UNIVERSITY OF SOUTHAMPTON

SCHOOL OF ENGINEERING SCIENCES

Fabrication and characterization of superconducting BiPb2223 tapes in new configurations for AC losses reduction.

by

Javier Tundidor Sarasa

Thesis for the degree of Doctor of Philosophy

November 2003

UNIVERSITY OF SOUTHAMPTON

ABSTRACT

SCHOOL OF ENGINEERING SCIENCES

Doctor of Philosophy

FABRICATION AND CHARACTERIZATION OF SUPERCONDUCTING BIPB2223 TAPES IN NEW CONFIGURATIONS FOR AC LOSSES REDUCTION.

by Javier Tundidor Sarasa

Superconductivity is a phenomenon occurred in some materials at very low temperatures. The two main properties are the lack of electric resistance and the expulsion of magnetic fields in the bulk. In the first discovered superconductors materials, superconductivity was only achieved just over liquid Helium temperatures. The properties of these superconductors could be a source of improvements in many industrial applications but the high operational cost for this range of temperature prevented the industry from using them widely.

From 1986 the investigations done in superconductivity have given an amazing progression. New superconductors in the copper oxide families have been found with much higher running temperatures than the previous known materials. These new superconductors have similar properties but very useful differences. The most promising superconducting material for electrical transport are composites of $(Bi,Pb)_2Sr_2Ca_2Cu_3O_{10}$ or BiPb-2223, $(Bi,Pb)_2Sr_2Ca_1Cu_1O_8$ and $YBa_2Cu_3O_7$.

The higher temperature obtained in the new type of superconductor puts at hands new applications as for example current cables. Nowadays, copper wires are used for the transport of electrical energy from the sources of generation to the points of consumption. Copper, even being a good metallic conductor and cheap material, has losses in electric transport. In some cases, superconducting materials can replace its use where the size and the amount of energy are critical.

Electrical energy is generally distributed by Alternating Currents (AC) that generate losses in the material that should be minimized. AC losses in superconductors come from the protective metallic sheath currents and from the hysteretic losses of superconductors. These losses can be reduced by an optimum selection of barrier materials and configurations.

The purpose of this thesis is the study of superconducting tapes characteristics and the development of new tapes for the reduction of AC losses.

TABLE OF CONTENTS

LIST OF FIGURES

LIST OF TABLES

Acknowledgements

Thanks to every one who has helped me in this period. Specially, thanks to my family and friends for all the good times, their support and company, thanks to my supervisors Carlo and Yfeng, our technician Mike and colleagues for their advises, help and support, without them it would have not been possible this work. Thanks to all the University staff and services which improved the development of my work and leisure. Finally, a special gratitude to National Grid Company and EPSRC for their sponsorship.

Chapter 1: SUPERCONDUCTIVITY.

1.1 Definition.

Superconductivity is a condensed matter phase characterized by the total loss of electrical resistance. This early definition explains the property firstly discovered in these materials but indeed they have another important properties. Superconductors have a perfect diamagnetism and magnetic flux expulsion as main factors for characterization. Superconductivity is only found in some materials at low temperatures due to its quantum origin; some of them related to the lattice and electron vibration coherences, some others still unknown.

1.2 History of Discoveries.

The first discovered property in the early years of this century was *Zero Resistivity* when Kammerlingh Onnes[1] was measuring the electrical conductance of metals at very low temperatures using Helium as refrigerant. The opportunity to measure at these temperatures the properties of some elements led to the discovery of the first property of superconductivity, the *Zero Resistivity.* The second of the properties, *Perfect Diamagnetism*, was found years later by Meissner and Ochsenfeld[2] in 1933. There are two aspects to perfect diamagnetism, flux exclusion and flux expulsion.

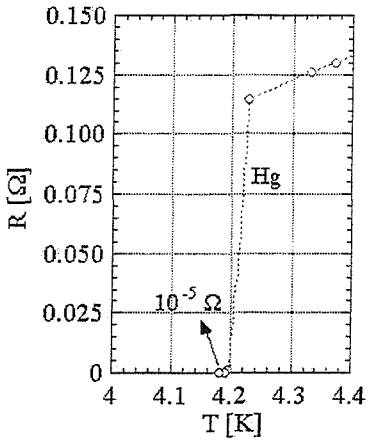

Fig. 1: Zero resistivity in Hg (Onnes, 1911).

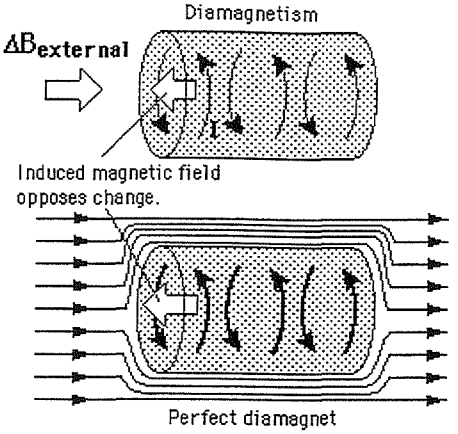

Fig. 2: Perfect diamagnetism.

The first superconducting materials were pure metals as mercury (Onnes, 1911), lead (Onnes, 1913) and tin. These metals have very low critical temperature (<30 K) and low critical magnetic field. In the 50's and 60's some Niobium based alloys (also called A15 compounds) with higher magnetic critical field were discovered. Nowadays, many applications are using them such as Magnets, Magnetic Resonance Imaging (MRI), magnetic separation, coils and other devices such as SQUID's.

It was on April 17, 1986, in an article titled "Possible High T_c Superconductivity in the Ba-La-Cu-O System" written by J. G. Bednorz and K.A. Müller[3], when a new generation of superconductors was discovered. They were called High Temperature Superconductors and the breakthrough given was impressive since the critical temperature jumped from the 23 K until the present 133 K (at atmospheric pressure). We can see the timeline of discovered superconductors in Fig. 3.

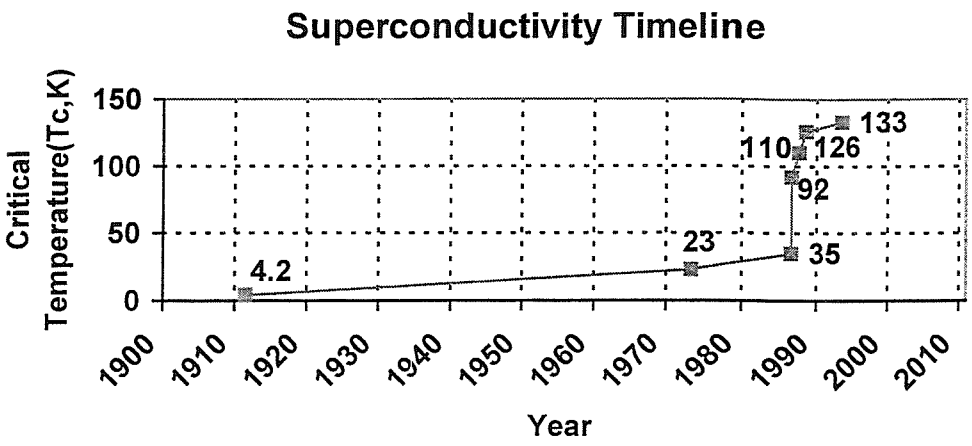

Fig. 3: Evolution of superconducting elements discovered.

These new superconductors, by difference to the previous ones that works with liquid Helium, can operate at liquid Nitrogen temperature, 77K, and therefore the operating cost is substantially reduced.

Nowadays, the discovering of a new superconductor (MgB_2(2001))[4] has brought us a new family of superconductors which may operate between 20K and 30K improving the properties of classical materials.

1.3 History of Theories.

Last century a wide range of materials with unrelated electrical, structural and chemical properties in their normal state have been found to be superconductors and the theories of superconductivity have been developed accordingly. But still there are discrepancies and unknowns and the origin of the superconducting properties of HTS materials is not yet understood.

A first phenomenological and macroscopic theory based on electromagnetism to explain superconductivity was given by F. London and H. London[5] in 1935. This theory explained the Meissner effect and the exponential decay of the magnetic field inside the superconductor by the parameter called London penetration depth. In 1937, Shubnikov et al[6] were the first to suggest the fundamental nature of type II superconductors. In 1950, Ginzburg and Landau[7] gave a derivation for the London equations, and their theory was the base of a thermodynamic theory. In 1950, H. Frölich[8] predicted the called isotope effect, which was observed experimentally in the same year by Maxwell and Reynolds[9].

The Ginzburg Landau theory was supplemented by the more complete and microscopic BCS theory (Bardeen, Cooper and Schrieffer[10]). In this theory, the superconductivity is explained by the change of state of the electrons. A slight attraction between these electrons through the lattice coupling make them pairs which travel without scattering. Nowadays, this is the most complete and closer approach to the superconducting state but it can not explain the pairing of HTS materials. Abrikosov[11] described in 1957 the mixed state of type II superconductors as a vortex state. Some other secondary properties were described after this general approach of superconductivity theory.

1.4 General Description.

1.4.1 Properties

Resistivity Zero, Critical Field, Current and Temperature

At low temperatures, resistivity of non-superconducting materials behaves as Drude model which states that conduction is restrained by three kinds of particle interactions: material defects, electron-phonon and electron-electron interactions.

Molecular defects interrupt the regular crystalline structure scattering the electric particles from its path. Electron-phonon interaction is due to scattering on the electron wave function with a discrete atom lattice. And finally, Electron-electron interaction is a Coulomb repulsion between the electrons.

Superconducting materials do not follow Drude conduction Model and at a Critical Temperature, T_c, resistivity drops to zero. Below T_c, electrons have lower energy if they join in pairs (BCS Theory). These pairs consist of electrons with opposite spins and opposite and equal momentum so that the net momentum and the net spin of the pair are zero[12] in low temperature superconductors. In HTS, pairing is different (net spin is 1) and still unclear mechanism. Nevertheless, not all the electrons behave in the same way and we can find normal electrons and superconducting electron pairs flowing on the material. As the superconductor temperature decreases further, unpaired electrons become superconductors.

Superconductivity is destroyed when the temperature is raised above T_c, and certain large value of magnetic field B_c called critical magnetic field. This magnetic field can be produced by an external source or by the superconductor own transport current. When the magnetic field exceeds its critical limit due to a current the superconductor is driven into a normal state due to so-called *Silsbee effect*, which explains the existence of a critical current density, J_c. It is not surprising that these three parameters, temperature, magnetic field and current density are closely coupled in determining the state of the superconductor. In Fig. 4 we can appreciate a standard relation between these parameters:

Critical Surface Phase Diagram

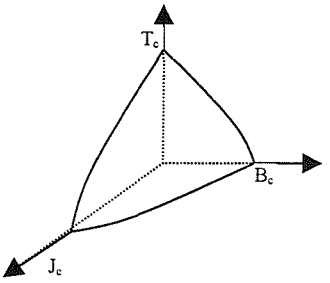

Fig. 4: Critical Surface Phase Diagram with limits in T_c, B_c and J_c.

In the case of the plane B-T, the critical magnetic field and critical temperature approximately follows next relation:

$$B_C = B_C(0)\left(1-\left(\frac{T}{T_C}\right)^2\right) \qquad \textbf{Eq. 1}$$

The critical current density distribution is different depending on the type of superconductor.

Perfect Diamagnetism. Meissner Effect.

The magnetic behaviour of a superconductor is different from a perfect conductor. If a superconductor were cooled in zero field below its critical temperature, it would react to an applied field in the same way as a perfect conductor. Both will exclude the magnetic field from the interior of the material due to the induced screening currents. They behave as a perfect diamagnetic material, i.e. the local magnetic induction within the body is zero.

$$B_i = B_a(1+\chi) = 0 \Rightarrow \chi = -1 \qquad \text{Eq. 2}$$

If now the superconductor is cooled below T_c in the presence of a magnetic field, it behaves in a different way than a perfect conductor. A local field in a perfect conductor does not change because there are no induced screening currents. However, a superconductor will expel the magnetic field and this is called *the Meissner-Öchsenfeld effect.* It implies that the final state of the system does not depend on whether the magnetic field is applied before or after cooling, indicating a thermodynamic equilibrium state.

Type I Superconductor.

Superconductors are generally divided into two categories called type I and type II superconductors. Type I superconductors are those up to a given critical field H_c remain superconductor (see Fig. 5). The superconducting state has lower free energy than the normal state. The energy cost of removing the magnetic field, sometimes referred to as the condensation energy of the superconducting state, is $\frac{1}{2}\mu_0 H_c^2$ per unit volume. This value is the difference in the energy of the normal and the superconducting state in zero magnetic fields. Since the currents generate self fields, a low tolerance to magnetic fields leads to a low tolerance for current transport. Superconducting currents are in a surface sheath of depth λ. Type I superconductors are pure metallic elements such as mercury, lead and tin and have only practical operations in relatively low magnetic fields.

Type II Superconductor.

At low magnetic fields, type II superconductors fully expel the magnetic field inside the material, the same as type I superconductors does. This state remains below a critical magnetic field B_{c1}, different from B_c, and is called Meissner state. However,

at higher magnetic fields, type II superconductors have a way to maintain the magnetic field in the body of the superconductor below the critical field B_{c2} (See Fig. 5 and Fig. 6). In type II magnetic fields penetrate deeper and coexist as fluxes with superconducting currents. The magnetic fields are confined to an internal array of normal state flux tubes called vortices since they are surrounded by a circulating supercurrent. This state is energetically favourable for $B_{c1} < B < B_{c2}$ and is called mixed state or Abrikosov state which allows the superconductor to reach higher levels of applied magnetic fields and transport current. Type II are usually alloys or compounds (niobium and Vanadium are exception to this rule) and most of the industrial applications are made with this type of materials.

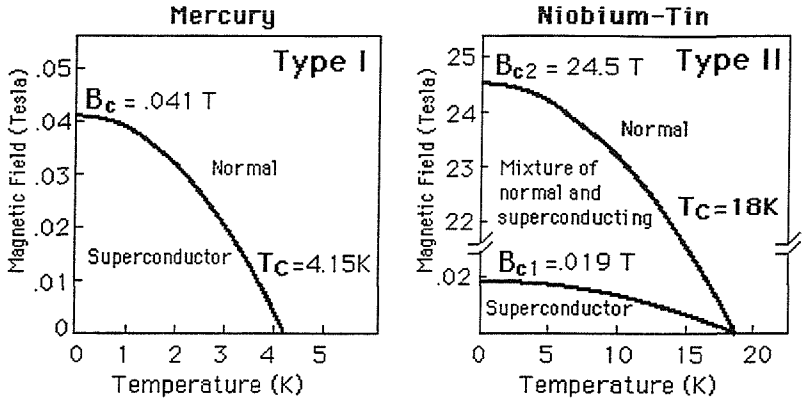

Fig. 5: B-T characteristics of type I and type II.

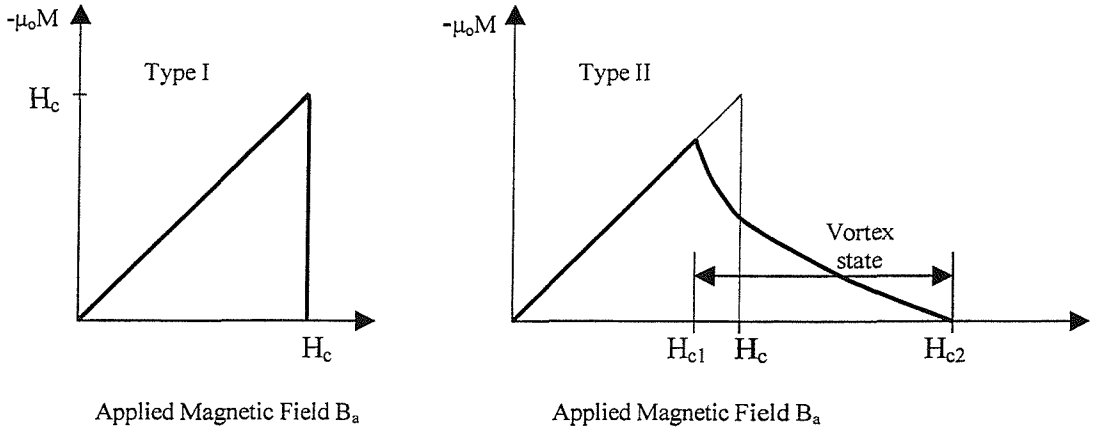

Fig. 6: Magnetisation curve of type I and II superconductors.

Flux Pinning and Hysteretic losses

In type II superconductors where a magnetic field is supplied, the flux vortices, also called fluxoids, would start to appear from the external surface of the superconductor. In the case of a homogeneous material vortices move freely and spread homogeneously in the superconducting material organising themselves in regular hexagons since this is the lowest energy structure. Any change in magnetic field would change the amount of vortices and therefore, all the vortices would move to the next equilibrium state.

However, these fluxoids should remain stable, since motion results in dissipation by normal currents induced in the fluxoid cores. This stabilisation can be achieved if any impurity or defect hinders its movement, this is what is called pinning the fluxoids. The pinning centres in HTS are mainly provided by point defects such as oxygen vacancies, holes or precipitate particles and grain boundaries.

When the repulsion forces between the vortices are comparable to the pinning forces then the fluxoids start to move, hence energy is invariably dissipated. The dissipation is generally distinguished and referred to as "flux creep" when the pinning forces dominate, and as flux flow when the Lorentz forces are dominant.

1.4.2 London Theory.

Fritz and Heinz London[13] focused on the electromagnetic properties of superconductors introducing a set of phenomenological equations; the key aide is to separate the conduction electrons into two components, namely normal and superconducting electrons. As we know for normal metals, Drude model is valid and follows next relation:

$$\vec{J} = \sigma \cdot \vec{E} \qquad \textbf{Eq. 3}$$

That in variable electric fields formulae becomes:

$$\vec{J}e^{-i\omega t} = \sigma(\omega) \cdot \vec{E}e^{-i\omega t} \qquad \textbf{Eq. 4}$$

Where, in Drude theory the complex conductivity turns to be

$$\sigma(\omega) = \frac{ne^2\tau}{m^*(1 - i\omega\tau)} \qquad \textbf{Eq. 5}$$

$\tau \equiv$Average time between collisions

$m^* \equiv$Effective mass

In a simple drude-like description, the superconducting electrons are postulated to have an infinite scattering time, as they did not suffer from scattering processes ($\tau = \infty$). So the formula becomes in this way:

$$\tau \to \infty \Rightarrow \sigma_s(\omega) = -\frac{n_s e^2}{i\omega m^*} \qquad \textbf{Eq. 6}$$

$$\sigma(\omega) = \frac{n_s e^2}{i\omega\, m^*} + \frac{(n-n_s)e^2\tau}{m^*(1-i\omega\tau)} \qquad \textbf{Eq. 7}$$

The first term is purely imaginary and it does not dissipate any energy. Therefore, the first London equation is then defined as:

$$\frac{d\vec{J}_s}{dt} = \frac{n_s e^2}{m^*}\vec{E} \qquad \textbf{Eq. 8}$$

If we manipulate a bit more the conductivity equation (Eq. 3) and Maxwell equation we shall get:

$$(\vec{\nabla}\times\vec{J})\cdot e^{-i\omega t} = \sigma(\omega)\cdot(\vec{\nabla}\times\vec{E})\cdot e^{-i\omega t} = -\sigma(\omega)\cdot\frac{d(\vec{B}e^{-i\omega t})}{dt} = i\omega\sigma(\omega)\vec{B}e^{-i\omega t} \qquad \textbf{Eq. 9}$$

London postulated that, for some reason, the wave function of the superconducting electrons is "rigid", i.e. the average momentum is zero, <p>= 0, even in external applied field. Therefore, if there is no time dependence, when ω tends to 0 and using the other Maxwell equation implies:

$$(\vec{\nabla}\times\vec{J})\cdot e^{-i\omega t} \rightarrow -\frac{n_s e^2}{m^*}\vec{B}e^{-i\omega t} \qquad \textbf{Eq. 10}$$

And therefore, the second London equation can be shown as:

$$(\vec{\nabla}\times\vec{J}) = -\frac{n_s e^2}{m^*}\vec{B} = -\frac{1}{\mu_0\lambda^2}\vec{B} \qquad \textbf{Eq. 11}$$

And applying Maxwell equation in absence of magnetization and displacement currents:

$$\vec{\nabla}\times(\vec{\nabla}\times\vec{B}) = -\mu_0\left(\frac{n_s e^2}{m^*}\right)\vec{B} = -\frac{1}{\lambda^2}\vec{B} \qquad \textbf{Eq. 12}$$

This gives an exponential decay parameterised by λ, called *penetration depth* of the superconductor, being the distance inside the surface over which the magnetic field decrease by the factor "e" by 1/e. In a vortex, the magnetic field goes to zero outside a radius of order λ.

1.4.3 Ginzburg-Landau Theory.

This theory is also a phenomenological approach of superconductivity from the point of view of phase transition theory that was developed in 1950. It adopted some assumptions that seem to be valid since many of the properties were predicted successfully.

As in many other phenomena involving phase transitions they characterized the superconducting state as an order parameter that explains the transition between the superconductor and the normal state.

Ginzburg-Landau theory assumes that there is a complex order parameter $\phi = |\phi(\vec{r})|e^{i\Theta}$ such that $|\phi|^2$ is proportional to the density of superelectrons (n_s). The theory also assumes that the superconducting currents are the motion of superelectrons of effective mass m*, charge e^* with absolute value |2e|; the order parameter n_s is zero in normal state but it increases to $\pm\frac{1}{2}n_s$ for 0°K.

The theory postulates that below the transition temperature and close to T_c, the Gibbs free energy per unit volume $G_s(\phi)$ may be expanded as a power series of the order parameter:

$$G_s(\phi) = G_n + \ldots$$
$$\ldots + \frac{1}{V}\int d^3\vec{r}\left[\frac{1}{2m^*}\times\left(-i\hbar\vec{\nabla} + e^*\vec{A}\right)\phi + \frac{1}{2\mu_0}B^2(\vec{r}) - \mu_0\vec{H}(\vec{r})\vec{M}(\vec{r}) + a\phi\phi^* + \frac{1}{2}b\phi\phi^*\phi\phi^* + \ldots\right]$$

Eq. 13

where G_n is the free energy density of the normal state, M is the magnetisation, A is the magnetic vector potential and a and b are functions of the temperature only and related by ½ (a^2/b) which is the condensation energy per unit volume of the super electrons or the energy released by transformation of normal electrons to the superelectron state and -a/b is $|\phi|^2$.

The Ginzburg-Landau Equations are determined by two requirements. The free energy must be a minimum in relation to variations in the order parameter and in the vector potential.

In conclusion, the two Ginzburg-Landau equations are:

$$\frac{1}{2m^*}\left[\hbar^2\vec{\nabla}^2\phi - 2i\hbar e^*\vec{A}\cdot\vec{\nabla}\phi - e^{*2}\vec{A}^2\phi\right] + a\phi + \frac{1}{2}b\phi|\phi|^2 = 0$$

Eq. 14

and

$$\vec{\nabla}\times(\vec{\nabla}\times\vec{A}) + i\hbar\left(\frac{e^*}{2m^*}\right)(\phi^*\vec{\nabla}\phi - \phi\vec{\nabla}\phi^*) + \left(\frac{e^*}{2m^*}\right)\vec{A}|\phi|^2 = \vec{0}$$

Eq. 15

Normalizing these equations, the theory give us, as natural parameters, the penetration length, the coherence length (ξ) and the flux quantization already explained, where:

$$\lambda_L = \frac{m^*}{\mu_0 e^{*2}|\phi_\infty|^2}\ ; \quad \xi^2 = \frac{\hbar^2}{2m^*|a|}$$

This length scale, ξ, measures how long it takes for a perturbation of the equilibrium value of the order parameter ϕ to heal. For example, ξ measures the typical width of a domain wall between the superconducting and the normal phase, in the absence of magnetic fields. Meanwhile λ_L is similar to the parameter of London equations, in fact London equations, can be derived from this theory by applying these equations in weak fields and to first order in B, and therefore discriminating small fluctuations of $|\phi|^2=n_s$.

The ratio of these two characteristic lengths $\kappa = \lambda_L/\xi$ is another order parameter of this theory that explains the limit where the superconductor becomes unstable with respect to the formation of a normal-superconducting interface, therefore vortices and type II behaviour appears for a determined constant ratio as it is shown below:

$$\kappa < \frac{1}{\sqrt{2}}\ ; \qquad \text{Type I Superconductor}$$

$$\kappa > \frac{1}{\sqrt{2}}\ ; \qquad \text{Type II Superconductor}$$

Yet, the relationship between the thermodynamical critical field (B_c) in type I and type II and the upper and lower critical field in type II superconductors are related by this parameter as:

$$\frac{B_{C2}}{B_C} = \sqrt{2}\,\kappa \qquad \textbf{Eq. 16}$$

$$\frac{B_{C1}}{B_C} = \frac{\ln \kappa}{\sqrt{2}\,\kappa} \qquad \textbf{Eq. 17}$$

1.4.4 The Bardeen, Cooper and Schrieffer (BCS) Theory.

The excitation spectrum of a superconductor was studied through low-temperature electronic specific heat and electromagnetic absorption measurements. An energy gap, Δ, of order $k_B T_c$, was found in the single-particle excitation spectrum in different materials. Despite Ginzburg-Landau theory has a successful phenomenological approach to the superconductivity phenomena, does not explain the origin of this energy gap neither its microscopically behaviour. The BCS theory was developed under three major insights:

- It seems that forces between electrons can sometimes be attractive in a solid rather than expulsive.
- Even a week attraction makes the electrons at the Fermi surface bind into pairs.
- BCS make a many-particle wave function in which all the electrons are paired up.

To explain the whole theory requires a deep explanation but there are some textbooks that explain it (Tinkham (1985)[14] or Fetter and Walecka (1971)[15]). But generally speaking, theory started in 1956, when Cooper addressed the problem of a single pair of interacting electrons above a non-interacting filled Fermi sea and showed that the kinematical constraint imposed by the Pauli principle always leads to the existence of a bound state for any arbitrarily weak attractive potential. Bardeen, Cooper, and Schrieffer realized that the idea of pairing among electrons was crucial to understand the phenomenology of superconductivity.

According to the BCS theory, in the superconducting ground state, electrons of opposite spin and momentum develop strong correlations. These paired electronic states are called Cooper pairs. Above the superconducting transition temperature, these pairing correlations are broken up by thermal fluctuations and play no important role in the metallic phase. But what is the physical origin of such an attractive interaction? The screened Coulomb interaction cannot be responsible for

superconductivity, being a repulsive interaction. A key experiment that shed some light on this question is the measurement of the isotope effect, the critical temperature T_c and the thermodynamic critical field H_c of a superconductor are proportional to $M^{-\alpha}$ with $\alpha \sim 1/2$ for isotopes of the same element (where M is the nuclear mass). Thus, T_c and H_c are larger for lighter isotopes. The most obvious way in which the different atomic masses may affect the critical temperature is if the attractive electron-electron interaction is phonon mediated. Qualitatively speaking, the first electron attracts the positive ions of the lattice and, because the relaxation times of the lattice are of the order of the inverse Debye frequency $\omega_D << \omega_p$ (the plasma frequency), when another electron passes by, it will feel an attraction by the displaced lattice. If the electron-phonon coupling is strong enough, the effective attractive electron-electron interaction could overpower the repulsive screened Coulomb interaction. It turns out that this effective interaction is attractive only if the electron energy differences are smaller than the phonon spectrum cut-off $\hbar\omega_D$. Therefore, the electrons in an energy shell of width $\hbar\omega_D$ around the Fermi surface turn out to be the players for superconductivity.

As a last result of the BCS theory, the gap parameter Δ is the characteristic energy determining the range of one-particle states involved in the superconducting ground state. For typical elemental superconductors, the size of a Cooper pair is of the order of $\zeta = 3000$ Å, much larger than the typical distance between electrons in a metal. The BCS theory adds to the Ginzburg-Landau Theory the value of the mass and charge of superconductor particle to be $2m_e$ and $2e$ respectively.

1.5 High Temperature Superconductors(HTS).

The superconductor materials can be divided in different groups based on their electromagnetic properties or by operating temperature. As mentioned earlier the superconductors can be divided in type I and type II by its electromagnetic behaviour, in parallel to this definition, the superconductors are also classified by the operating temperature in High Temperature Superconductors (HTS) and Low Temperature

Superconductors (LTS) (although HTS is also a different class microscopically and means certain behaviour). Among the HTS, the more interesting are those with a critical temperature above liquid Nitrogen temperature, while for the LTS, the only cryogen available for cooling is liquid Helium (4K). All HTS materials are type II superconductors.

The High Temperature Superconductors fall into a restricted number of systems. These systems are delineated by their compositions and corresponding crystal structures. The systems generally contain extensive families, in which individual members are related by elemental substitutions but have similar crystal structures. The families all have complex crystal chemistries, and in many of them, processing problems are associated both with imperfect stoichiometry and with intergrowths of similar phases. Recently, new superconductor LTS-like with higher critical temperature has been discovered[16] in systems much simpler, which are under study.

The principal HTS groups are listed below but for further details on the crystal structure of various families of compounds described here are given by Hazen[17]:

1. Alkaline Earth Doped La_2CuO_4, with a layered-perovskite K_2NiF_4 structure and $T_c \cong 30$ K.
2. $La_{2-x}M_xCuO4$ family ($x<0.5$; M= Ca, Sr, Ba), has octahedrally coordinated structure and $T_c \cong 31$ K. Oxygenation increases their I_c due to decreasing their vacancies and increasing holes.
3. $Y_aBa_bCu_cO$ System (abc = 123, 124, 247) $T_c \cong 93$ K, 81 K and 55 K respectively. Their I_c can be increased by oxygenation during sintering process. The Y can also be substituted by next lanthanide elements: Nd, Sm, Eu, Gd, Dy, Ho, Er, Tm, Yb and Lu.

4.$A_2B_2Ca_nCu_{n+1}O_{2n+6}$ Systems (n = 0-4; A= Bi, Tl, Hg; B= Sr, Ba), with T_c up to 133 K. This family includes the BiSCCO system which will be further explained because of its practical importance.

1.6 The BSCCO Family.

From all the HTS materials discovered so far the more successful systems are Bi-Sr-Ca-Cu-O (BSCCO) ceramics, which consists of three superconducting phases and Y-Ba-Cu-O (YBCO) (with lower critical temperature but higher critical magnetic field). It was Maeda[18] who found BSCCO material in 1988, and since then, many studies have improved our acknowledge in these ceramics.

The three superconducting phases belonging to the $Bi_2Sr_2Ca_{n-1}Cu_nO_{2n+4}$ series[19] are:

1. *$Bi_2Sr_2CuO_6$ (2201).*

This phase has T_c of about 22K and tetragonal structure (a= 5.4 Å, c= 24.6Å)[20], being stable at temperatures below 600 °C with melting temperature of 910 °C. The stoichiometric compound is semiconductor, however the out of stoichiometry compound $Bi_{2,1}Sr_{1,9}CaO_6$ is superconductor[21].

2. *$Bi_2Sr_2CaCu_2O_8$ (2212).*

This phase has T_c values about 95 K and a pseudo-tetragonal structure (a= 5.4 Å, c= 30.85 Å)[22] and the melting temperature is around 895 °C.

3. *$Bi_2Sr_2Ca_2Cu_3O_{10}$ (2223).*

The T_c is about 110 K, this phase has an orthorhombic structure (a= 3.8 Å, c= 38 Å)[23] and a melting temperature of about 850 °C with a narrow range of stability around 50°C.

While the 2201 and 2212 phases are easy to obtain, the 2223 one has a lower stability and only in a narrow window of a few degrees is obtainable with a high final formation percentage. However, by substituting some Bi by Pb (BiPb2223), a wider range of stability is obtained[24,25], achieving at the same time, a higher conversion of 2223 phase in the final product related to the precursor 2212 phase. Some characteristics of the BSCCO system common with all copper oxide superconductors are listed below:

- There are intergrowth layer structures[26,27], producing anisotropic properties.
- Cations have mixed valences[28], being the origin of charge carriers.
- They have extremely short coherence lengths and large penetration depths that lead to two problems, weak links at grain boundaries and large magnetic flux line creep.

But some other characteristics are particularly stronger in BSCCO system such as:

- A magnetic behaviour dominated by giant flux creep[29].
- A wide reversible regime and low melting temperature of the Abrikosov lattice[30].

1.7 Commercial achievements.

Superconducting technology of HTS materials has reached several areas of competitiveness: Substitution of low temperature superconductors and new technology that cannot be reached otherwise. The application field is very broad going from mechanical and electrical transportation, medical analysis, magnetic material separation, electrical generation, storage and production, electronics and computers.

In the field of transport, the use of superconductors by magnetic levitation (MAGLEV) is attracting the interest of the developed countries with overloaded transport systems and where public services needs to improve time response. Economy scaling and lower energy consumption are the keys in the use for passengers and freight transport. The idea is the use of a magnetic rail over which a superconducting train is lifted and stabilized keeping a security distance of several centimetres from the edges and the floor of the rail. The main train passenger projects are made in Japan (Yamanashi Maglev)[31], Germany (Berlin-Hamburg project)[32], China (Shanghai-Pudong airport) and US (Virginia College campus test)[33]. For the case of freight transport, the reasons for its use are the high traffic and the construction of ships bigger than the size allowed by the Suez and Panama channels. A land bridge could be used for freight interchange on these areas, a project in the Mexican Tehuantepac isthmus and in the Suez channel are under study[34].

In the area of medical studies, superconductivity has been used in the creation of homogeneous magnetic fields that serves for the body examination with non invasive methods as Nuclear Magnetic Resonance Interference (NMRI)[35]. The better the homogeneity, the better the resolution and superconductors can make this homogeneity better than normal windings.

Superconductivity is also used in particle physics experiments, where high magnetic fields are demanded, laboratories as CERN in Switzerland or Fermilab in USA are using superconductors in particles colliders as the new LHC (large hadron collider)[36] or in the proton antiproton collider[37] respectively.

Other applications particularly interesting are the construction of high efficient motors and generators and magnetic energy storage prototype that are under way in companies as General Electric and Energy alliance in collaboration with American Superconductors. The Engineering department of Southampton, which has built a 20 KVA transformer[38], a 600 A-13 kA current lead for CERN[39] and at this moment is building a superconducting asynchronous generator[40]. Current fault limiters with higher time response have been tested by ABB company[41], Advanced ceramics limited[42] or Intermagnetics General (IGC)[43].

For electrical power transmission, superconductors are only tested in short lengths and places where high currents and impracticality of copper wires extension due to the lack of space made them economically viable. Some HTS wire has been placed in the electrical grid in Copenhagen[44] and Detroit[45].

The paper industry needs of strong magnets for the separations of impurities during kaolin extraction, it is therefore another technology that could be substituted for energy cost reduction.

In the electronics and computers industry, it has been used in the production of electronic filters for the cellular telecommunications. It is also studied the implantation of ultrahigh speed processors and memories by josephson junctions creating petaflop computers but for this issue there are several technologies competing for the future like molecule-based and quantum transistors.

Another emerging technologies as satellite gyroscopes or superconducting x-ray and light detectors are under study.

Chapter 2: FABRICATION OF BiPb2223 TAPES.

2.1 Introduction.

Due to their brittle and reactive nature of these ceramics the HTS materials require a careful processing and handling. One of the most important engineering parameters determining the successful practical application of these materials is the critical current. In order to reach high critical currents the production of BiPb2223 requires a good chemical composition of the precursors and a proper optimisation of the mechanical and thermal procedures. Due to the large number of parameters, the optimisation of the fabrication process is a very difficult task.

The most common way used for fabrication of BiPb2223 conductors is the OPIT Method where a precursor powder oxide is packed into a metal tube in a controlled environment. This sheath is required to avoid:

a) The mechanical fragility: BSCCO ceramics are granular and brittle. So, composite with a metallic sheaths are needed for mechanical processing and manufacturing.

b) Quench stability: Eventually, some local unstable areas in a superconductor which have lower transport current capabilities may become non superconducting under a current flow. The heat produced by the current transport of a resistive zone would propagate the instability along the wire causing it to quench. Therefore, the design of superconducting wires must take into account for this behaviour providing alternative paths for the current. A metallic sheath, due to their good thermal and electrical conduction, can

provide alternative path for heat dissipation and current transport allowing the superconductor to stabilize.

The selection of the sheath material also should satisfy:

1. Reactivity during processing. The sheath must have low reactivity with the precursors during the heat treatment as well as melting points higher than processing temperatures. Also the sheath must allow oxygen diffusion at the processing temperatures.
2. Low cost: The choice of the sheath material for large scale applications should keep the costs lower enough. This is because the applicability in the industries requires to keep the investment and operation costs of the new devices at competitive values compared with present technology.

Unfortunately, it has being found that only noble metals (gold and silver) and some of their alloys do not react during heat treatment with the precursor powders. The most common sheath materials are silver and silver alloys. They have a good thermal and electrical conductivity, ductile and they allow the Oxygen diffusion at processing temperatures. Silver has a melting point of 960°C in air at 1 atm., higher than temperatures of common heat treatments used for 2223 tape production. Also, the lower peritectic temperature of 2223 in the presence of silver allows its diffusion into de core causing the partial melting of the superconducting material and enhancing the reaction[46]. Gold and Paladium silver alloys which have a higher thermal conductivity and complemented with ternary elements as Mg, Ni to increase the mechanical strength are the optimum materials for BSCCO tapes and wires but their cost is still high; therefore, another cheaper alloys based in elements such Mg, Cu, Ti or Ni are used with a lower electrical resistivity at operating temperatures[47].

In the diagram of Fig. 7 is described the general processing of a BSCCO tape. In some experimental processing, the wire is swaged or squared rolled instead of drawn, in some others; a pressing or continuous pressing can substitute the rolling of the wire/tape.

PROCESSING A TWISTED MULTIFILAMENTARY TAPE

a) Filling of reactant mixture of oxide powder in a billet.

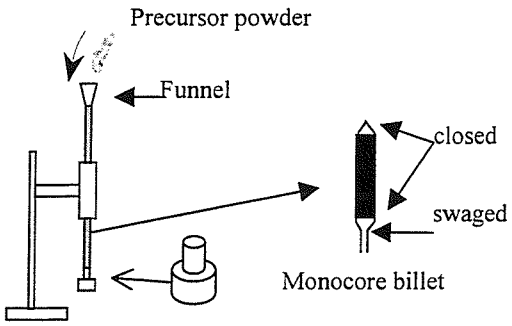

b) Drawing and annealing several times monocore wire.

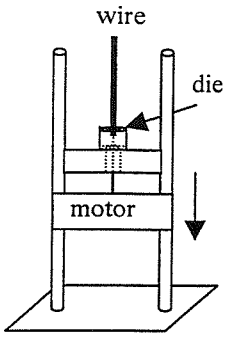

c) Packing a multifilamentary tube.

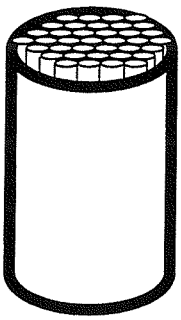

d) Drawing and annealing multifilamentary wire.

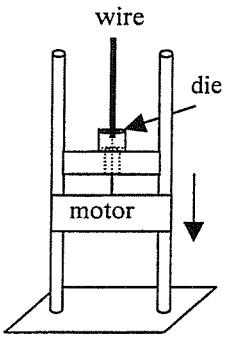

e) Twisting/braiding and annealing the wire.

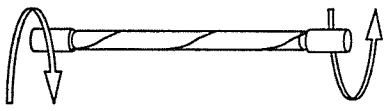

f) Rolling the wire into a tape.

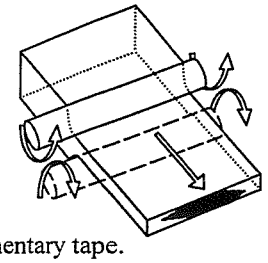

Fig. 7: OPIT process for a multifilamentary tape.

In the standard OPIT method, a well mixed mixture of unreacted powders with the 2223 stoichiometry are used as precursor powder and packed into a silver tube (see Fig. 7). A pure Argon atmosphere is used to avoid the water and the carbon presents in the air, which are a likely source of contamination for the powder[48]. The packed tube is then cold drawn into 1 to 2 mm of diameter resulting in an increase in the core density.

For silver alloys based in elements such as Ni, Mg, Mn or Cu, the hardening of the sheath during cold working is higher than the pure silver so that the new elements act as discontinuous points of sliding planes. When the stresses induced in the silver sheath reach their tensile strength limit it may provoke inhomogeneous deformations and the breaking of the wire; therefore, some intermediate softening steps will be necessary. The annealing temperature must be kept low so that the powder does not start undesirable reactions. Depending on the sheath material, change the number of annealings needed during the OPIT process and even it could be unnecessary for soft material as pure silver.

The wire drawn down to 1-2 mm diameter can be processed in two different ways:

a) The wire can be rolled (or axially pressed) into monofilamentary tapes. This configuration is not optimised for industrial applications due to its high hysteretic losses, fragility and inhomogeneous superconducting properties along the tape, but is used for investigation of the main properties of the material.

b) The monocore wire is divided and packed into another silver or alloyed tube to form a multifilamentary wire. Then, the multifilamentary wire is drawn in several steps, with intermediate annealings if necessary, down to 1-2 mm diameter. The wires are packed in a hexagonal or rectangular

shape, being more stable the hexagonal for circular or hexagonal drawing and rectangular in the four-roll machine. The number of filaments used in hexagonal shape is commonly 19, 37 and 61 filaments. Then, the wire is repeatedly rolled or pressed in small steps for a good deformation process obtaining tapes of about 200-300 μm thickness, 3-5 mm width. Moreover, if a twisted multifilamentary wire is required, the twisting process can be carried out prior to the rolling or pressing step.

Finally the tape is thermomechanically treated. The as-rolled tapes are heat-treated in a temperature range of 810-840°C in order to convert the stoichiometric precursor into BiPb2223. It is generally accepted that core densification and grain alignment are improved with subsequent rolling-pressing/sintering processes[49], promoting higher critical currents. The use of tapes instead of wires is also due to the lower handling damage caused in the tape; additionally, the contact surface with silver is higher, therefore cryogenic stability is also improved and the superconducting core layers in close vicinity to the silver sheath have higher phase conversion from Bi2212 to Bi2223.

2.2 Precursor powder synthesis.

In the production of tapes with high I_c using OPIT method, the starting precursors are partially calcined powders, which mainly consist of 2212 phase grain and oxides of Ca_2CuO, Ca_2PbO_4 and CuO. There are several synthesising methods[50,51] of such precursor. Some of these methods are:

a) *Solid state reaction*[52]. The solid state reaction takes place by diffusion at temperatures or below the melting temperature of component oxides. These processes are repeated several times with grinding in between and require long annealing times and close temperature control of the sample.

b) *Coprecipitation*[53]. In this method, soluble ionic compounds such as carbonates, nitrates, oxalates, etc are dissolved in water before adding acid to bind all the metal ions. After precipitation the water can be evaporated prior to the calcination process to yield the desired phase. The difficulty of this method is that the stoichiometry and contamination are difficult to control.

c) *Evaporation Decomposition of Solution (EDS) method*[54]. A solution of cations is sprayed as a fine mist in a hot furnace and the resulting oxide mixture is collected. Further grinding and sintering steps allow the homogeneous reaction of the powders.

d) *Burn technique*[55]. A nitrate solution of cations plus organic species is heated to remove water and to react the nitrate ions with the organic species. The resulting mixture of powder can be fired to eliminate the carbon containing compounds to produce the phase.

e) *Freeze drying*[56]. An aqueous nitrate solution spray of compounds is sunk in liquid nitrogen. The droplets are then collected and at the same time the water is removed by freeze drying. A very good mixture of powder with no contaminants is obtained.

f) *Sol gel*[57]. By adding water or alcohol to an alcoxide solution of cations, a gel is formed through polymerisation and condensation reactions. The organic compounds are then, burnt by heating at high temperatures. It gives a powder with some residual carbonates.

All these methods affect the powder properties in different ways. From a chemical point of view, the right proportions of compounds and high purity are very important for the achievement of the pure 2223 phase. Any contamination, whether external or from the powder composition can inhibit the production of high quality phase. The chemical composition of components affects the driving force of chemical reaction and grain growth during the synthesising process. Also, the

reaction during the synthesis affect the degree of agglomeration, the final phase composition and the particle size, which in turn determine some features of the thermomechanical processing of the 2223 tapes. The average particle size of the powder can influence the homogeneity of the packing and the amount of liquid phases during sintering process. It is generally accepted that higher phase formation rate can be achieved with small particle size.

2.3 Mechanical Processing.

To achieve high J_c tapes, it is advantageous to have well aligned dense core. It may appear that a high initial packing density will result in high final core density. However, Wolf et al[58], has clearly shown that the final core density, as a function of the wire diameter, tends to reach asymptotic value, which is independent of the initial packing density, as a consequence, further mechanical cold work can develop sliding and fracture of the core and therefore inhomogeneities in both core and sheath. High initial packing densities have been shown to produce irregular interface between silver and core (sausaging) and bursting between filaments. Therefore, the initial densities used in most cases are in the range of 20%-50% of the theoretical 2223 phase density (6.6 gr/cm^3).

Once the powder is packed into the silver tube, the size is reduced to 1-2 mm diameter by drawing using successive dies. The stresses involved are a longitudinal tension, and a radial compression superimposed, which is accomplished by an axisymmetric reduction of the cross-section and an elongation. This is obtained by pulling the wire through a number of dies. The prominent characteristic of the drawing method is that the deformation is not homogeneous, especially for small reductions, the tendency is for the outer layers of the wire to be worked more severely than the inner regions.

The die geometry, which determine the material deformation, is quantitatively parameterised by G_d that relates the mean diameter and the inclined length drawn:

$$G_d = \frac{(D_1 + D_2)}{(D_1 - D_2)} \sin\vartheta \qquad \text{Eq. 18}$$

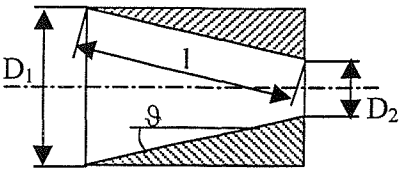

Fig. 8: Die geometry.

where D_1 is the income die diameter assuming to be the initial wire diameter, D_2 is the final diameter and ϑ is the die angle. This effect is most marked when the length of the deformation zone is small and the die angle is large. The geometry of deformation also gives rise to redundant deformation because some of the shearing that occurs at the entry to the deformation zone is reversed at exit and thus not contribute to the final shape change. Smaller unitary radius reduction and longer die angles give greater G_d values reflecting an inhomogeneous and redundant deformation. Therefore, the parameter G_d may be considered as an indication of the homogeneity of the deformation and core densification.

According to Crane[59] when G_d falls below 0.9 for a metal rod, the inhomogeneous deformation is negligible, nevertheless these results can not be extrapolated to the drawing of the soft/hard composites resulting in the OPIT method. In fact, the value of G_d in composites is much more bigger (between 5 and 15 in Ag-Bi2223 composite). In this case, powdered cores cannot support tension stresses and a more detailed study is necessary. Also the stresses over each material affect the density across multifilamentary wires. Denser materials could be found in the outer wire parts and this inhomogeneous density developed across sectional area is the reason why some multifilamentary wires can burst in the centre.

The reduction per pass is limited to avoid sausaging of the cores; hence for Bi-2223/Ag wires the reduction must be kept low (<15%). The drawing process induces the first stages of texture into the material and an increase in density of the powder due to the directional compression[60].

The next step in the tape formation is rolling (See Fig. 9 and Fig. 10). The material is compressed in the roll gap, and thus, it expands longitudinally and spreads laterally. At entry the roll surfaces tend to drag the surface portions of the wire forward, but on exit drag them back again, relative to more central portions of the wire, the change of direction of the frictional drag may be imagined to occur instantaneously in a plane called the neutral plane.

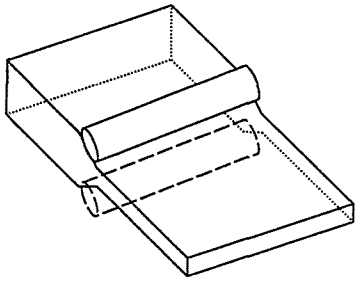

Fig. 9: Rolling sketch.

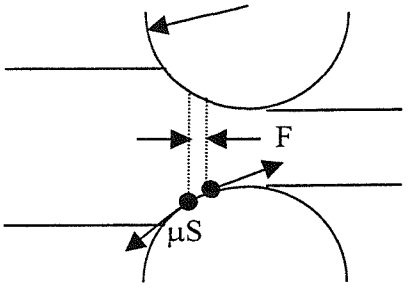

Fig. 10: Rolling forces diagram.

The friction thus generates an inward-acting longitudinal force, which may be supposed to be distributed over the cross section of the tape as a shear stress. The radial roll pressure is generally sufficiently high to cause the roll surfaces to undergo a significant change in curvature. A bigger roller diameter was shown to give more width strain and hence a wider tape[61], improving the aspect ratio and therefore the grain alignment and the silver contact surface. Also, the application of some tension in the front and the back of the tape improves the final critical current density[62].

The main defect associated with rolling is sausaging. It is caused by differing strains in the sheath and core due to the different mechanical resistances to the deformation. Wang et al[63] has detailed this defect. It is believed that sausaging interferes with the path of the current flowing preferentially near the silver ceramic interface. This inhomogeneous response is exaggerated as the degree of deformation increases, specially after annealing to softening the sheath. Wang concludes that stronger sheath material and smaller wire size prior to rolling would reduce sausaging. Yoo et al[64] has found that the use of harder alloy sheath reduces the effects of sausaging.

2.4 Heat Treatment.

The Bi2223 tapes made by the OPIT method need to be thermally processed to convert the 2212 phase to the desired Bi2223 one. Furthermore, in order to reach high critical current, in this case, a good intergranular connectivity of the 2223 grains and a strong pinning, in case of external magnetic field, has to be reached.

The heat treatment of the tape is dependent of many parameters; the initial powder composition (purity and stoichiometry), the silver area in contact to the core and its texture, the ramp rates, temperatures and dwell times during thermal processing, the intermediate rolling parameters and further treatments are all interdependent and they need to be controlled in each case.

From the point of view of powder composition, it is well known that the addition of small amount of Pb substitute the Bismuth and promotes the growth of the 2223[65], several powder stoichiometries are used as a green powder, the most common are:

$Bi_{1.72}\ Pb_{0.34}\ Sr_{1.83}\ Ca_{1.97}\ Cu_{3.13}\ O_{10+z}$ Yamada composition[66]

$Bi_{1.84}Pb_{0.34}Sr_{1.91}Ca_{2.03}Cu_{3.06}O_{10+x}$ Endo composition[67]

$Bi_{1.8}Pb_{0.4}Sr_{2.0}Ca_{2.1}Cu_{3.0}O_{10+x}$ Sato composition[68]

These three stoichiometries share:

1. A proportion of Ca higher than Sr, to compensate the lower diffusivity of Ca.
2. A Cu in excess, because copper phases behave liquid formers and therefore enhances the kinetics of Bi2223 formation.
3. An excess of Bi+Pb to avoid the evaporation losses of them during heating.

The sintering atmospheres also affects the reaction dynamics because a low partial pressure of oxygen increase the solubility of lead into the 2223 phase[69], allowing lower reaction temperatures. The reactions involved in the conversion of the green powder into the 2223 phase are not well understood. Nowadays, several authors are still discussing on the main reaction as mechanism, intercalation of extra layers of CuO_2-Ca or/and nucleation and growth from a liquid phase.

Generally, at temperatures over 770°C the initial 2212 phases start dissolving with other phases, forming a liquid that enhance the conversion to BiPb2223. The composition and amount of this liquid phase is fundamental and small variation during heat treatment changes the solubility of compounds as well as other parameters such as the speed of reaction. During this conversion several intermediate phases are present. The intermediate phases that seems to play an important role at the beginning of liquid formation are the so called 1:1($(CaSr)CuO_2$) and CuO, and the 2:1($(CaSr)_2CuO_3$) and 14:24($(CaSr)_{14}Cu_{24}O_z$) above 820 °C. There are also in the

liquid leaded phases as $(CaSr)PbO_4$ and $(CaSr)_5(PbBi)_3CuO$ or '3321' $(Pb_3(Sr,Bi)_3Ca_2CuO)$. That promotes the conversion.

Although the purity of the precursor powders and a good composition are essential for the conversion to the 2223 phase, inhomogeneous mixture may produce uneven distribution of the other phases along the tapes. At sintering temperatures, these phases melt giving the conditions necessary for the 2223 phase growth, When the distribution is not homogeneous, local areas may have unfavourable liquid composition causing low 2223 formation and as a consequence, a final larger amount of secondary phases.

Upon rolling some alignment of the 2212 grains is achieved. The degree of texture increases close to the silver surface[70]; however, the 2212 grains are not so easy to texture as the 2223 ones[71], then in a standard thermomechanical treatment of BiPb2223 tapes there are a first sintering, an intermediate rolling and a final heat treatment. During the first reaction stage, the BiPb2223 grains start to growth resulting in an overall increase of porosity. After the intermediate rolling the alignment is increased and the intergranular distance shortened while the intergrain connectivity is deteriorated. In the final sintering, the enhancement of grain growth and annealing of cracks improves significantly the critical current density of the tape.

Ramp rate for heating[72], sintering time[73], atmosphere[74], dwell temperature[75] and cooling rate[76] are the parameters to control the liquid phase formation and the BiPb2223 conversion during the solid state reaction and liquid phase sintering periods. Depending on the grain size if the system is heated to quickly and the equilibrium is not reached it may be possible to melt the grains below the peritectic point of the system[77], therefore the amount and composition of the liquid phase would depend on the heating rate. Also, the longer the sintering time would be, the smaller the amount of remained liquid phase for grain enhancement on the second sintering

period. Depending on the atmosphere used, the annealing temperature has to be optimised. The lower the local oxygen partial pressure would be, the lower the melting temperature and therefore the sintering temperature are. Finally, during cooling other phases as the 2201("$(BiPb)_2Sr_2CuO_6$") or 3221, which at the grain boundaries are weak links for superconducting currents, deteriorate the critical current density values of the tape[78,79]. In these cases, an optimal cooling rate or two step process is needed.

In the intermediate rolling or pressing between subsequent heat treatments the alignment of the grains, the densification of the core and, therefore, the mean intragrain distance is improved. When it is too large the relative thickness reduction, the cracks produced in the new sintered grains may be not healed in the afterwards annealing because the liquid phase would be less abundant[80]. Upon rolling, the cracks are distributed perpendicular to the tape, while pressing are parallel and subsequently has better conditions for current transport along the tapes[81], however for long tape production, rolling are much cost efficient. Normally, the thickness reduction in this intermediate rolling/pressing is less than 25%, being the optimum around 13%[82].

In second sintering period the cracks produced during the intermediate rolling are healed and the densification of the core improves connectivity. The best reaction temperatures in air of the 2223 Ag sheathed tapes are in the range of 830 °C to 840 °C. The oxygen partial pressure alters the sintering process, lowering the temperature by 15 degrees when 0.07 atm. oxygen partial pressure are used instead of air and the optimum sintering time is also reduced by a quarter of that in air[83]. The optimal temperature window for the 2212 to 2223 phase conversion, which is less than 5 degrees in air, become approximately 15 degrees in reduced oxygen atmosphere[84].

All these thermomechanical parameters make very complex the optimisation of the 2223 tapes for high critical currents. The J_c of the tape is going to depend on the

reaction kinetics (temperature, healing and cooling rates, reaction time), mechanical parameters (density, homogeneity, wire diameter or final tape thickness) for only an individual powder precursor. Slight changes of the precursor type, of the nominal composition may lead to a shift of all parameters, which are interactive and which have to be optimised again as a result.

2.5 Experimental

2.5.1 Precursor Powder

The precursor powder used in this project is partially calcined (BiPb)2223 which consists mainly of 2212 phase element. The powder is produced by Merck Limited Company with the Endo[85] composition: $Bi_{1.84}Pb_{0.34}Sr_{1.91}Ca_{2.03}Cu_{3.06}O_y$.

The method used by Merck for the powder fabrication is the Evaporation Deposition of Solution (EDS), where a mixture of unreacted metal oxides and nitrates without any of the superconducting phases are thermally treated in 80%Ar-20%O_2 atmosphere. The partial calcined powder undergo the thermal process shown in Table 1:

Degrees/hour	Final Temperature	Dwell time (h)
60	500 °C	15
10	750 °C	30
20	800 °C	15
-60	Room Temp.	End

Table 1: Table of temperatures, ramp rates and dwell time used for partial powder calcination.

In the first step the unreacted oxides are heated at 60°C/hour up to 500°C and dwelt for 15 hours to eliminate moisture. In the second step, the powder is ramping up to 750 at 10°C/hour and maintained for 30 hours. The slower heating rate prevents the appearance of small, sub-micron particles of the unreacted oxides taking place by overpassing the reaction temperatures. Within the liquid phase sintering theory it is widely accepted that the homogeneity and amount of liquid are influenced by the initial particle size, density of the material, heating rate and the final sintering temperature. The slow heating rate was employed primarily to improve the homogeneity such that the partially reacted powder contain a narrower distribution of 2212 grain sizes, thus improving the reactivity of the powder during conversion to the 2223 phase. A CO_2 free air atmosphere is used to avoid possible carbon contamination, which is detrimental for the final transport J_c[86]. Finally, the powder is heated to 800 °C and dwelt for 15 hours to reduce carbon contents and complete the conversion of remaining nitrates to oxides. The resulting powder contains mainly 2212 phase grains as well as $CaPbO_4$ and $CaCuO_3$. This partially calcined powder is usually supplied in sealed containers to reduce the carbon and moisture intake.

2.5.2 Packing A Tube

The as-received powders undergo a preliminary heat treatment in pure oxygen, as shown in Table 2, to further eliminate any water or carbon contamination absorbed during transport and storage. The powder is then packed in Ag tube (99% of purity) with 10 mm outer diameter (OD) and 1.2 mm wall thickness.

Grades/hour	Final	Dwell time(h)
60	800	10
-60	Room Temp.	End

Table 2: Table of thermal process to ensure no contamination of carbon and water content in the air before packing into a tube.

In one experiment, which requires the increase of the sheath electrical resistivity, we have used silver alloy, 0.2%Ni-0.28%Mg-99.99%Ag with 10 mm OD and 1mm wall thickness.

About 0.2 g of precursor powder is introduced in the tube each time and maintained under constant pressure of about 0.5 kg/cm^2 for a minute and the process repeated until the complete tube filling. By doing so, a homogeneous packing density of about 1.5 g/cm^3 (25% of the BiPb2223 density) is achieved along the packed length. The tube is then evacuated and filled with Oxygen before sealing with Indium.

2.5.3 Drawing.

The packed tube is sealed for density control at both ends using Indium, also one of the ends has being swaged along 40 mm as a head for the drawing process. It is used Indium as a sealer due to its softness for handling. Upon drawing the packed tube is transformed into around 1.6 mm diameter wires and increased the density of the powder. When some intermediate annealing is necessary during the mechanical work, the Indium has to be taken away because its low melting point that makes it very contaminant for the powder. A sketch of the packed tube prior drawing process is shown in Fig. 11.

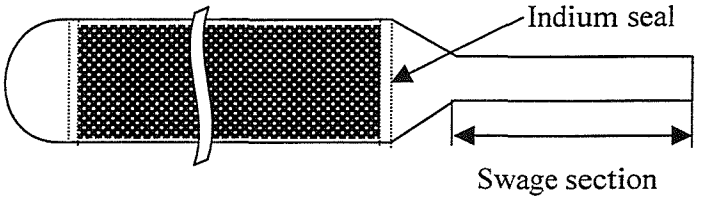

Fig. 11: A billet prepared for being drawn.

Our aim is to produce a homogeneous core density both in longitudinal and radial directions. Longitudinal homogeneity can be obtained by a good control of the density along the wire but radial homogeneity depends on the reduction step. As

silver wire passes through a die (see Fig. 12) the external area hardens more than the internal and therefore density in the ceramic core may vary radially. On the other hand, there is a maximum tension that is possible to apply to the wire for each step, which depends on the ultimate strength of the material. Over this limit, drawing may produce cracks and the appearance of necking in the sheath. Moreover, the drawing process induces the first stages of texture into the material due to the directional compression[87].

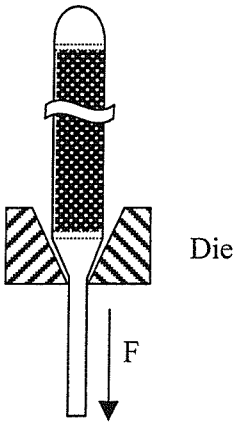

Fig. 12: Sketch of a drawing processing through a die.

The standard reduction ratio initially used for silver wires was (12±5)% with a hard steel die with angle reduction of about 12°. An increase of the reduction ratio has been studied and presented in next chapter in detail.

2.5.4 Rolling.

Once the wire reach the diameter required (< 2 mm), it is deformed into a tape by rolling. In our experiments 100 mm diameter rollers and controlled linear speed of 2.4 mm/s are used. A more homogeneous density across the tape has been reached by adding tensions of (0.5 kg/cm^2) in the back and forehead sides of the tapes during rolling.

The lubrication with oil has been removed spraying acetone over the rollers to reach a higher shear deformation and two guides control the perpendicular entrance of the tape respect to the rollers (see Fig. 13). Typical rolling step reductions used in most of the experiments are firstly 20 μm/step reduction for tape thickness bigger than 1300 μm (shape formation phase), 40 μm/step until tape thickness is between 400μm and 500μm and a final and single step reduction of more than 100 μm.

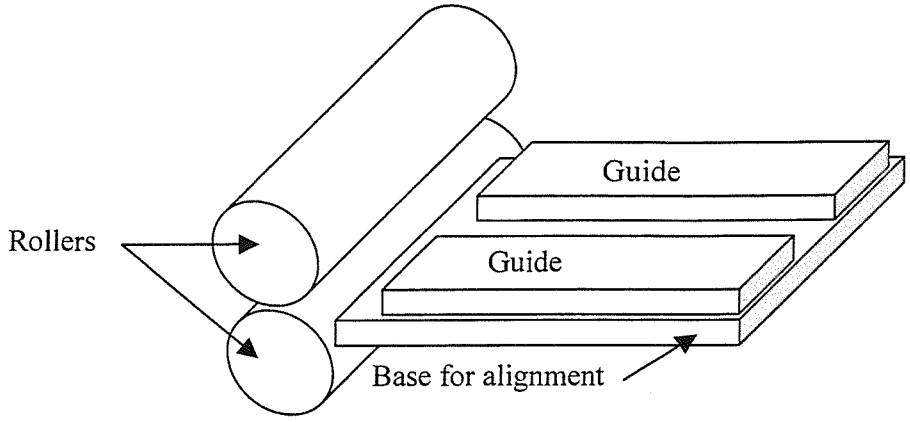

Fig. 13: Sketch of the rolling machine used. The tape is aligned vertically by the base and horizontally by the two guides.

In the first steps, the tape area which undergoes deformation is small and the pressure applied large, therefore mainly involves the external and central filaments, meanwhile the other will remain almost unchanged, with further deformation steps the inhomogeneity will increase, as we will be seen in further chapter. The reduction ratio in these shaping are to be reduced to the minimum being also desirable some annealing at this stage to reduce the hardness of the sheath. As an example, in Fig. 14 we show the results on a tape fabricated with high ratios per pass and therefore the inhomogeneity will be higher, clearly showing the different zones.

Fig. 14: A tape with 37 filaments of Au-Ag alloy (10%), rolled in the first steps at 100 μm ratio per pass.

Once the tape shape is obtained, our aim is to achieve in each step the maximum number of the filaments under the same deformation condition. As explained by Lee et al[88], upon tape rolling there are three zones of deformation, one with compression stresses, another with shear or deformation stresses and finally a dead zone without stresses (See Fig. 15).

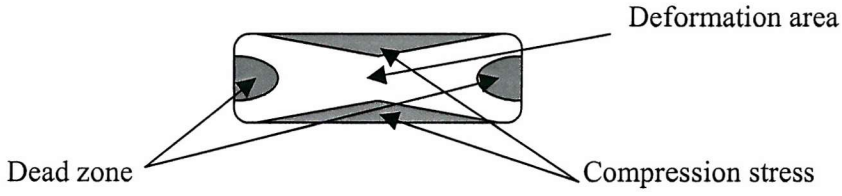

Fig. 15: Schematic cross section of a tape showing th e areas of deformation during a rol ling process.

In the area of compression stress, at the top and bottom of the tape, the deformation is small but the compression high. Therefore, porosity and dense areas are mixed on the filaments located in this zone. Also due to the higher softness and plasticity of the sheath the filaments can be taken from the sheath out, producing leak of superconducting material. In the Dead zone, placed at the free ends of the tape, no deformation neither densification is produced, keeping unaltered after processing. In the deformation area, compression and shear stresses densify the filaments in a coordinate process. The bigger this area could be the more homogeneous and textured

will be the filaments. The shear stress reconfigures the shape of the filament elongating them along the tape width and increasing the compression zone. Therefore, due to the Bi-2212 high degree of texture, the density of the filaments increases.

The size of each deformation area is controlled by several variables; friction between the tape and the rolls, roll diameter, deformation resistance, the reduction thickness per pass and the presence of front and back tensions. Several studies have been made in the analysis of these parameters. Lee et al. studied the friction, reduction per pass and surface conditions of the rolls, showing that in multifilamentary tapes, critical current is increased with higher deformation ratio per pass because they limit the dead zone. Zeng et al[89] have reported that a gradual increasing of the reduction per pass improves the critical current of multifilamentary tapes. Utsunomiya et al[90] found that back and front tension suppress sausaging and improves grain alignment. Some other techniques have been used in order to homogenize the filament density and distribution as two axial rolling[91] and periodic pressing.[92]

2.5.5 Thermal Processing.

The sintering process is needed for the conversion of the precursors into $Bi_2Sr_2Ca_2Cu_3O_{10}$ phase and to reach intergranular connectivity of the superconducting material. Initially, the green powder is a mixture of Bi-2212 and secondary phases as Ca_2PbO_4 and CuO. During the packing, drawing and rolling processes, densification and grain orientation has been improved. The derived multifilamentary tapes should undergo a thermally optimised treatment for derive the maximum current.

Oxygen partial pressure combined with sintering temperature varies the formation rate of the superconducting grains[93]. Low partial pressure decreases the sintering temperature and increases the temperature range at which conversion is produced[94] due to the increase of solubility of lead into the 2212 and 2223 phases[95]. In our case,

the optimum sintering temperature for a 8% oxygen partial pressure is 817,0 ± 7,5 °C and for 21% is 840,0 ± 2,5 °C although the ranges changes with powder stoichiometry and oxygen diffusion for different sheaths. This is the range used in general for pure silver, Ni-Mg silver alloys and Au-Ag alloy sheaths.

The ramp rate for achieving the sintering temperature and cooling down is also found determinant in the reaction dynamics[96,97,98]. In our experiments, the heating rate mostly used was 60 °C/h and in some cases 100 °C/h and 20-40°C/h ramp rates. According to Young et al[99] higher ramp rates, allows the production of more liquid phase for sintering and at the same time avoids the production of secondary phases non desirables. On the other hand, a relatively low ramp rates gives more homogeneous liquid formation and avoid overheatings. In tapes with insulation barriers, bubbling can appear for high ramp rates because do not allow the gases to be eliminated. A set of samples made with an insulator layer of Sr-zirconate layer surrounding the filaments has been produce in order to investigate reduction of AC losses. As shown in Fig. 16, only by decreasing the ramp rate, it was possible to eliminate some bubbling that had appeared on first sintering.

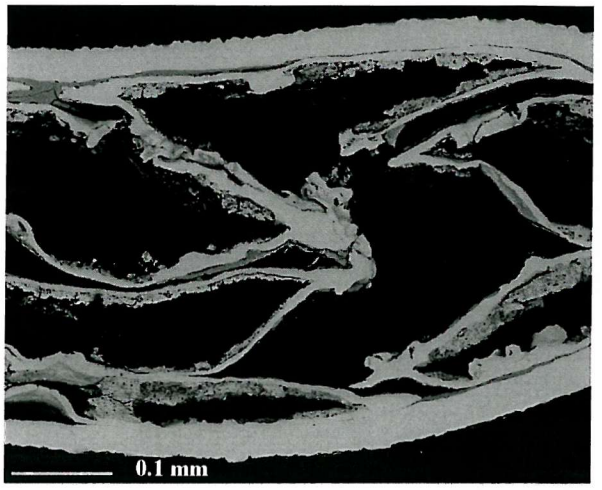

Fig. 16: Silver sheathed composite tape with 19 filaments insulated with a Sr-Zirconate layer. The bubbling appears when no escape of the oxy gen is found in relatively short periods of time.

At ramp rates of 2 °C per hour and increasing sintering temperature at 844°C in air, the tapes do not show bubbling and the current reach a final critical current of 6.45A for a 19 multifilamentary tape. The sintering temperature increase might be due to the higher local oxygen partial pressure. As the oxygen cannot be released easily from the tape, a higher temperature might be needed for liquid formation. A window temperature of 844.5 ±1.5° C was found as optimum sintering temperature. A sample of this tape with no bubbling is shown in Fig. 17:

Fig. 17: 19 multifilamentary tape with Sr-Zirconate insulation layer and no bubbling performed during sintering periods.

Further improvements in optimisation of the sintering reaction should be desirable for the use of this kind of configuration.

As shown in Table 3, the cooling process has been done in two different ramp rates.

Fast cooling

Step	Rate °C/h	Temp. Reached	Dwell time
1	60°	600° C	0
2	20°	822° C	X
3	1°	800° C	0
4	60°	0° C	0

Slow cooling

Step	Rate °C/h	Temp. Reached	Dwell time
1	60°	600° C	0
2	20°	822° C	X
3	1°	740° C	0
4	60°	0° C	0

X= Sintering time

Table 3: Thermal processing of silver tapes using different cooling rates.

These two procedures must get the same conversion but slow cooling allows bigger grain size of new Bi-2223 particles. This grain size allows measuring a bigger amount of particles in x-rays in order to get more realistic conversion[100].

Temperature control.

Due to the small window for optimum sintering temperature, it has been necessary to assure the temperature control in the furnaces and their dynamic behaviour as well as the accuracy of the temperatures read by the thermocouples.

The furnaces control the temperature with type N or S thermocouples placed in the external central part of the heater tube (see Fig. 18). The controller fixes the temperature and the heating rates during dynamic and stable heating in relation to the point of measurement (thermocouple). However the sample is in different place and therefore, in a different temperature that should be known. This adjustment is done both, in the profile along the tube and for different temperatures of the central

point. The profile has been done with an accuracy of ±1°C at 800°C and the useful length will be called 'hot zone'.

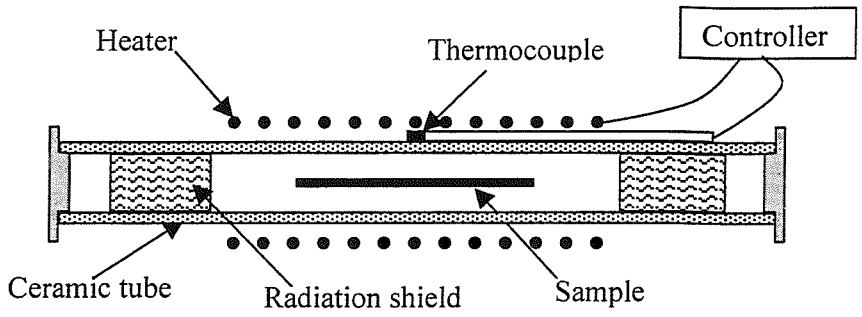

Fig. 18: Sketch of a standard furnace.

The furnaces have been prepared and calibrated for homogeneous and gradient temperatures along the tube (the later are used for a quicker characterisation of the sintering temperature). It has been taken into account the conductivity of the thermocouple and the reaction for changes in temperature and temperatures rates. As it can be seen in Fig. 19 different dynamic steps have been tested to check the reaction time of the furnace. The test demonstrates a high-speed reaction in time with small overheating, which is critically important in the production of tapes.

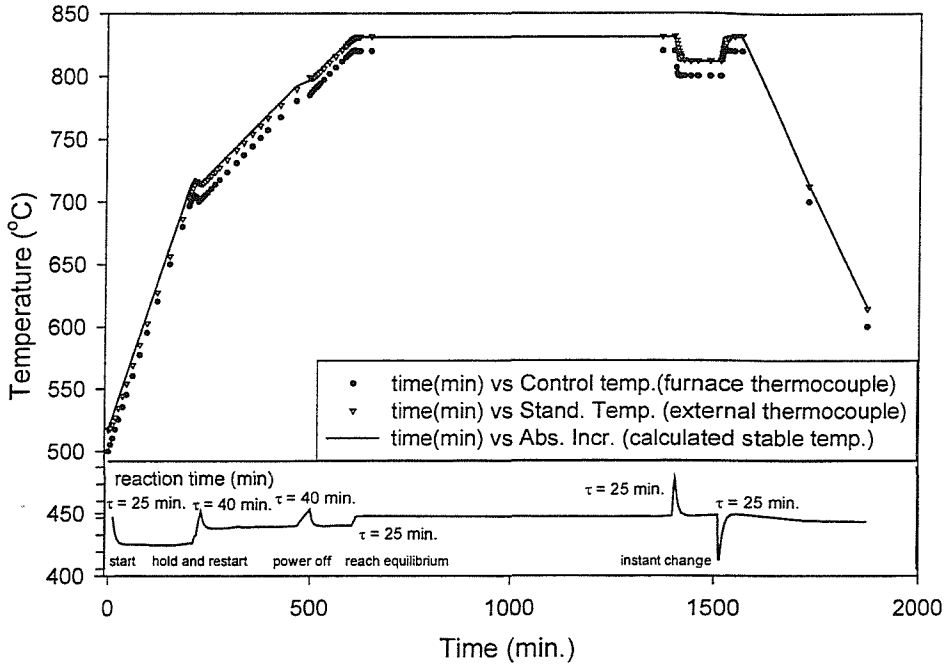

Fig. 19: Temperatures and reaction times measured in different sensors for control of the dynamic behaviour of temperatures inside a furnace.

Incubation curves.

Incubation curves are one parameter that gives us an idea of the amount of BiPb-2223 created from Bi-2212. The dynamic of each powder is different; density, grain size and homogeneity make likely unpredictable the conversion and this is why is necessary an experimental derivation.

The conversion degree is obtained by X-rays diffraction measurements over the tapes sintered for first time, which will be explained in section 2.5.6 . With that information the tapes are processed with one or two intermediate rolling steps in order to improve grain alignment. The tape thickness before intermediate rollings is 300÷400 μm. It has been seen that a good time length for the first sintering is when the conversion reaches 30% of BiPb-2223[101]. An intermediate rolling down to 25%

of the thickness is used, some studies have found the optimum rolling reduction being between 10% and 20% of the initial thickness[102] depending on the sintering temperature and a closer approach give an optimum at 13%[103]. During the intermediate rolling high angle grains links are broken and the phases are remixed. Then, a new intermediate sintering rolling process lead to a 60% conversion. If some other intermediate rollings are needed the percentage reduction must be lower since it remains a less amount of liquid. In the final sintering, the tape is optimized at different temperature and time to obtain the higher critical current.

J_c Optimization.

Once the conversion from Bi-2212 to BiPb-2223 is completed, from further annealing the material start to degrade due to the appearing of 2201[104] and other secondary phases that hinder intergranular connectivity and diminishes the overall J_c, There is an optimum point where almost all the filaments are fully converted and the secondary phases start to appear, for which we achieve the maximum current. To find out this point the current is measured for different second sintering times. Every tape, with different processing or starting powder and sheath, has a characteristic curve and this process has to be made for every single tape production.

Other secondary process can be implemented in the production as preannealing before rolling, a secondary dwell or annealing at low temperatures after final sintering but a fully analysis has not been made. These procedures that has been studied otherwise also improves the critical current.

2.5.6 XRD.

X-ray diffraction (XRD) is a versatile, non-destructive technique used for identifying the crystalline phases present in solid materials and powders and for analysing structural properties of the phases such as grain size, phase composition, crystal orientation, etc. The incident X-rays are diffracted (according to Bragg's law) by material crystallites and varying the angle of incidence, a diffraction pattern emerges that is characteristic of the sample. The pattern is identified by comparing it with an internationally recognized database containing tens of thousands of reference patterns.

In our case, Bi2212 or (BiPb)2212 and other secondary phases react to convert in (BiPb)2223. The X-ray pattern can give us the grain texture, the conversion rate between superconducting phases and the different intermediate phases involved during reaction. The x-rays pattern in a tape with textured grains is different from the one of randomly oriented grains showing higher (00X) peaks the former.

For the conversion from Bi2212 to (BiPb)2223 phases, two peaks, the (008) peak from the Bi2212 phase and (0010) from the (BiPb)2223 are used as the reference, since these angles are not superposed with others and they present the closer approximation to their actual values. An example of pattern can be seen in Fig. 20:

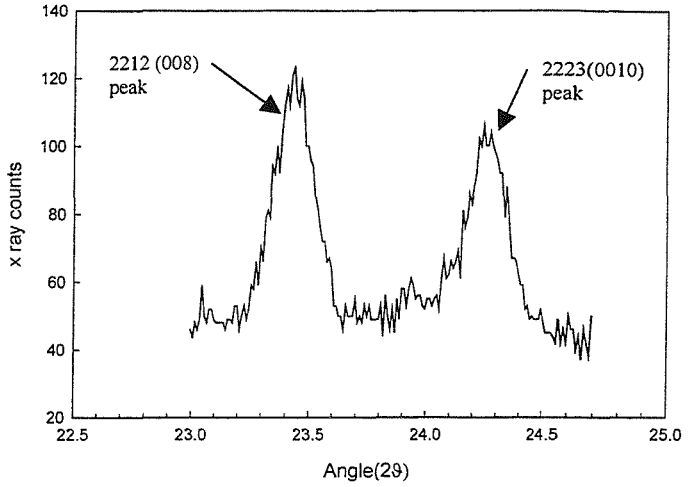

Fig. 20: X-ray diffraction pattern peaks of a (BiPb)2223 tape.

The conversion rate is measured by the relation:

$$conversion\ (\%) = \frac{2223\,area}{2223\,area + 2212\,area} \cdot 100 \qquad \textbf{Eq. 19}$$

The data are treated with a noise filter (integral of the area) and the areas are normalized.

The X-ray diffractometer

We are using a Phillips X-rays diffractometer with CuKα radiation and α-Cu Filter. The power of the X-ray is set to 30 kV and 20 mA. The parameters used for the counting average time have been studied and the results show to be much less noisy with expositions longer than 5 seconds by step. The step size can be as small as $0.01^{\circ}(2\theta)$ but for practical purposes it is normally used 0.02° and the beam area is a (3x5) mm ellipse as mayor axes.

Preparing samples for X-ray exposition.

For the X-ray exposition we use tape samples of 7-8 mm length that are pressed during 10 seconds at 4-5 bar. The pressed sample has parallel surfaces suitable for the polishing preparation and reference alignment. Once the sample is pressed, it is soldered with tin to a silver base (holder) that was previously flattened, and polished. During soldering, we must keep the sample parallel to the holder by placing a weight over during the cooling of the tin.

Further, the holder is stuck over the polishing utility by heating wax in its surface and gently set the sample holder over it. After the wax is hardened, the polishing tool is placed over wet sand paper. The water is used for a lower abrasion and the grit of the sand paper for polishing might be P1200 or lower grain size. The polishing must be as homogeneous as possible and the sample must be polished in all directions.

2.5.7 V-I measurements.

Current-voltage measurements (V-I) give us the correspondent critical current of a tape. The sample is fixed with varnish to a flat base and the end soldered to the current leads as it can be seen in Fig. 21. In order to get a homogeneous current along the area of voltage measurement a distance of 1 cm is kept below the current feeding and voltage contact. Also the distance between voltage taps is selected as 1 cm and the V-I criteria used to derive the critical current was the appearance of electric fields above 1 μV/cm. In the first measurements the voltage contacts were soldered to the tape (Fig. 21) but we have used other new device that can obtain good contacts only by pressure. In this case copper needles are in contact with the tape and a spring keeps enough pressure for electric good contact (See Fig. 22).

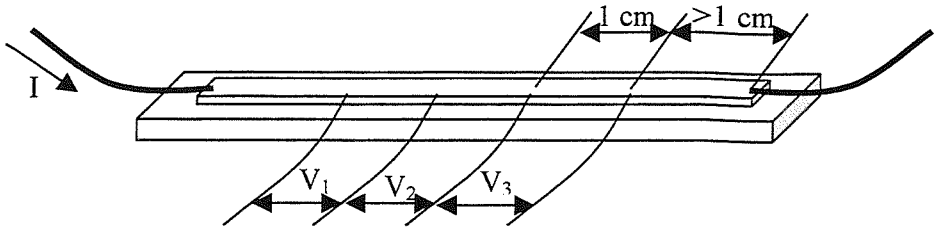

Fig. 21: Measuring tapes with soldered wires connected to the tape.

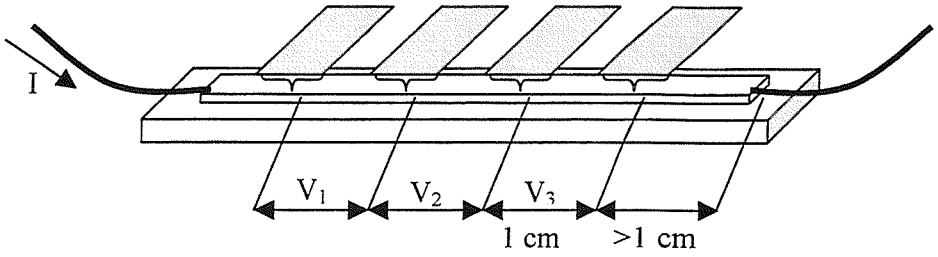

Fig. 22: Measuring tapes with springs pressing in the middle of the tape.

The same device was also used for measurements under both parallel and perpendicular magnetic fields in the range of 0-0.48 T. A typical V-I curve is shown in Fig. 23:

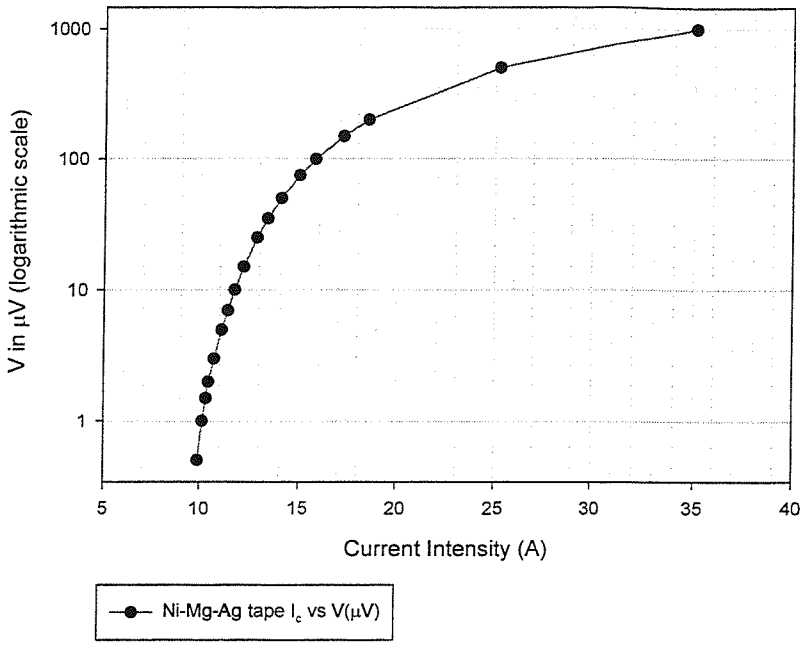

Fig. 23: V-I curve from Ni-Mg-Ag tape sample.

Chapter 3: STUDY OF MECHANICAL DEFORMATION OF 2223 TAPES.

3.1 Introduction.

The production of superconducting tapes for the experiments presented in this thesis requires the study of multiple techniques. Some of the techniques has been adapted or developed to the specific requirements necessary in each experiment. Specially, it has been developed a procedure for the production of more homogeneous multifilamentary wires with a sheath of Ni-Mg-Ag alloy, other technique for rolling where the tape is spread more widely in order to achieve a higher aspect ratio and finally, an adapted measurement of X-ray data for each filament independently.

3.2 Production of Ni-Mg-Ag alloy tapes

3.2.1 Introduction

Silver is a good sheath material for BiPb2223 tapes, however, the critical current density obtained with this configuration is far away from the experimental value obtained in grains or thin films[105, 106] (10^5-10^6 A/cm^2). Furthermore, Ac losses produced by eddy currents across the sheath could be reduced by higher sheath resistivity. Therefore, it is interesting to investigate some other materials that could improve critical current by a higher texture and densification of the core as well as increasing the electrical resistivity of the sheath. Ni-Mg silver alloys are good candidates for achieving our aim; however, the mechanical processing demands a different path than for the tapes with pure silver.

3.2.2 Change of deformation drawing steps by the parameter G_D

In this section, it is proposed a new set of dies that will enhance a better drawing. In the case of a Ni-Mg-Ag sheathed wire, the set of dies used for drawing are shown in Table 1 (as Optimal Diameter). The data of the column named as "initial diameter" correspond to the dies used previously for silver wires with good results. It is used a rough decrement of about a 10% until a medium diameter that is 5.1 mm, further drawings are realised at an approximately 14% decrement or over. The diameter (in mm.) of the dies used is shown in the first column and the decrement in area in percentage is the following column.

Initial Diameter		**Optimal Diameter**		**Initial Diameter**		**Optimal Diameter**	
9.6	**Area %**	9.6	**Area %**	3.25	12 %	3.25	12 %
9.1	10 %	9.1	10 %	3.03	13 %	3.03	15 %
8.66	9 %	8.66	9 %	2.83	13 %	2.83	13 %
8.2	10 %	8.2	10 %	2.63	14 %	2.63	14 %
7.8	10 %	7.8	10 %	2.44	14 %	2.44	14 %
7.4	10 %	7.4	10 %	2.27	13 %	2.27	13 %
7.0	10 %	7.0	10 %	2.07	17 %	X	
6.65	10 %	6.65	10 %	1.97	9 %	1.97	25 %
6.3	10 %	6.3	10 %	1.8	17 %	X	
6.0	9 %	6.0	9 %	1.7	11 %	1.7	17 %
5.7	10 %	5.7	10 %	1.6	11 %	1.6	21 %
5.4	10 %	5.4	10 %	1.48	14 %	1.48	14 %
5.1	11 %	5.1	10 %	1.38	13 %	1.38	13 %
4.85	10 %	X		1.28	14 %	1.28	14 %

4.62	9 %	4.62	18 %	1.19	14 %	1.19	14 %
4.42	8 %	X		1.11	13 %	1.11	13 %
4.26	7 %	4.26	15 %	1.03	14 %	1.03	14 %
4.0	12 %	4.0	12 %	0.96	13 %	0.96	13 %
3.72	13 %	3.72	14 %	0.9	12 %	0.9	12 %
3.6	6 %	X		0.83	15 %	0.83	15 %
3.46	8 %	3.46	14 %				

Table 4: Diameters of dies used in the drawing of Ag sheathed wires (initial diameters) and suggestions for Ni-Mg-Ag ones. The area variation is also included.

In Fig. 24a, the parameter G_d has been calculated for the sequence of dies shown above. As it can be seen, G_d increases to higher values at some stages of drawing process. By eliminating the use of some of the dies a lower G_d values has been obtained (as seen in Fig. 24b) leading to a better density distribution. For Ni-Mg-Ag alloy sheath, we have used the sequence of dies optimised by the parameter G_D as is shown in Fig. 24b with the addition of some lubrication. The die diameters represented in mm that have been suppressed are 4.85, 4.42, 3.6, 2.07 and 1.8 because are the higher peaks of the original G_d values. From Fig. 24b, it can be seen that the parameter G_d is reduced in these steps, which may result in a more homogeneous deformation. Also the use of a fewer number of dies will reflect on the production time and consequently the cost.

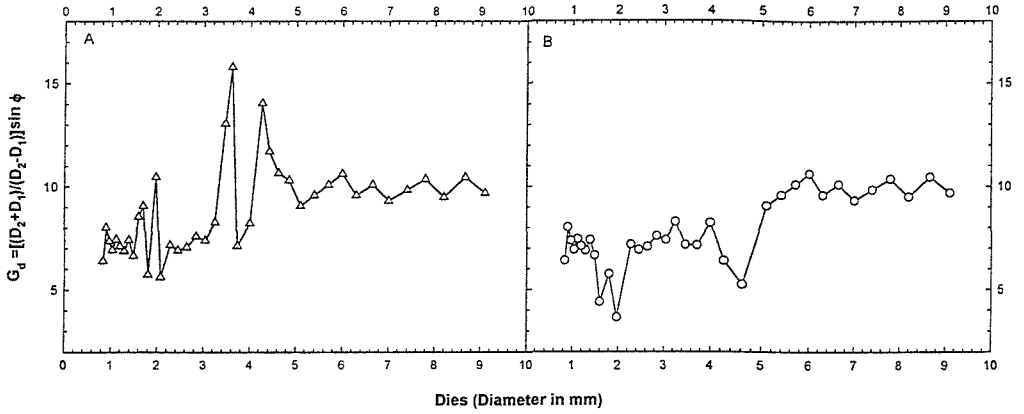

Fig. 24: Change of G_d values before (A) and after (B) the suppression of dies 4.85, 4.42, 3.6, 2.07 and 1.8 in the drawing processing.

The results obtained by the new dies were successful since the sheath was stable until the end of the drawing and no mechanical inhomogeneities were found neither along nor across the wire.

3.2.3 Annealing of the alloy sheath.

As a result of cold working, the hardness, tensile strength, and electrical resistance increase, while ductility decreases. There is also a large increase in the number of dislocations, and certain planes in the crystal structure are severely distorted. Most of the energy used to cold work the metal is dissipated in heat, and a finite amount of energy is stored in the crystal structure as internal energy associated with the lattice defects created by the deformation.

During annealing the high density of lattice defects produced during cold work is reduced by crystallization to another distribution strain free. This process is carried out entirely in the solid state.

Each sheath material, depending on its composition requires different time and temperature of annealing. In our case, we have silver gold (10% wt.) alloy, a Ni

(0.2% wt.)-Mg (0.28% wt.)-Ag (99.5% wt.) alloy and pure silver that needs half an hour annealing in order to recover its original softness. On the other hand, the annealing temperature should be low enough to avoid chemical reactions of ceramic cores. From these three materials the hardest is the Ni-Mg alloy. A comparison of Vickers hardness after annealing for Ni-Mg-Ag sheathed outer at different temperatures is shown in Table 5 indicating that 400 °C will be sufficient for our purpose.

HV_{before} (kgf/mm^2)	T(°C)	HV_{after} (kgf/mm^2)
108	400	52.8
104	500	50.1
107	600	49.5

Table 5: Vickers hardness for a Ni0.2%wt.-Mg0.28%wt.-Ag99.5%wt. Alloy sheathed wire after and before annealing at different temperatures.

The annealing process is carried out initially in Argon atmosphere due to the high reactivity of the alloy components with air or oxygen. In particular, annealing the Ni-Mg-Ag alloy in atmosphere with oxygen produce Mg and Ni oxide precipitate causing an irreversible hardening of the alloy[107]. Therefore, oxidation of particles must be avoided during annealing.

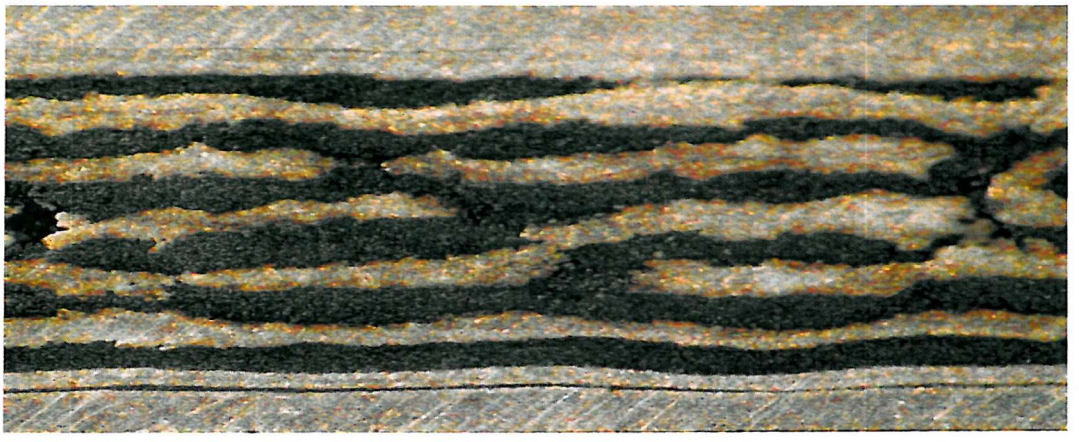

Fig. 25: Longitudinal section of a burst wire of ϕ=3,46mm.

Fig. 25 and Fig. 26 show the longitudinal and transversal cross sections of a multifilamentary round wire 3.46 mm diameter annealed at 410 °C in Argon for 30 minutes. Even when the mechanical cold working was at the initial stages, the Ni-Mg-alloy sheath of some filaments burst because the inhomogeneous hardening. From the picture, it is possible to see some fracture of the sheaths and also some bursting of the filaments as a consequence of both these fractures and the sausaging of the filaments.

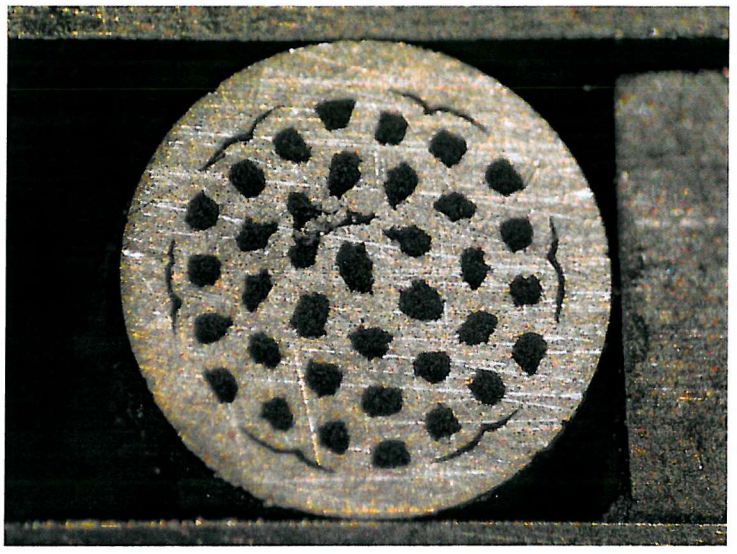

Fig. 26: Cross section of a burst wire of ϕ=3,46mm.

Two reasons may explain the filaments break: hardening by oxidation of the sheaths during the process, which would lead to fracture and secondly, the inhomogeneous hardening of the drawing process where the outside parts are more heavily deformed. The solutions to this problem are the change in the atmosphere to avoid oxidation and the optimisation of the drawing process by improving the die sequence, explained in previous section, which also will improve the homogeneity of the density through the cross section.

To minimize the oxidation, the Argon atmosphere, during the annealing to soften the sheath, was substituted for a continuous vacuum. This, with the changes in the die sequence has allowed the fabrication of Ni-Mg silver alloy wires and tapes.

3.3 A rolling experiment.

3.3.1 Introduction

In order to improve the texture of BiPb2223 tapes a new rolling configuration has been tested. The experiment is based on previous results where a higher deformation and better aspect ratio of the filament take place in the central tape areas. This suggests the use of a thicker outer sheath to avoid the presence of filaments at compression areas where no deformation exists.. However, the use of these thicker sheaths increases the cost and the AC losses while decrease the engineering critical current of the tape. This theoretically may be foreseen using another sheaths only during rolling but has not been yet studied. These configurations could place the compression area in the outer sheath and the filaments in the deformation zone improving their homogeneity and the aspect ratio.

3.3.2 Experiment

To enlarge the aspect ratio, several tapes have been deformed by cold rolling between metallic tapes of a soft material (in this case copper) and compared to the standard rolling procedure.

Initially, the wires have followed a standard procedure by packing Merck powder at 25% density. Lately, 37 of these filaments were packed inside a pure

silver tube and drawn down to 1.6 mm diameter and rolled by 20 μm reduction steps until a 1300 μm thick tape, and 40μm reduction steps afterwards, the final and common tape size for the experiment is 500x2600 μm.

The thickness of the copper tapes is 520-550x2750μm. The material used for sandwiching the superconducting tape is copper because is a cheap material with mechanical properties similar to the silver, and available in different sizes and aspect ratios.

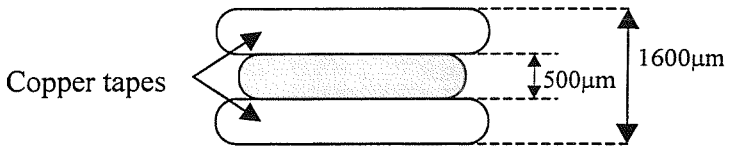

Fig. 27: Superconducting tape sandwiched between copper tapes.

The sandwiched configuration is not mechanically stable during rolling; and the tapes are kept in place by strong glue (Cyanoacrylate), and soldering with tin the tape ends for keeping the configuration after the rolling step. Different thickness and width ratios between the copper sheets and the tape has been tested being more stable the ratio 1:1 for both parameters In this way, the total thickness of the sandwich is roughly three times of a single tape (see Fig. 27). A slightly longer width (or 1.05:1) for the copper is necessary to drive the rolling because if the copper plates do not cover the tape the rolling becomes unstable and the edges shear the tape instead of spreading. The single roll step changes the total thickness of the sandwiched tape from 1600μm to 500μm. As a result, Ag-BiPb2223 tapes with thickness 210 and 240μm are obtained with wavy shape surfaces, therefore a further rolling step down to 170μm is made.

In the other hand, the standard tape is rolled from 500μm to190μm in a single step with a further one to match the 170μm thickness. Finally, the tapes where processed with a sintering at 817 °C for 10 hours in 8% oxygen partial pressure, followed by an intermediate rolling down to 90% of initial thickness in a single step and a second sintering at 820 °C during 40 hours and 800 °C during 30 hours.

3.3.3 Discussion and results

As it can be seen in Fig. 28, the tape rolled sandwiched between copper plates is 25% wider than the one rolled by standard steps (Fig. 29):

Fig. 28: Tape rolled between copper tapes of the same overall size with a further standard rolling of the tape to 170 μm (width= 4.64 mm).

Fig. 29: Standard tape rolled in a single step from 500 μm to 190 μm with a further rolling at 170 μm. (width=3.70 mm).

We can appreciate (See Fig. 31 and Fig. 32) that the tapes fabricated by standard rolling procedures are flatter than the ones rolled between tapes. As the copper is as soft as the silver (both are annealed before processing), the core deformed by the former adapt the material to zones with harder filament by plastic flowing to its edges and will displace more silver and copper to the edges than areas with lower density. As a consequence, an indentation of the copper over the tape is produced (See Fig. 30). Furthermore, the areas with low density of filaments will spread more than the denser ones.

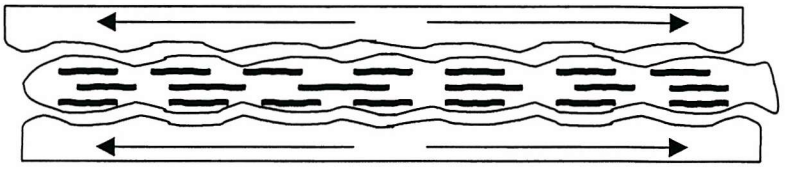

Fig. 30: Mass displacement along the tape cross section.

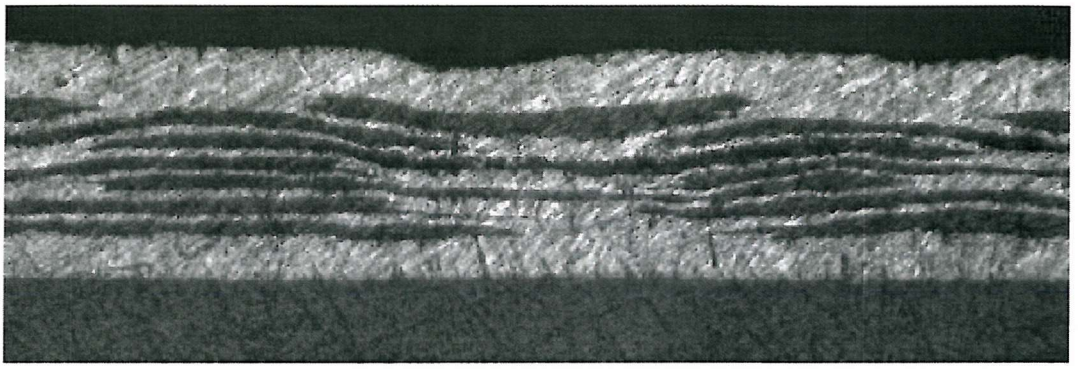

Fig. 31: Observation in detail of the tape rolled between copper tapes.

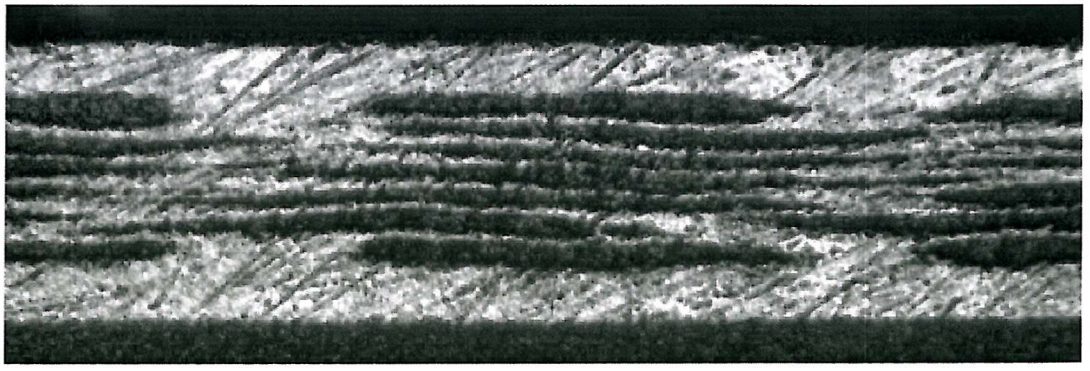

Fig. 32: Observation in detail of the filaments in a standard tape.

A comparison between both procedures can be seen in Fig. 33 and Fig. 34. For all the positions except for filaments placed at the edges and the top and bottom of the tape, the mean filament width of the samples rolled between copper tapes is larger than the one reached by the standard procedure and the standard deviation increase. This increase is mainly due to the lack of spreading of filaments placed at

positions without shear stress. Even more, some filaments have a width lower than the standard tape one.

One of the tape edges is thinner because the shear of the copper tapes shifts the axes of deformation to the indented side (see Fig. 28 at the right edge).

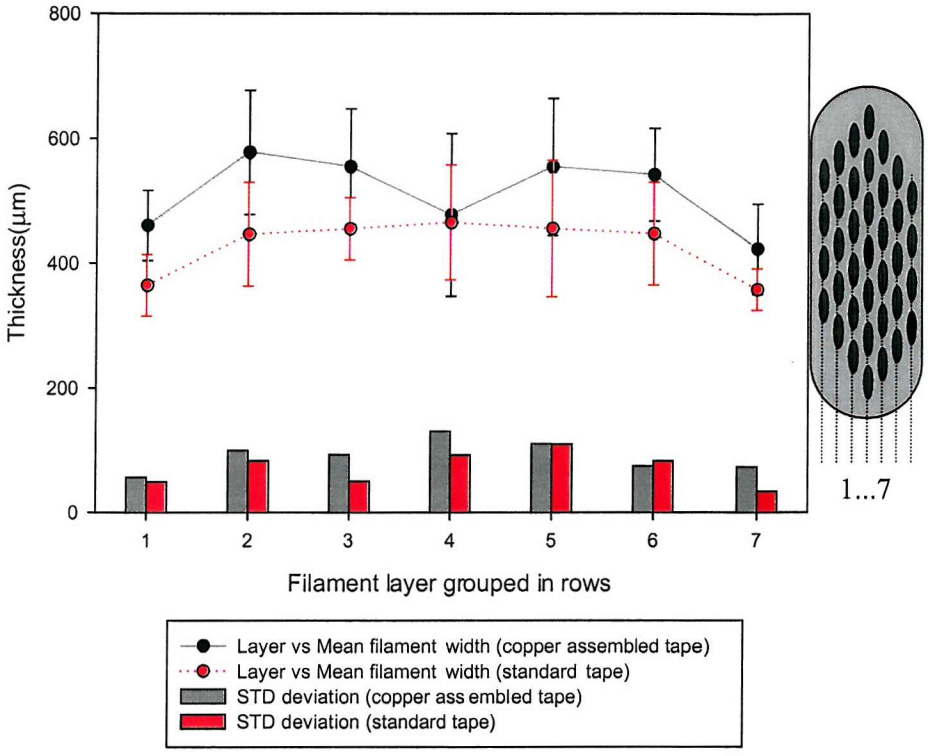

Fig. 33: Mean values and standard deviation of the filame nts width placed in the showed rows. The data for copper assembl ed tape is described by the black symbol and solid lines while the standard ones by the red symbol and dotted lines. Their standard deviations are shown in columns filled black and grey respectively.

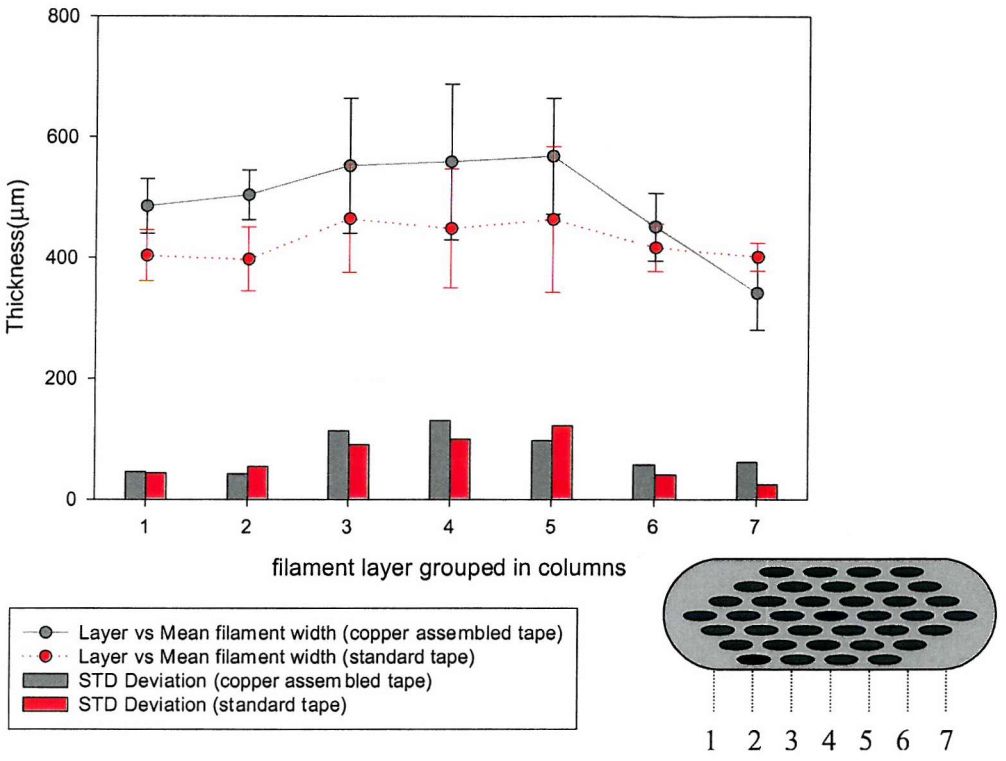

Fig. 34: Mean values and standard deviations of the filaments wi dth taken in columns. The sandwiched tape is described by green symbols and solid line while the standard tape by the red and dotted line one. Their standard deviations are shown in columns filled black and grey respectively.

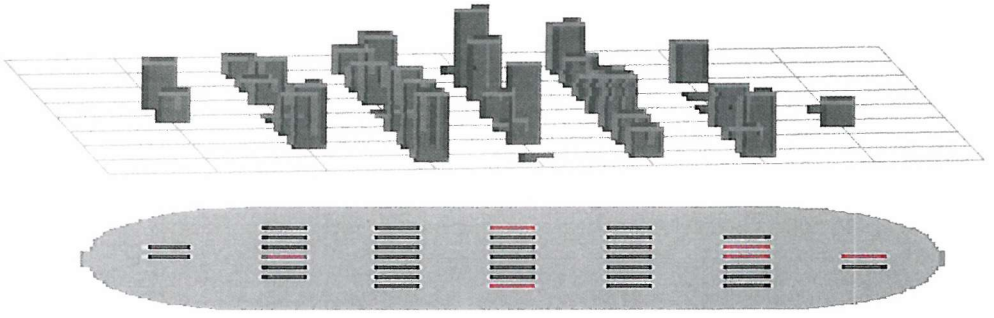

Fig. 35: Mapping of the width difference between th e sandwiched tape and the standard tape. Grey areas means p ositive difference in width, read areas means negative difference. It is observed that the increment of width in the sandwiched tape is general (grey areas) respect to the standard tape (red areas).

The current reached in the sandwiched tape is lower than the standard tape (see Table 6). In order to diminish the inhomogeneous deformation it should be desirable to find a matrix yielding to a more homogeneous distribution with longer

number of filaments as well as a more stable and controlled rolling. Also, different selection of materials for gluing or tapes harder than copper for sandwiching would help. Also, I suggest testing the same experiment in different composite configuration in such a way that the presence of the superconducting material was more distributed along the perpendicular direction of the rolling plane.

Critical current density (A/cm^2)	First Sintering	Second Sintering
SANDWICHED TAPE	913	1941
STANDARD TAPE	1558	3542

Table 6: Critical current density for the evaluated tapes after the first and second sintering.

Finally, it has been tested the action of a wire introduced in a copper wire for rolling (see Fig. 36). In this picture it is possible to see that the spreading is stopped by the copper tube, this reason and the difficulty of getting rid of the copper sheath does the experiment not interesting.

Fig. 36: Wire rolled inside a copper tube.

3.4 Improvements to get the best X-ray measurements.

The XRD measurements, which are essential to understand the conversion mechanisms in BiPb-2223 tapes, requires a high precision. Various improvements of our data acquisition were made. As the samples are textured within a tape, the measurements depend on angular sample position. The original X-ray base holder was not enough parallel to the surface exposition so we have made a flat sample holder with an error lower than 5 microns in a base area of 3x3 cm.

Secondly, the samples measured are small filaments with very low count sensitivity and noise must be avoided as much as possible. Different sample holders of glass, copper, alumina and silver were searched with minimum noise for alumina (See Fig. 37) and silver. Since silver is also the tape sheath material it was finally used as a base.

Also it was tested the way to stick the sample on the sample holder. It was used resin and tin where it was found that tin had a lower noise. For a better XRD reference angle, it is necessary to guarantee the flatness of the sample respect to the holder by some weight added during the drying or cooling of the resist or tin respectively.

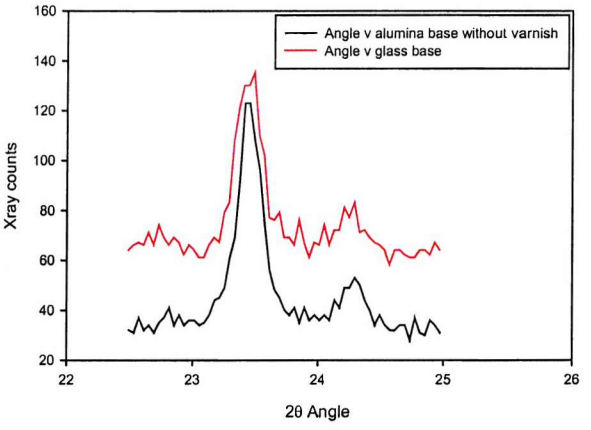

Fig. 37: X-ray diffraction diagram of a multifilamentary tape section on different sample holder of alumina and glass.

The number of counts for each angle was also tested, three different counting times, 2, 5 and 10 seconds (see Fig. 38). The noise for 2 seconds counting periods is much higher than the rest. As 5 seconds counting period give results with similar precision than for 10 seconds hereafter 5 seconds counting will be used.

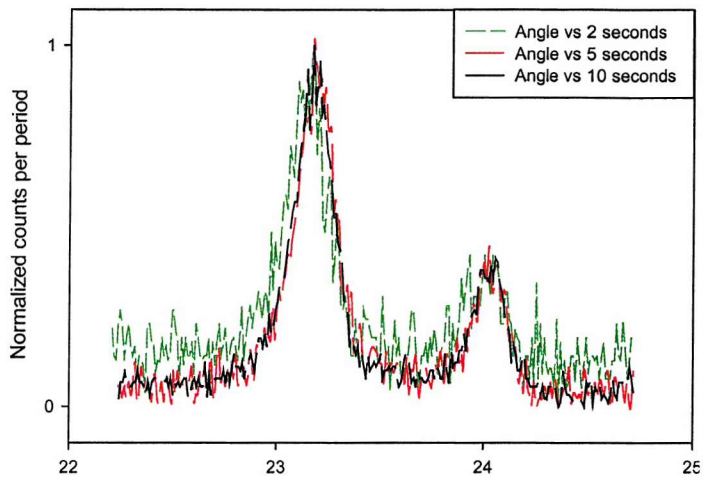

Fig. 38: Normalised number of XRD counts measured in the same sample for different counting periods of 2, 5 and 10 seconds.

The shape of the X-ray beam was also studied. The beam zone, which was about 3 x 5 mm2, gives problems in the single filament measurements because they are about 0.5 mm width and 0.7 mm distance. Thus, the measurements would give of the average phase conversion rate of several filaments. In order to improve our measurements, it was made a window slit (see Fig. 39) 0.8 mm of width. It was placed over the sample holder and moved horizontally for every filament measurement.

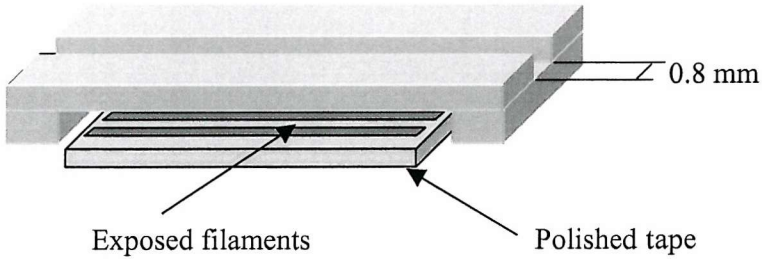

Fig. 39: Sketch of the window slit and the silver base used for the selection of the x-rayed filam ent.

The conversion between Bi-2212 and BiPb-2223 phase was measured by XRD on different layers and position of filaments. The results obtained with this technique are shown in next chapter.

Chapter 4: ANALYSIS OF Bi-2212/(BiPb)2223 CONVERSION BETWEEN FILAMENTS IN MULTIFILAMENTARY NiMgAg ALLOY SHEATHED TAPES.

4.1 Introduction.

Application of HTS requires materials with high critical currents. In tapes, this is achieved, among other variables, by texturing induced by cold working and successive step of sintering. The cold working procedure will determine the degree of texturing obtained[108] and the local variation of core density, both having significant influence on the critical current[109,110].

An important parameter that affects directly the critical current of a tape is the homogeneity[111]. Some studies addressing longitudinal and transverse inhomogeneities in the conversion and densification have been made previously[112,113]. The Longitudinal inhomogeneities such as sausaging and microcracks have been also the focus of several studies[114,115]. Transverse inhomogeneities, however, mostly concern to non-uniform phase conversion by the limited contact with the Ag sheaths or core density difference. While affinity to Ag is a minor problem for multifilamentary tapes, the non uniform densification difficulties remain especially for tapes with some Ag alloy sheath where the hardening becomes more inhomogeneous.

In the other hand, most of the current transport applications are made in AC regime; therefore the losses produced whether of the sheath or the filaments (hysteresis losses) have to be reduced. As increasing the electrical resistance of the sheath the losses could be reduced, different sheaths have been studied. The high

reactivity of the superconducting powder during sintering and the superconducting cryostability of final conductor reduce the available materials to some silver alloys in multifilamentary tapes and pure silver in other configurations such as multifilamentary tape with electrical insulation barriers.

In this scenario, we have studied the production of a tape with Ag-Ni-Mg alloy sheaths which double the electrical resistivity and mechanical hardness of pure silver. Although the convenience of increasing the electrical resistivity is interesting for decreasing AC losses, the increment of mechanical hardness requires a higher tensile strength during drawing. As a consequence, silver alloy sheath reaches more easily its mechanical intrinsic limit, hindering further processing and annealing to soft the sheaths has to be introduced. Furthermore, this annealing requires optimised temperatures and atmospheres since permanent hardening of the sheaths by oxidised agglomerates may occur and powder reaction at moderate high temperature could change reaction dynamics.

The purpose of this chapter is to determine the degree of homogeneity of the conversion ratio Bi2212/(BiPb)2223 of different filaments in Ag-Mg-Ni alloy multifilamentary tapes deriving solutions for this alloy sheath processing.

4.2 Experimental Details.

The studied material was a 37-multifilamentary tape embedded in Ag (Mg (0.28%wt.), Ni (0.2%wt.)) alloy sheath. Precursor powders of Merck Ltd. with stoichiometric composition $Bi_{1.84}Pb_{0.34}Sr_{1.91}Ca_{2.03}Cu_{3.06}O_y$ were packed in an alloy tube (Inner Diameter (ID)= 8.86 mm and Outer Diameter (OD)=10 mm) with a relative density to 25-30% to the BiPb-2223 one.

4.2.1 Mechanical Processing.

The wire was drawn until 1,19 mm. diameter and then, cut in 37 pieces. These were inserted together in an Ag-Mg-Ni alloy tube of similar size than the initial one. A hexagonal shape was formed by some small silver tapes inserted on the face of the hexagon (See Fig. 40). The multifilamentary billet was drawn until a final diameter of 1.9 mm.

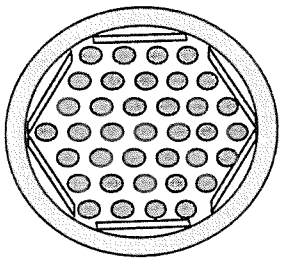

Fig. 40: Cross section sketch of a multifilamentary billet.

The drawing increases the hardness of the sheath and as it has been explained in chapter 3, due to the difficulties of cold work processing and some intermediate annealing are necessary. The annealings were made in a vacuum for 30 minutes at 400° C. The multifilamentary drawing and annealing steps are shown in next Fig. 41:

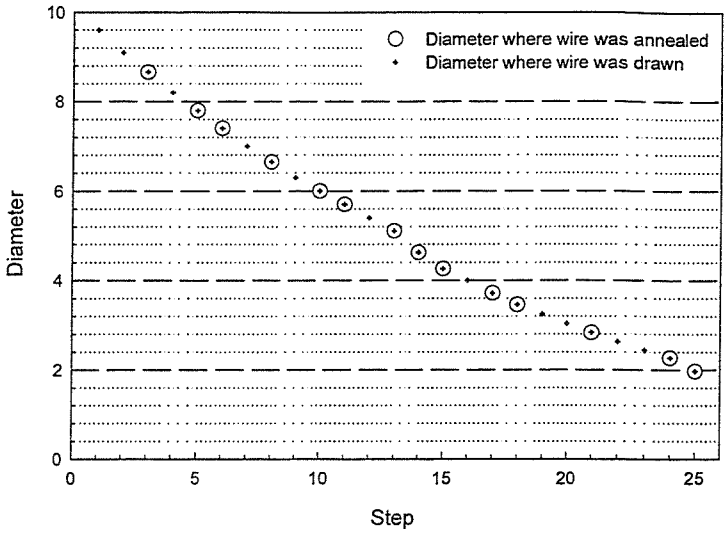

Fig. 41: Diagram showing the drawing diameter of each step of the process. The circles mark the intermediate annealing made at different steps.

The rolling of the wire was done in three different steps. At the beginning, during shape formation, 20 μm thickness reduction was used in each step until reaching 1300 μm thickness. Later, 40 μm reduction for rolling step was used down to 500 μm thick tape and then, a single step of 100 μm reduction finishes the rolling process obtaining a tape with a thickness of 400 μm.

4.2.2 Thermal Processing.

After rolling, two annealing-rolling processes and a final sintering were employed. The parameters used in the furnaces for sintering and annealing are collected in Table 7. The annealing has a dwell time of 3 hours at 812° C and the intermediate rolling steps reduce the thickness by 20% each time. The temperature of sintering is 818° C and the dwell time ranges in this study from 50h until 150 h. The atmosphere used for sintering and annealing was 8,5% Oxygen in Argon.

Step	Rate (° C/h)	1st thermal treatment		2nd thermal treatment	
		Annealing (°C)	Dwell time (h)	Sintering (°C)	Dwell time (h)
1	60	600	0	600	0
2	20	812	3	818	50-100-150
3	1	800	0	800	0
4	60	0	0	0	0

Table 7: Thermal parameters for tapes with three different final sintering times (50, 100 and 150 hours).

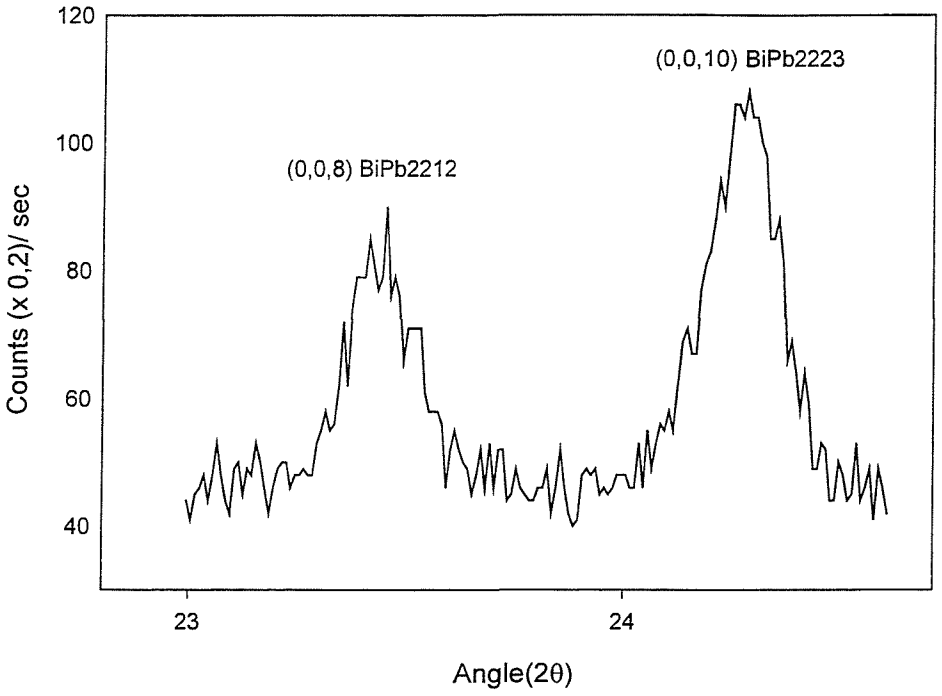

Fig. 42: XRD diagram of a filament, showing the intensity and scan angle.

The dwell times were selected to have a 30% of conversion of Bi-2212 into BiPb-2223 in the first annealing and 60% in the second. The final dimensions of the tape were 256 μm thickness and 3.8 mm width. An example is shown in Fig. 42.

The estimation of the conversion Bi-2212 into BiPb-2223 was done from the X-ray measurements of three tapes with different sintering times.

4.3 Results And Discussion.

Three tapes were selected for the mapping of the conversion; sintered during 50 h (short sintering), 85 h (with the highest critical current) and 150 h (over sintered). This will show the fine evolution of the conversion in each filament allowing the determination of the optimal time to achieve higher critical currents.

Two typical XRD results from an outer and a central filament (see Fig. 43) are shown in Fig. 44. The peaks used to estimate the relative fraction of conversion of Bi-2212 and BiPb-2223 were the (0,0,8) and (0,0,10) that correspond to the angle 2θ of 23.16° and 23.92° respectively. It is assumed 2212 and 2223 peaks are comparable so that the alignment of these phases is presumably similar, see peak (1,1,5) how slightly change proportion related to the (0,0,8) peak due to a preferred orientation. The conversion was estimated by integration over the area of the peaks. The conversion map obtained for the different tapes are presented in Fig. 48.

Outer filament Inner filament

Fig. 43: Position of the studied filaments.

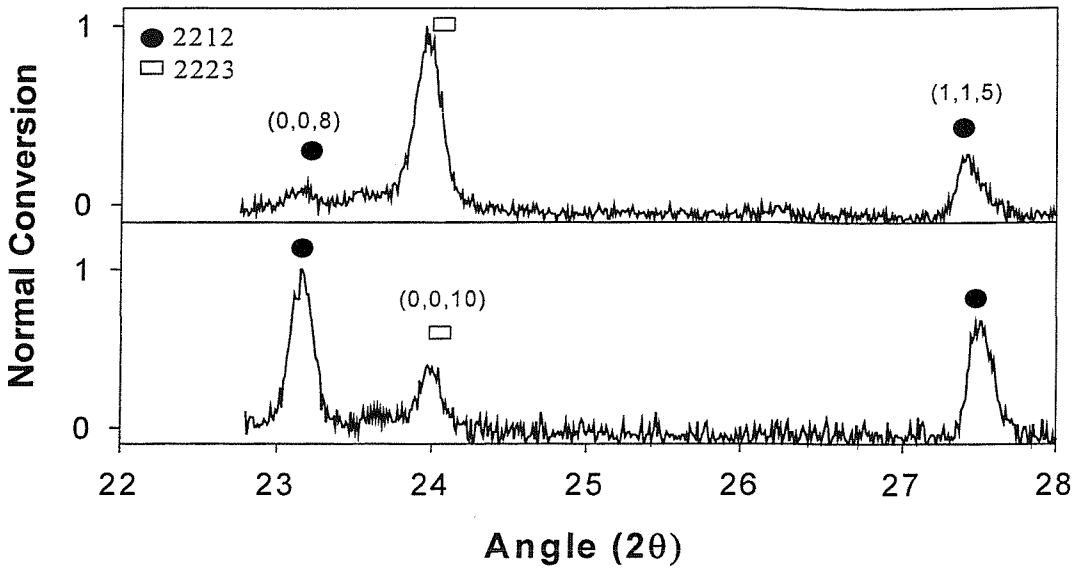

Fig. 44: X-ray data of two filaments form outer and inner areas with different conversion fraction.

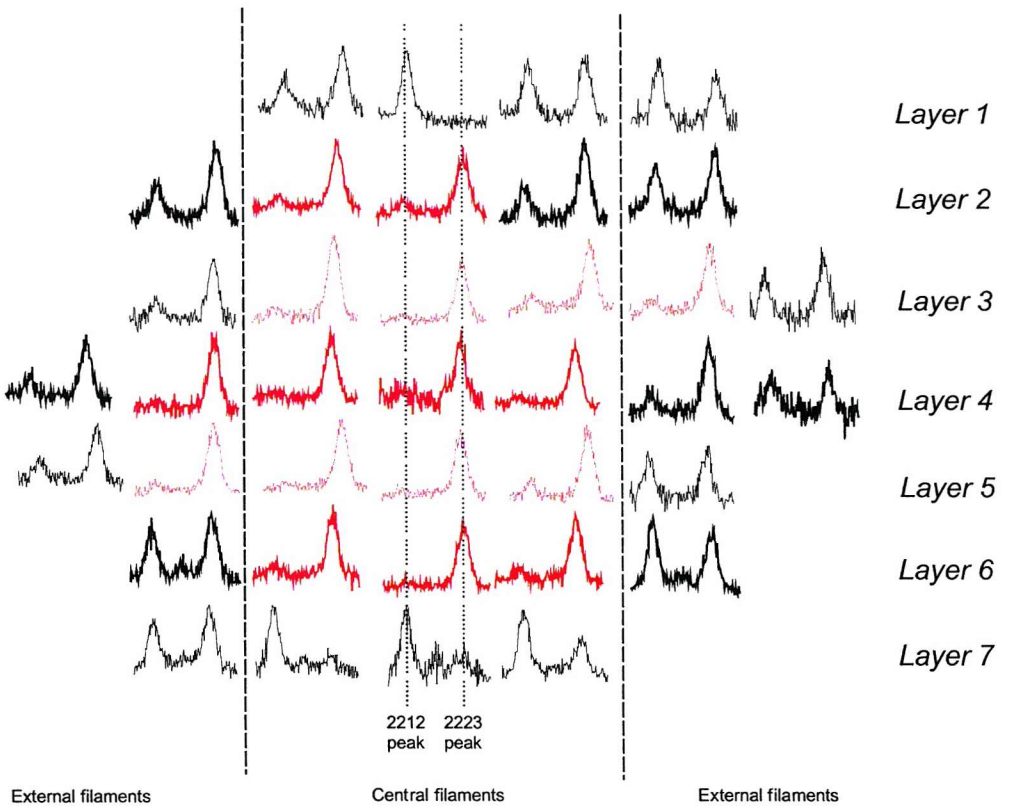

Fig. 45: XRD data of different filament of a multifilamentary tape sintered during 50 hour showing the evolution of the (0,0,8)BiPb2212 and (0,0,10)BiPb2223 peaks. Black diffractogram correspond to filament with lower conversion.

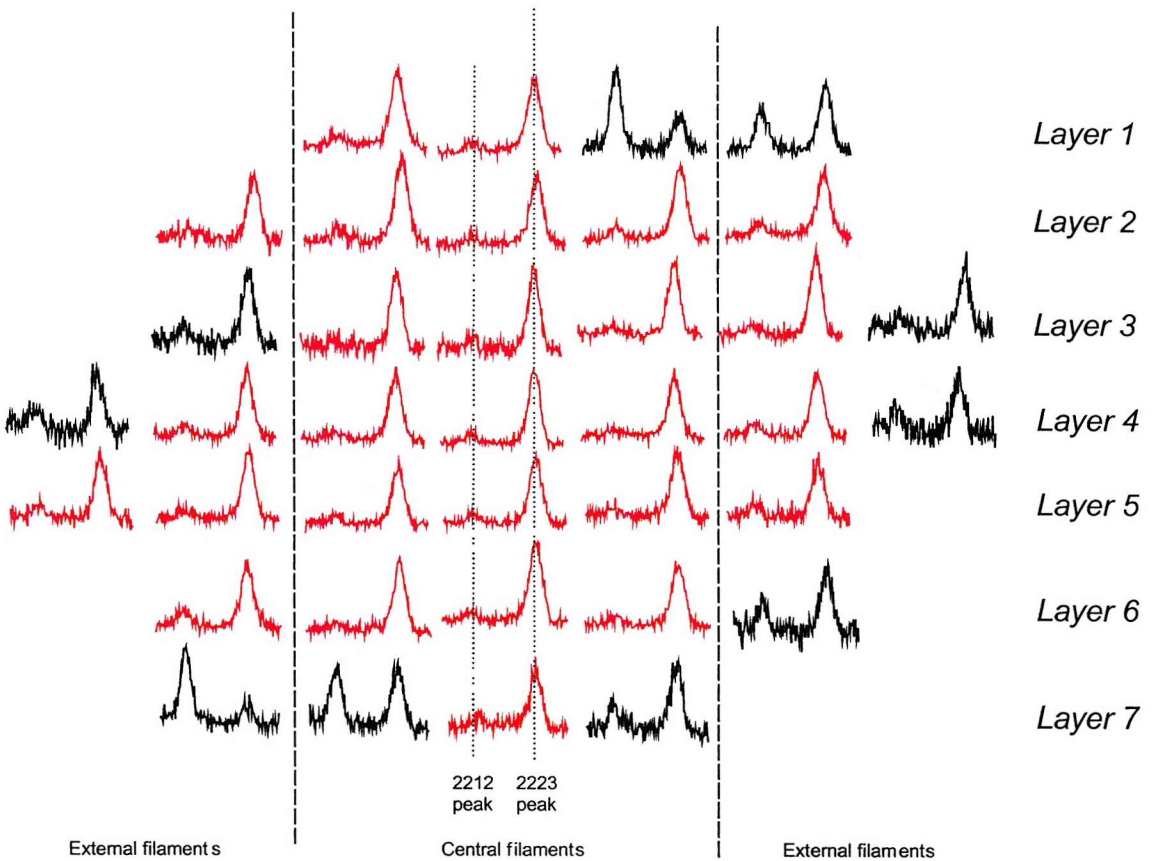

Fig. 46: XRD data of different filament of a multifilamentary tape sintered during 85 hour showing the evolution of the (0,0,8)BiPb2212 and (0,0,10)BiPb2223 peaks. Black diffractogram correspond to filament with lower conversion.

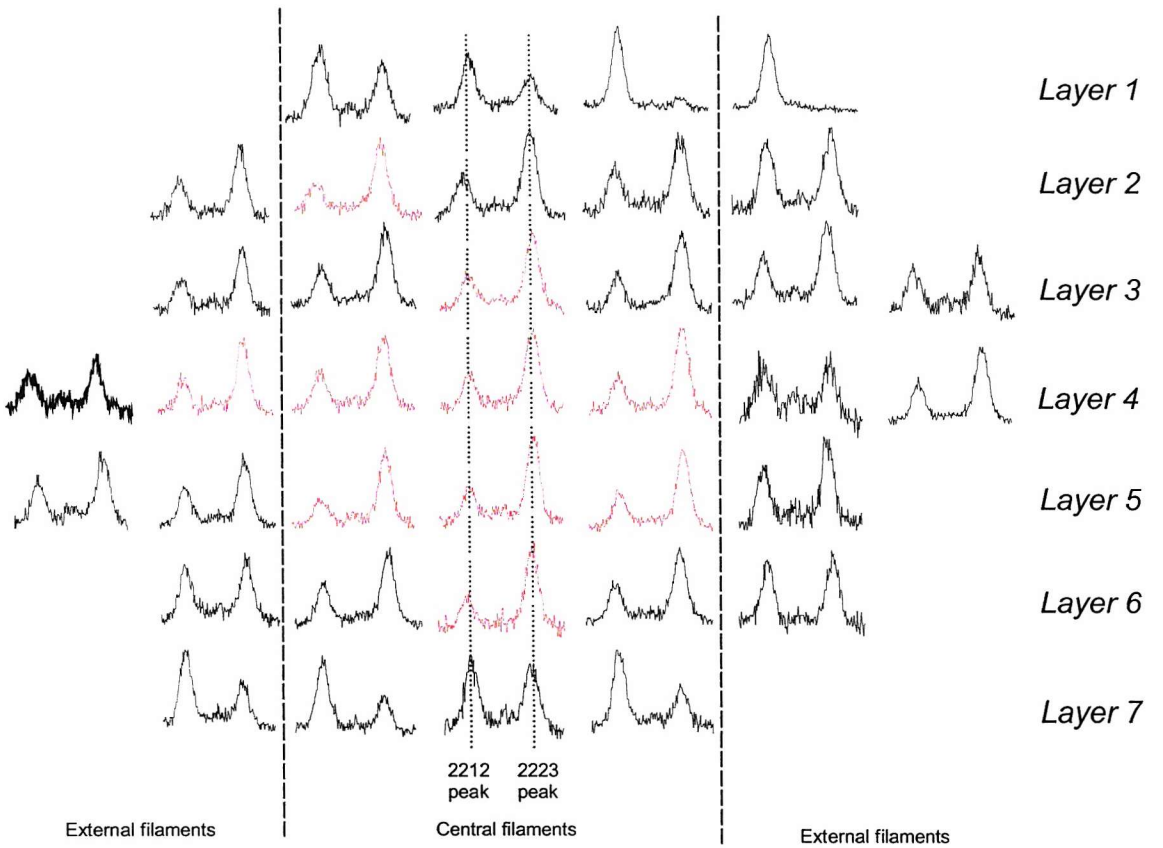

Fig. 47: XRD data of different filament of a multifilamentary tape sintered during 150 hours showing the evolution of the (0,0,8)BiPb2212 and (0,0,10)BiPb2223 peaks. Black diffractogram correspond to filament with lower conversion.

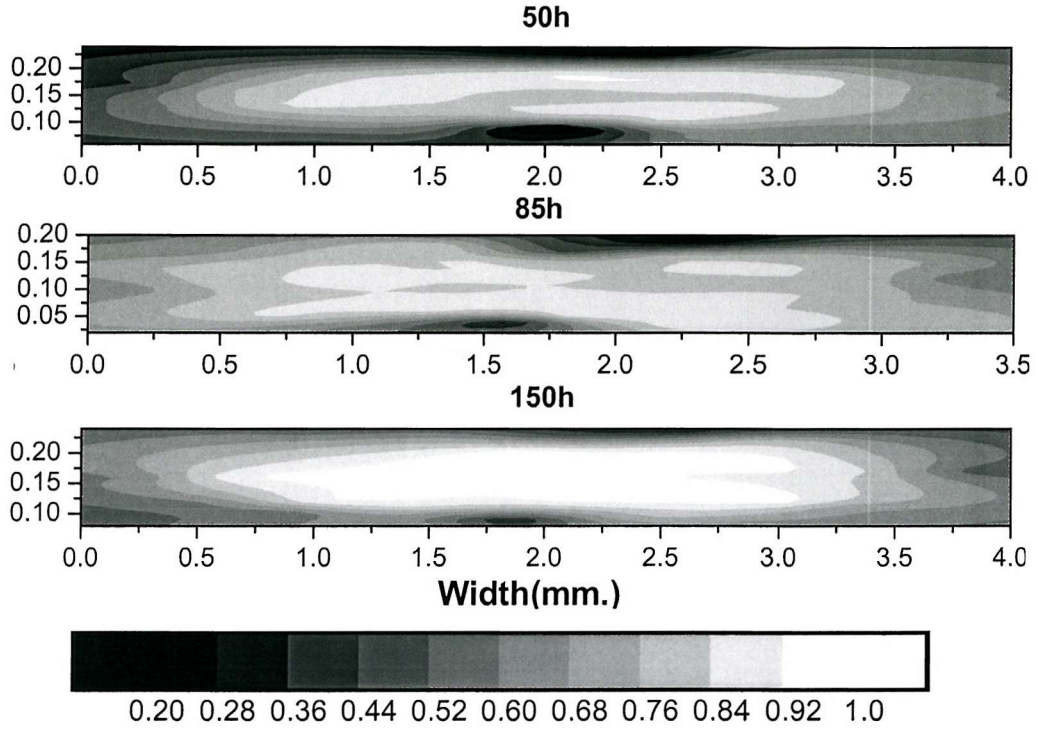

Fig. 48: Normalized conversion map in the cross sectional area of a tape for different sint ering times (50, 85 and 150 h).In the last graph is presented the grey scale.

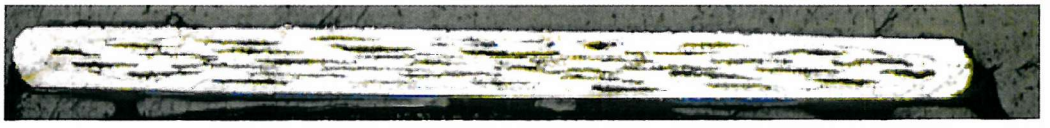

Fig. 49: Cross-section of the tape with optimum sintering time.

From Fig. 45 to Fig. 50 it may deduced that the filaments from the outer layers (A and G) always show the lowest conversion. A 50% difference between the lower conversion of outer layers and inner centre filaments is observed on the three tapes while the other external filaments are 30% lower in the worse case. This inhomogeneity is more pronounced in NiMgAg alloy sheathed tapes than in pure silver ones due to its higher hardness after cold working. In fact, in pure silver tapes the differences between filaments is lower. Fig. 50 shows that the conversion of

outer filaments (see Fig. 43) reaches maximum value when the critical current is optimised and decreases for longer times, whereas still increases after 150 hours in inner filaments. A smaller conversion in the central layer appears to be a common trend at all sintering times. Although conversion inhomogeneities are observed in all samples, they decrease for increasing sintering times.

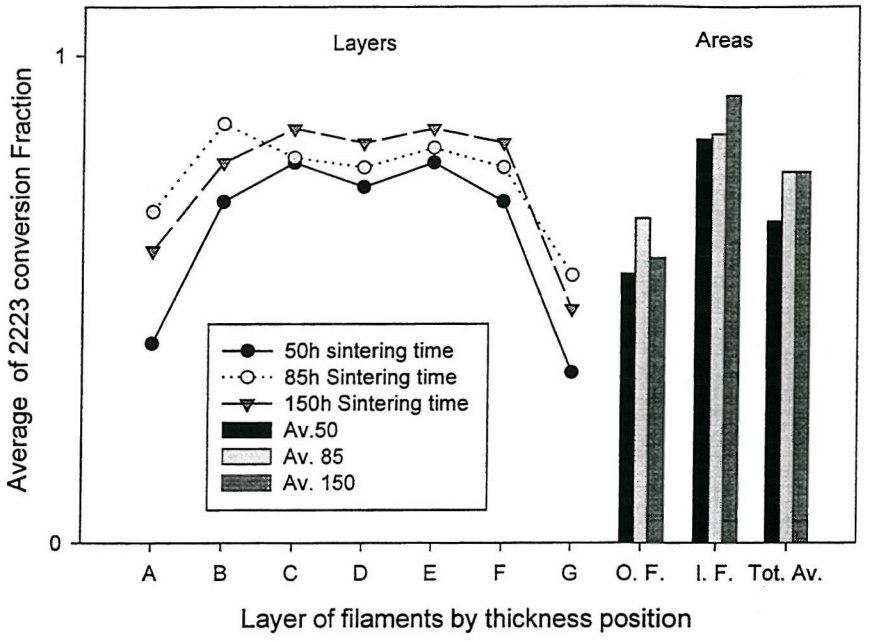

Fig. 50: Averages values of phase conversion as a function of the layers for different sintering time where O.F represents the Outer Filaments, I.F the inner filaments and Tot is the whole tape.

The difference in the local density might be the responsible of the behaviour of the filaments, and higher conversion rates are achieved for lower density (see Fig. 50, I.F. area conversion related to O.F. area). This is consistent with published result where the density has been found to play an important role for the conversion of Bi-2212 to BiPb-2223[116]. Local variations of the density are produced during both drawing and rolling processes. Upon drawing the outer filaments become denser than the inner ones in a radial distribution. Moreover, this also happens in monofilamentary wires (See Fig. 51), which display two areas clearly separated with different densification, and the outer core, zones which are denser than the

inner ones, do not conform the powder along the wire as the internal powder, creating an interface in the core. In the centre the powder is so loose packet that during abrasion is lost.

On the other hand, higher powder densities during cold working induce more irregular silver core interfaces and therefore lower alignment. Although the proximity of outer filaments to the external oxygen atmosphere could help the liquid formation has lower total silver interface area and the higher thickness of these external filaments operate in the opposite way.

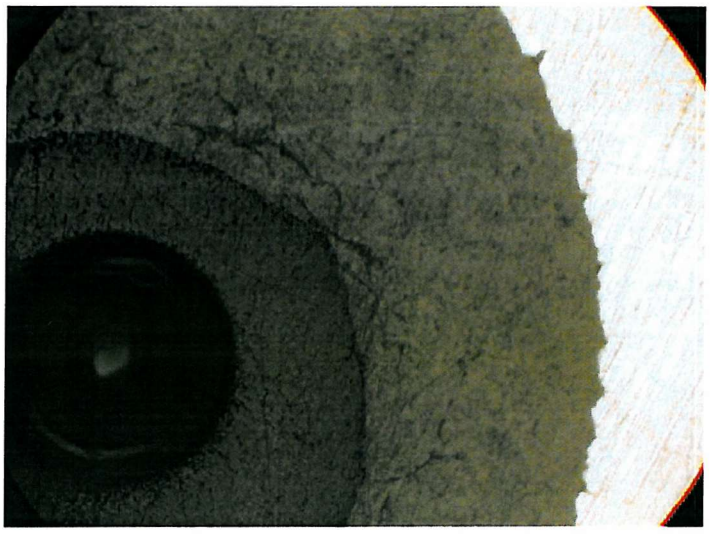

Fig. 51: Cross-section of a monocore Ag-BiPb2223 wire showing two core zones of different density.

Similarly, during rolling an ellipsoidal inhomogeneity may be produced. Broadly speaking, this distribution takes the form of four sectors defined by the diagonals with the top and bottom sectors being denser than the side sectors[117].

Adding the area already densified during drawing the overall map of densification would be similar to Fig. 52:

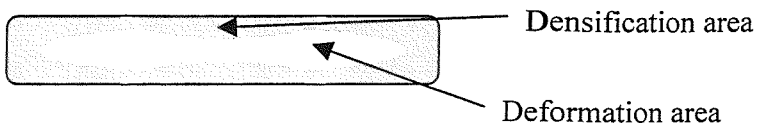

Fig. 52: Densification area of the tapes after drawing and rolling.

The critical current as a function of the final sintering time displayed in Fig. 53 shows a typical behaviour with higher critical current densities for longer sintering periods at short times due to the conversion of BiPb2212 to BiPb2223. It reaches a maximum when the conversion is nearly completed and longer sintering period induces the growth of secondary phases which deteriorate the intergrain connectivity and therefore, the critical current. The critical current density at the top is approximately 6 kA/cm^2.

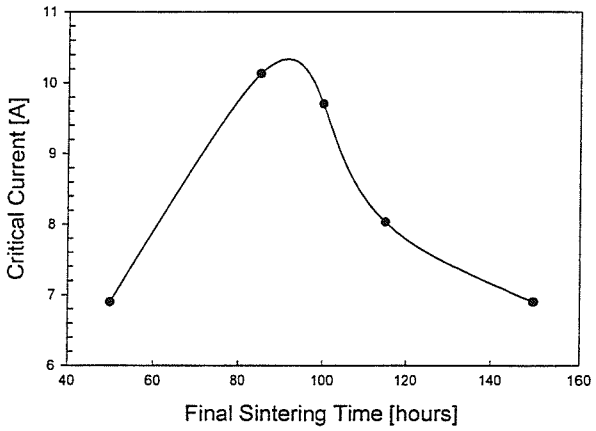

Fig. 53: Self-field critical current versus final sintering time of a Ni-Mg-Ag sheathed tape.

The correlation of the phase conversion with the changes in transport currents could be hidden by other parameters of the filaments such as disposition, shape and higher reactivity of external filaments which have not been characterised.

4.4 Conclusions.

The analysis of BiPb-2212/2223 conversion in the filaments of multifilamentary Ni-Mg silver alloy tapes has been done. The XRD measurements have shown that the conversion is not homogeneous across the tape. There are differences in the filaments conversion that makes difficult to optimise the 37 filaments at the same time. A possible reason of this inhomogeneity is the relationship between the conversion rate and the local core density. Further improvements in mechanical treatment and homogeneity are required to obtain higher critical currents in multifilamentary tapes.

Chapter 5: AC LOSSES IN SUPERCONDUCTORS.

5.1 Introduction.

Superconductors do not exhibit losses in direct current (dc), but most of the electrical devices and applications for electric transport and transformation operates in Alternating Current (AC) transmission regime. In a changing magnetic field, the magnetic flux that penetrates into a superconductor generates hysteretic losses in the superconductor and eddy current losses at the normal sheath. To these energy losses we must add the energy needed to keep the device at working temperatures (liquid Nitrogen in the case of HTS). If the total energy losses and the production cost is less than the losses and costs for the copper at the operational temperature then the device may be feasible with superconducting technology.

Moreover, the thermal stability of superconductors imposes the use of multifilamentary tapes in a silver sheath and this arrangement adds new losses from the resistive silver. These losses can be diminished by several routes that are going to be presented in this chapter.

5.2 Hysteretic Losses.

The hysteretic losses are produced by the flux flow under variable magnetic fields. The losses are coming from different mechanisms. In high frequency losses it is due to electron acceleration and interaction with trapped flux and normal cores. In low magnetic fields into the Meissner state, losses happen in the London penetration depth. Finally the losses at large amplitudes and low frequencies are subdivided into two different regimes, when the magnetic field applied reach the

center of the superconductor, and those where the field is confined to the surface. I will be concentrated in the later case because most of the industrial applications are into this range.

The magnetic or hysteretic losses can be measured in different ways. The electrical method is based in the relationship between the voltage produced by a variable magnetic field. The energy losses would be given by eddy current losses $P = \int \vec{E}\vec{J}dV = \int J\frac{d\phi}{dt}dV$ where ϕ is the magnetic flux. But the highly non-linear superconducting V-I dependence can lead to significant errors. In the case of external magnetic fields the hysteretic losses given by $Q = \int MdH$ are also present

$$M = \frac{1}{V}\int_S \mu_0 i dS \qquad \textbf{Eq. 20}$$

Using London and Bean[118] approximation for superconductors the external magnetic field penetration in a superconductor material is set independent of the current density. In the case of a slab in an external field B_{ext} of thickness d the magnetic field therefore is given by:

$$\frac{dB}{dt} = \mu_0 J_c = constant \Rightarrow B(x) = \mu_0 J_c\left(|x| - \tfrac{d}{2}\right) + B_{ext} \qquad \textbf{Eq. 21}$$

In the case of a cylinder of diameter D:

$$B(x) = \mu_0 J_c\left(r - \tfrac{D}{2}\right) + B_{ext} \qquad \textbf{Eq. 22}$$

The losses produced in these configurations are therefore:

$$q=\frac{2}{d}\int_0^p J_c\Delta\phi(x)dx=\frac{B_m^2}{2\mu_0}\frac{\beta}{3}=\Gamma(\beta) \qquad \textbf{Eq. 23}$$

Where $\beta=B_m/B_p$ (m=maximum, p=penetration).

This function reach the maximum at $\beta=1$. So, in order to reduced losses in the superconducting core, whether we applied a magnetic field with small penetration (wasting most of the superconducting material) or we apply a magnetic field far above penetration field that, for the same volume, is obtained by subdivision of the core in small filaments.

There are some other approaching models that we have not used for calculations, it should be mentioned Kim[119] model where it assumes pinning force is constant:

$$J_c(B)=\frac{J_{c0}B_0}{B+B_0}\Rightarrow B(x)=Kx^{1/2}+B_{ext} \qquad \textbf{Eq. 24}$$

By simplicity and following the Bean model, the analytical resolution of the losses has been studied by several authors for different configurations, some of them are presented below:

Norris[120] calculated the self-field losses for different configurations on hard superconductors:

A) Self field losses under penetration field ($I<I_c$)

for elliptical wires:

$$Q=\frac{I_c^2\mu_0}{6\pi}\left(\frac{I}{I_c}\right)^3 \qquad \textbf{Eq. 25}$$

for strips of finite width:

$$Q = \frac{I_c^2 \mu_0}{6\pi}\left(\frac{I}{I_c}\right)^4 \qquad \textbf{Eq. 26}$$

For BSCCO monocore Ag-sheathed tapes the predictions for both configurations are also consistent[121]. It has been shown[122] that multifilamentary tapes behave as monocore elliptical tape indicating that there is a strong interaction between the filaments.

B) at saturation peak current

- for elliptical wires: $Q = A\frac{I_c^2 \mu_0}{\pi}$; where A depends on the number of filaments, being A=0.5 the value for monocore tape.
- for rectangular (a,b) conductors: $Q = \frac{I_c^2 \mu_0}{\pi}(0.386 + \ln k)$; where k is given in the Table 8:

a/b	0	0.1	0.2	0.4	0.6	0.8	1
Ln k	0	-0.023	0.034	0.052	0.059	0.063	0.063

Table 8: ln K values for rectangular conductors with different thickness/width ratios.

B1) when is applied an external and parallel magnetic field for different configurations, it has been found:

B1A) Monocore slab of thickness d[123]

a) under penetration field ($H \ll H_c$)

$$Q = \frac{B^2 \beta}{6\mu_0} = \frac{B^2}{2\mu_0}\Gamma(\beta) \qquad for \beta < 1 \qquad \textbf{Eq. 27}$$

$$\text{being } \beta = \frac{B}{B_p} = \frac{B}{2\mu_0 J_c d}$$

b) above penetration field (H>Hc)

$$Q = \frac{B^2}{2\mu_0}\left(\frac{1}{\beta} + \frac{2}{3\beta^2}\right) = \frac{B^2}{2\mu_0}\Gamma(\beta) \quad for\ \beta > 1 \qquad \textbf{Eq. 28}$$

C1) losses in a perpendicular magnetic field.

In this case Brandt[124] presented some calculation that does not follow Bean's model completely but it assumes mean characteristic of fluxes only moved when current density reaches J_c

In the case of a elliptical wire:

$$Q = \frac{\mu_0 I^3}{6\pi I_c} \qquad \textbf{Eq. 29}$$

For a strip:

$$Q = \frac{\mu_0 I^4}{6\pi I_c^2} \qquad \textbf{Eq. 30}$$

For perpendicular magnetic fields Brandt calculated analytically the losses for a thin strip of width a. For small and large magnetic field amplitude the energy losses are:

$$\begin{cases} Q = \dfrac{2\pi\upsilon\mu_0 a^2 H^4}{3H_c^2} & H << H_c a \\ Q = 4\pi\upsilon\mu_0 a^2 J_c (H - 1.386 H_c) & H >> H_c \end{cases} \qquad \textbf{Eq. 31}$$

In the case of a multifilamentary tape with fully coupled filaments the hysteretic losses are predicted to be:

$$Q_S = \frac{1}{\mu_0}\pi\, w_s^2 B_d B_0 \left\{ -\tanh\left(\frac{B_0}{B_d}\right) + 2\left(\frac{B_0}{B_d}\right)\ln\left[\cosh\left(\frac{B_0}{B_d}\right)\right]\right\} \qquad \text{Eq. 32}$$

where $B_0=\mu_0 H_0$ and w_s is the width of the superconducting filament

5.3 Eddy Currents.

HTS tapes are normally sheathed with a metallic material such as silver for mechanical reinforcement and cryostability. For the same reasons the tape is multifilamentary structured, reducing, in addition, hysteretic losses.

When an AC magnetic field is applied or an AC current is transported in a tape, dissipations induced by eddy currents (See Fig. 54) on the sheath are added to the hysteretic losses, these dissipations are called eddy losses. These losses produced by the induced electric field created by the local magnetic field variation may give significant contribution to the overall losses.

Moreover, the lower hysteretic losses achieved by reducing the thickness of the superconductor filament are neutralized by the losses produced by current loops between the filaments. These currents would raise the magnetic fields in the external filaments, in such way that the multifilamentary area works as a monocore filament.

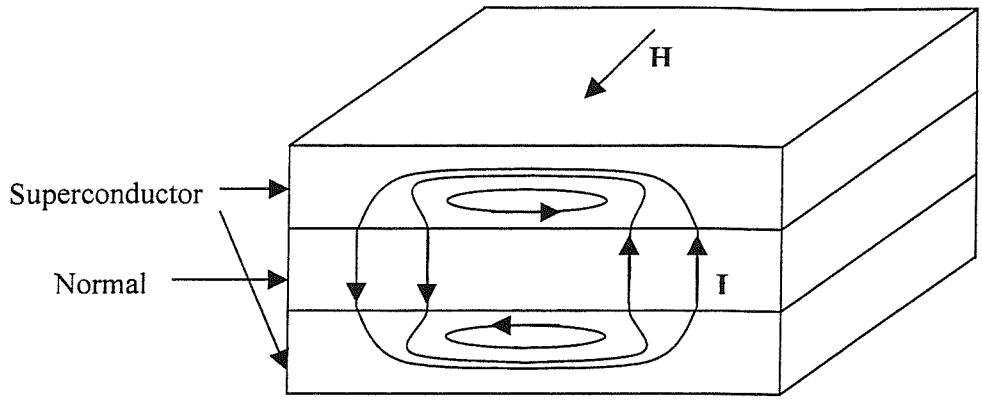

Fig. 54: Coupling currents induced by an AC magnetic field in a composite tape with metal and superconducting materials.

The most efficient method to reduce these eddy currents is the twisting of the filament. In such wire, the size of the current loops is limited by the twist pitch of the filaments. When it is smaller than the coupling length, the filaments uncouple effectively.

Unlikely another losses of eddy nature appear in a twisted tape. Looking from the magnetic field direction (See Fig. 55), the current path, follows the superconducting filament cross from one to another of the intersection. Thus, at this point flow is the same direction than the magnetic field across the sheath giving new losses called coupling losses.

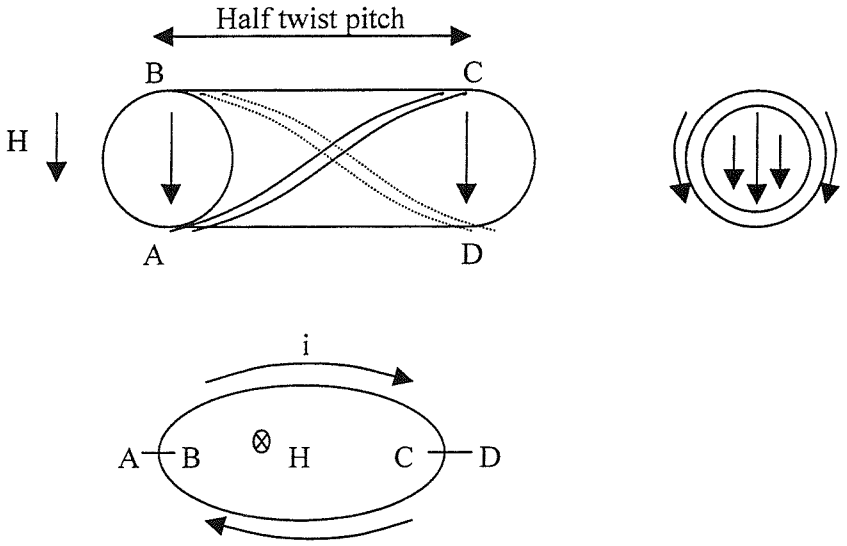

Fig. 55: Current coupling between two twisted filaments.

In a superconducting multifilamentary wire, coupling current losses under a sinusoidal magnetic field is given by

$$Q_c = \frac{B^2}{2\mu_0} \frac{\pi\omega\tau}{(\omega^2\tau^2+1)} \qquad \textbf{Eq. 33}$$

where $\tau = \frac{\mu_0}{2\rho_{ef}}\left(\frac{L}{2\pi}\right)^2$; $\rho_{ef} = \frac{1}{\rho_t} + \frac{w}{a\rho} + \frac{aw}{\rho}\left(\frac{2\pi}{L}\right)^2$ *and* $\rho_t = \rho\frac{(1+\lambda)}{(1-\lambda)}$

and λ is the fill factor in the cross sectional area.

From the Eq. 33, it is deduced that the losses of a tape are going to be higher for a perpendicular than for parallel magnetic field since $Q_e \propto a^2B^2$, where a is the width of the silver perpendicular to the applied field[125], The resistivity of the sheath, the amount of silver in the tape and the applied frequency also affect the magnitude of the eddy current losses. The best scenario is the reduction of the losses at

common industrial frequencies, as it can be seen in the coupling losses equation (Eq. 33) increasing sheath resistivity the losses can be reduced. This is possible by using different alloys that do not contaminate over the cores during annealing and increase the resistivity. Another possibility is to introduce insulating material between the filaments acting as barriers. Both paths have been investigated confirming its feasibilities.

For a tape in a perpendicular field, the equation is given by $Q_c = \frac{nB_0^2}{\mu_0}\frac{\pi f\tau}{(f^2\tau^2+1)}w_s t_s$, where the time constant τ, is given by: $\tau = 2\pi\mu_0 k\frac{L_p^2}{\rho_T}n$, and $n = \frac{1}{1-N}$ where N is the demagnetization factor of the superconducting filamentary region.

In the case of a non twisted tape L_p must be substituted by 2L.

5.4 Experimental.

For the self-field losses in a multifilamentary twisted tape, while the overall loss Q_T is proportional to the in-phase component of the first harmonic (E'_1), the hysteretic loss of flux pinning Q_S in the superconducting core is uniquely represented by the third harmonic[126] $|E_3|$. Therefore, the total loss per cycle is calculated by $Q_T = \sqrt{2}\frac{H_{AC}E_1' w}{f}$ and $Q_S = \alpha\sqrt{2}\frac{H_{AC}|E_3|w}{f}$ where E'_1 and $|E_3|$ are measured in rms voltage per unit length, w is the tape width, $\mu_0 H_{AC}$ is the peak AC field and α is the scaling factor given by the critical state model[127]. The coupling current loss can be estimated for comparison with $Q_C = \frac{V_{||}^2\lambda t}{\rho f w}$ where λt is the effective thickness of silver matrix perpendicular to the applied field.

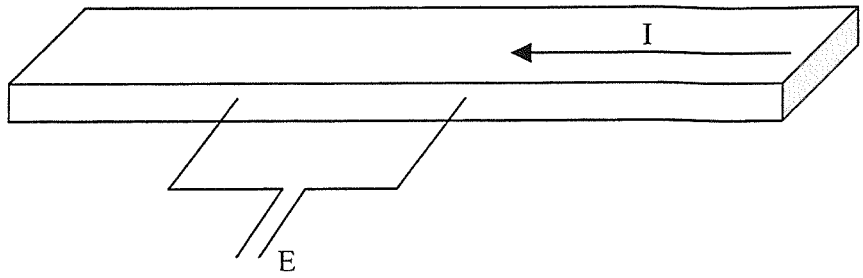

Fig. 56: Voltage taps for self field configuration in AC losses measurement.

In the case of a perpendicular field[128], hysteretic losses are determined by $Q_S = \frac{\pi}{2} w_c \frac{V_{S,RMS} H_{RMS}}{Lf}$, that is related with the 3rd harmonic by the factor $F(B_0)$ as:

$F(B0) = \frac{V'_{S,RMS}}{|V_{S,3}|}$, which is almost constant for the range used in Bi2223 tapes and approximately equal to 2. The voltage measurements are detailed in Fig. 57.

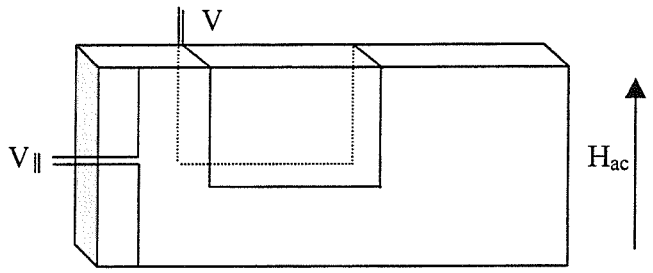

Fig. 57: Voltage taps in parallel configuration. $V_{\|}$: coupling, V: Total losses.

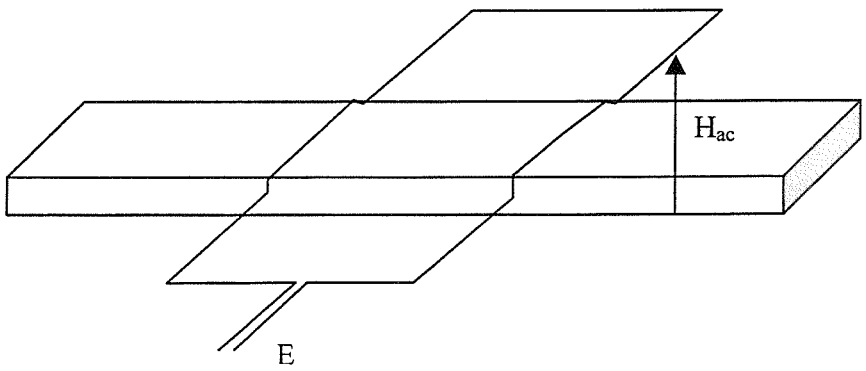

Fig. 58: Perpendicular magnetic field configuration for AC measurements.

Coupling losses calculated by effective medium approximation for conductors of rectangular cross-section give us coupling losses by: $Q_C = \frac{nB_0^2}{\mu_0}\frac{\pi f\tau}{\left(f^2\tau^2+1\right)}w_s t_s$, where the τ constant is given by $\tau = 2\pi\mu_0 k\frac{L_p^2}{\rho_t}n$ and w_s, t_s are the width and thickness of the superconducting region. Finally, eddy losses would be given by $Q_E = \frac{\pi^2 f B_0^2}{6\rho}w^3 t$ but only considerable at high fields ($B_0 > B_p$).

5.5 Equipment.

Fig. 59 represents the instrumentation and connections of the equipment used for the measurements:

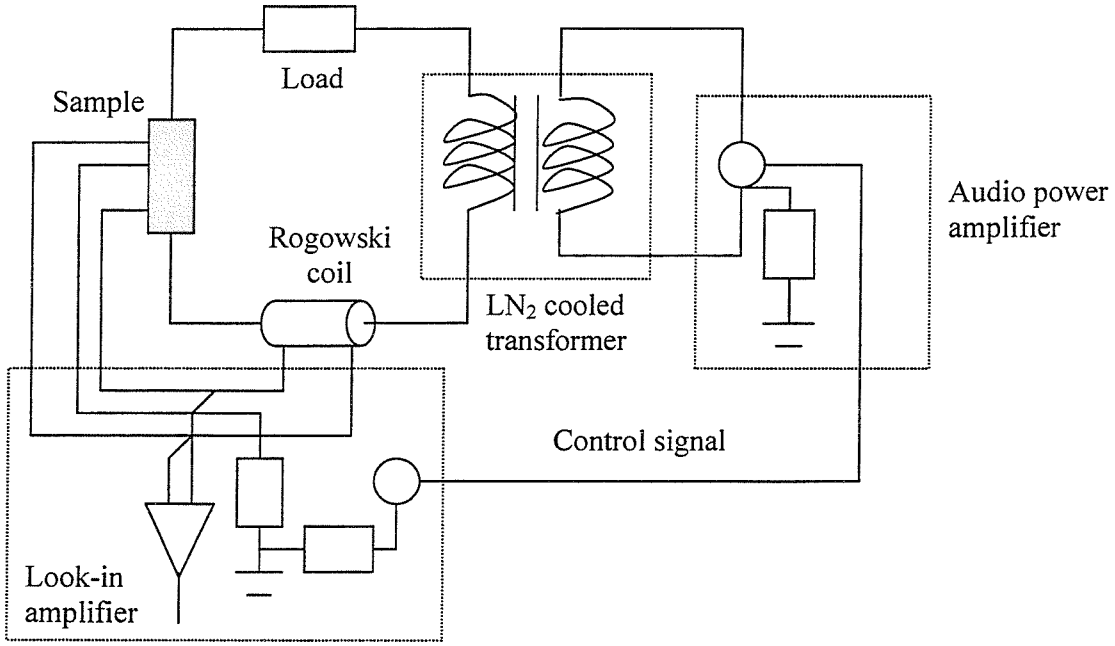

Fig. 59: Schematic of instrumentation and connections to the samples for measurements.

The sample is connected to a current circuit that is amplified by a transformer and audio amplifier. The signal is sent by the look-in amplifier which controls the input signal that is received whether sample (voltage) and Rogowski coil (current).

The Rogowski coil is a circuit that given a current the output is a very accurate voltage 90° out of phase. The lock-in amplifier will measure the in-phase and out of phase signals as well as different selected harmonics of the signal. Finally, all the signals are sent, collected and processed by a computer.

Chapter 6: AC LOSSES MEASUREMENT OF TWISTED MULTIFILAMENTARY BI-2223 TAPES WITH DIFFERENT CONFIGURATIONS.

AC losses of twisted multifilamentary BPSCCO-2223 tapes with different filament configurations have been measured under AC fields at 77 K. 37 and 111-filament tapes have been prepared where the 111- filament tape was made from three strands of 37-multifilamentary Ag-Au/BiPb-2223 wires. The strands were sintered together via silver alloy paste without any external sheath in order to maintain the metal/BPSCCO ratio. The final wires of 1.5 mm diameter were twisted at different pitches (Lp=8-17 mm) before rolling into tapes. Loss reduction has been found as the result of filament uncoupling by twisting. The different loss contributions in this regime, superconducting and current coupling losses have been obtained experimentally. The effect of the filament configuration and the number of filaments on the AC losses are analysed.

6.1 Introduction.

Loss reduction is one of the main research targets concerning the application of high temperature superconductors (HTS) in power devices. While flux pinning enables the transportation of macroscopic dc current without dissipation in superconductors, the same mechanism results in magnetic hysteresis and ac losses in an alternating magnetic fields[129,130]. The common strategy for loss reduction is by subdividing the superconductor core into fine filaments, provided they are uncoupled for the given frequency and amplitude of the ac field. In order to prevent the long lengths of conductors in practical devices from coupling, twisted filaments at a short pitch are required.

The main difficulties concerning the loss reduction for PbBi2223 Ag sheathed tapes are the low matrix resistivity of the silver sheath and the moderate critical current in the superconductor. Such a combination of the material properties leads to a low critical coupling field B_C and high coupling current losses Q_C. For fields applied perpendicular to the tape face, the problem is further compounded by the large aspect ratio, which proportional reduces B_C and increases the maximum level of Q_C[131,132]. As the minimum twist pitch is severely limited due to the ceramic nature of the HTS core, the only avenue for loss reduction is through the use of a high resistive matrix.

In this paper we focus on the loss behaviour of PbBi2223 tape in perpendicular ac fields. While conductors with high matrix resistivity such as oxides coated PbBi2223 tapes are being developed[133,134], the critical current density achieved to date is still relatively low. The use of Au-Ag alloy allowed us to obtain a moderately high resistivity without significant J_C degradation. Although such a sheath material may not be practical for real applications, it enabled us to carry out experimental studies in regimes otherwise inaccessible with other tapes.

Since the existing theories[131,132] for the coupling current loss are based on the effective medium approximation, their applicability to HTS tapes of relatively small number of filaments are uncertain. In this paper, two sets of tapes with different filament number and dimension are studied. Using a novel technique for separating the superconductor loss from the total losses, B_C and Q_C are obtained for direct comparison with the theoretical predictions.

6.2 Experimental Method.

The 37-filament Bi-2223 tapes were fabricated by the powder-in tube method using a high resistive alloy for the sheath/matrix, AgAu(10 wt. %), of $\rho \sim 2x10^{-8}$ Ωm, about seven times higher than for pure silver. Prior to deformation into tape geometry by rolling, the wire was cut in several pieces, each one being twisted at a different twist pitch.

To make the 111-filament tape, a 37-multifilamentary wire embedded in a 10 wt. % AgAu matrix was drawn until 1.6 mm diameter. The wire was cut in three pieces and pasted with a silver paint forming a tri-wire that was annealed at 800°C for 5 minutes and drawn until reaching 1.5mm diameter (Fig. 60a). The wires were then twisted at different twist pitches (final L_p= 8, 11,14 and 20 mm), and were further rolled up to ~300μm thickness (Fig. 60b) by a reduction ratio shown in Table 9, The gold alloy 37 multifilamentary tape had similar treatment but twist pitches were 7 and 13 mm.

Diameter range(Ø)	1500 μm-1300 μm	1300 μm-850 μm	850 μm-390 μm	390 μm-300 μm
Reduction step	20 μm	40 μm	30 μm	45 μm

Table 9: Rolling parameters, with low rolling reduction at the beginning for tape formation, constant % reduction in the middle range for homogeneous deformation and higher reduction at the end for increment of density.

The sintering process was done in two steps. A first sintering for 30 hours at 840°C in air with an intermediate rolling of 11% reduction in two steps (until 260 μm) and a second sintering of 75 hours duration at 840°C in air plus a dwelling at 818°C for 30 hours. See Table 10.

Atmosphere: Air	Ramp rate	Anneal/sinter. Temperature	Dwell time(hour)
1st sintering-ramp	60°C/h	700°C	0 h
1st sintering	20 °C/h	840 °C	30 h
1st sintering-cooling	60 °C/h	0 °C	0 h
2nd sintering-ramp	60 °C/h	700 °C	0 h
2nd sintering	20 °C/h	840 °C	75 h
2ndsintering-dwelling	2 °C/h	818 °C	30 h
2nd sintering-cooling	60 °C/h	0 °C	0 h

Table 10: Thermomechanical treatment for a 3x37 multifilamentary silver gold alloy BiPb2223 tape with no external sheath.

The transverse cross-section of the final tape is shown in Fig. 60e, and the longitudinal cross-sections of the top and middle layers of filaments are shown in Fig. 60c-d respectively. There is a distinctive non-uniformity in the filament distribution, as the three strands of wire revolve along the twisting helix.

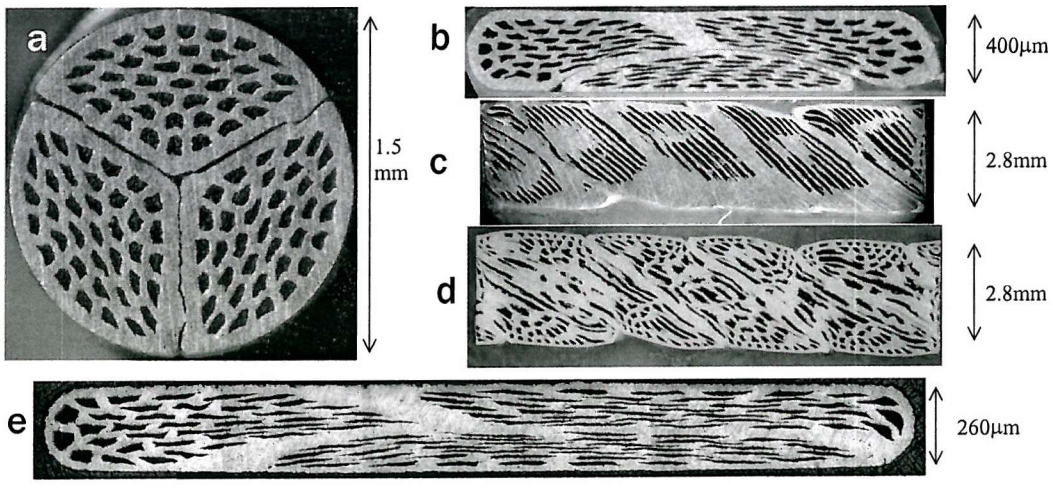

Fig. 60: Transverse cross sections of (a) the as-drawn stranded wire and (b) stranded tape prior to the first heat treatment; Longitudinal cross-sections of the stranded tape at (d) the top filament layer and (d) the middle filament layer; (e) the transverse cross-section of the final stranded tape.

The twist pitch of the measured tapes, L_P, together with their critical current, I_C, at 77 K are collected in Table 11. Degradations of 15-25% between the twisted and

the untwisted tapes are observed (see Fig. 61). All the tapes have the same final dimensions: width w=2.8 mm, thickness t=0.25 mm and length L=6.5 cm.

Samples	n_f	L_P (mm)	I_C (A)
S37-13	37	13	23.5
S37-7	37	7	23.2
S111-14	111	14	16.3
S111-8	111	8	15

Table 11: Tape characteristics.

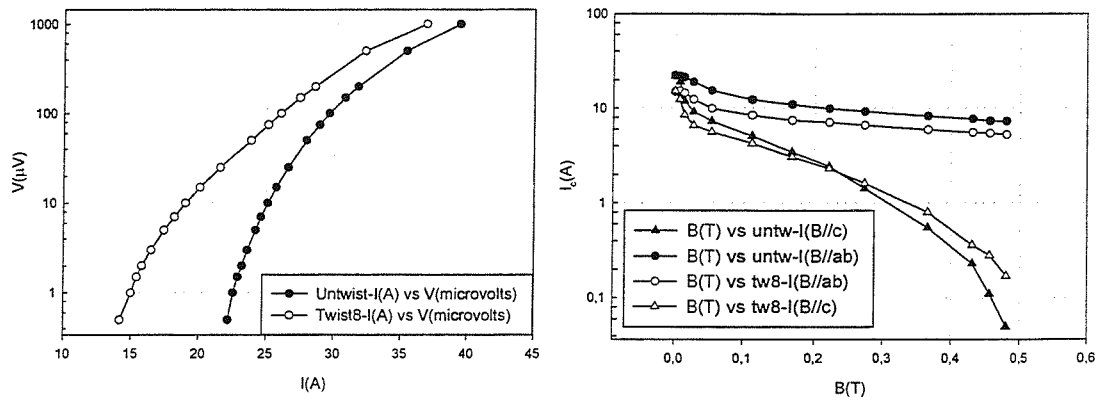

Fig. 61: V-I and I_c-B graphs of a 3x37 multifilamentary tape without external sheath that has been processed with the same thermomechanical treatment with a untwisted configuration (filled symbols) and twisted (white symbols) with a twist pitch of 8 mm.

AC losses were measured with the ac field perpendicular to the tape surface at 77 K using a saddle-like pick-up coil. The total loss Q and the superconductor loss Q_S are obtained form the 1st and 3rd harmonics of the pick-up voltage correspondingly using the procedure explained in reference.. The coupling current loss Q_C is attributed to the difference between Q and Q_S, neglecting eddy current loss for most cases.

6.3 Results and Discussion.

Fig. 62a shows the total loss Q and the superconductor loss Q_S of S111-14 as a function of applied field at 43Hz and 77K, obtained from 1st and 3rd harmonic of the pick-up signal. The large gap between Q and Q_S corresponds to the coupling current loss Q_C. The kink in Q_S marks the onset of filament coupling at the corresponding field amplitude and frequency.

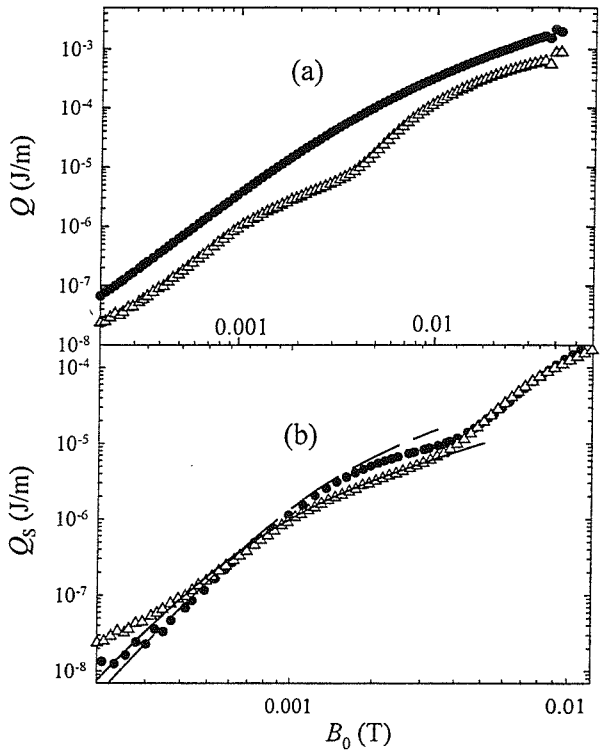

Fig. 62: (a) Superconducting and total loss of sample S111-14 at 43 Hz. (b) Superconducting losses, Q_S, of the tapes S37-13 (•) and S111-14 (Δ). The lines are the predictions given by (2) with *n*f=37, I_C=22 *w*f=*w*/9 (dashed line) and *n*f=111, I_C=16 *w*f=*w*/18 (solid line).

6.3.1 Superconductor loss.

The superconductor loss of multifilament tapes with coupled filaments follows the predictions of that of strips of zero thickness under perpendicular fields[135,136]:

$$Q_S = \mu_0 H_0 I_C w\left(\frac{2I_C}{\pi H_0 w}\ln\cosh\left(\frac{\pi H_0 w}{I_C}\right)-\tanh\left(\frac{\pi H_0 w}{I_C}\right)\right)\approx\begin{cases}\dfrac{\pi^3}{6}\dfrac{\mu_0 w^4}{I_C^2}H_0^4 & H_0 < H_P=\dfrac{5I_C}{2\pi w}\\ \mu_0 H_0 I_C w & H_0 \geq H_P\end{cases}$$

Eq. 34

When the filaments are uncoupled, which can be achieved by twisting for example, the superconducting loss is found by assuming identical filaments:

$$Q_{S,UC} \sim n_f Q_{Sf}$$

Eq. 35

where n_f is the number of filaments and Q_{Sf} the loss of each individual filament, which is given by Eq. 34 substituting w by w_f (filament thickness) and I_C by $I_{Cf}(=I_C/n_f)$, critical current of each filament. Note that for saturated filaments, the reduction of the superconducting loss by uncoupling the filaments will be by a factor w_f/w.

Fig. 62b shows the superconducting loss measured in the S37-13 and S111-14 samples at 77 k and 43 Hz (symbols). The lines are the predictions given by Eq. 35 using the values of I_C given in table I for each sample and values of the filament width $w_f=w/9$ and $w_f=w/18$ for the S37-13 and S111-14 samples respectively. Note that this factor should be the factor according to Fig. 60. As expected, the increase of the filaments number by using stranded tapes (S111s) results in a reduction in the filament width with respect to the mono-strand tapes (S37s), and hence a decrease of the superconducting loss. Nevertheless it has to be noted that there is a distinctive inhomogeneity among the filament width in the 111-filament tapes as is seen in Fig. 60. As a consequence, the assumption of identical filaments done in Eq. 35 is not

fulfilled. Although a more realistic approach would be to consider a distribution of both I_{Cf} and w_f, the main conclusions obtained here would remain. At B_0~4 mT, there is a sharp increase of Q_S marking the field at which the filaments start coupling, B_C[137] .

6.3.2 Coupling current losses.

The coupling current losses, Q_C, can be obtained experimentally by subtracting the superconducting loss to the total loss. For a superconducting tape under AC perpendicular fields, the frequency dependence of Q_C is given by.:

$$Q_C = n\pi\mu_0 H_0^{\,2} \frac{f\tau}{\left(1+f^2\tau^2\right)} S \qquad \textbf{Eq. 36}$$

where S is the area of the superconducting region, n is the shape factor (n~w/t) and τ is the time constant characteristic of the coupling currents expressed, in seconds, as reference. :

$$\tau = \frac{7\pi}{240}\mu_0 n\rho^{-1}L_p^2 \qquad \textbf{Eq. 37}$$

A different frequency dependence has been given by other authors.:

$$Q_C \propto \frac{1}{u}\left(\frac{\sinh u - \sin u}{\cosh u + \cos u}\right) \qquad \textbf{Eq. 38}$$

with $u = \pi\sqrt{\frac{f\tau}{2}}$

which differs slightly from Eq. 36 at higher frequencies. Moreover, for high frequencies the contribution to losses from normal eddy currents may become important:

$$Q_E = B_0^2 \cdot \frac{1}{f} \frac{\rho}{\mu_0^2} \frac{t}{\delta} \left(\frac{\sinh\gamma - \sin\gamma}{\cosh\gamma + \cos\gamma} \right)$$

Eq. 39

with $\gamma = \frac{w}{\delta}$

where Q_E is given in loss per cycle and per unit length and $\delta=[\rho/(\pi f \mu 0)]^{1/2}$ is the penetration depth.

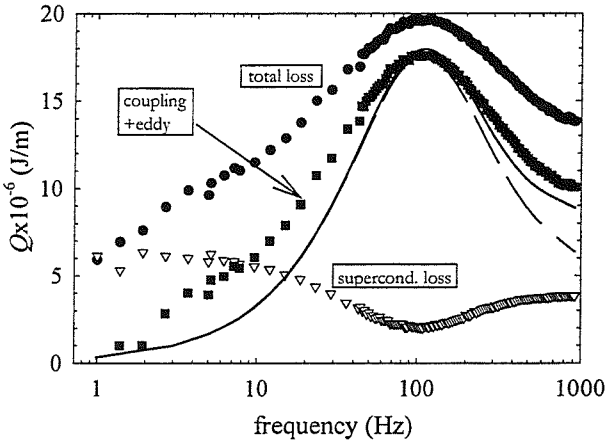

Fig. 63: Total (●), superconducting (▽) and coupling-current+eddy loss (■) measured at B_0=2mT for the tape S111-14. The solid line (Q_C) and discontinuous line (Q_C+Q_E) correspond to the predictions given by (3)-(6), as explained in the text.

Fig. 63 shows the total (Q, circles) superconducting (Q_S, triangles) and coupling + eddy ($Q-Q_S$, squares) loss contributions as a function of frequency measured for the sample S111-14 at B_0=2 mT. According to Eq. 36 and Eq. 37, the peak of Q_C would give us an estimate of the τ^{-1}, which in this case is τ^{-1}~105 Hz.

The dashed line in the figure corresponds to the $Q_C(f)$ dependence given by Eq. 38 with the value at the peak predicted by Eq. 36, using n~10. It is seen that although the value of Q_C measured at the peak agrees with Eq. 36, the losses measured at both $f < \tau^{-1}$ and $f > \tau^{-1}$ are higher than expected. At high frequencies ($f > \tau^{-1}$), the observed difference seems to be due to the contribution of the normal eddy currents, since the predictions of Q_C+Q_E (continuous line in figure) now approach the measured values. Nevertheless at $f < \tau^{-1}$ the reasons of the difference between measurements and predictions are still unknown.

On the other hand, at very low frequencies ($f < \tau^{-1/4}$), Q_S is almost constant, decreasing slightly with increasing frequencies due to the power-law I-V characteristic typical of high temperature superconductors. At higher frequencies, of the order of $f \sim \tau^{-1}$ the shielding of the superconductor by the coupling currents results in a sharper decrease of Q_S. Finally, the increase of Q_S at higher frequencies is due to the disappearance of the coupling current when the filaments start coupling..

Fig. 64 shows the measured coupling + eddy losses of the samples S111-8 and S37-7 at B_0=4 mT. It is seen than for the frequencies of technological interest (f~50Hz) this loss contribution is reduced considerably (by almost a factor of 2) for the 111-filament tape. This reduction is due to both a decrease of the Q_{C+E} at the peak, and an increase of τ^{-1} when increasing the number of filaments. The value of τ^{-1} obtained for the 111-filament tape is 310 Hz against the 180 Hz obtained for the 37-filament tape. Because of the similar dimensions of both samples, and according to Eq. 36, the reduction on the value of Q_{C+E} at the peak would give a value of the shape factor, n, lower for the S111-8 tape, by a factor ~0.8. On the other hand the observed difference on τ would indicate, according to Eq. 37, that the transversal resistivity of the sample S111-8 is ~1.4 times higher than for the S37-7 tape. Because both n and ρ depend strongly on the actual configuration of the tapes, as for instance on the existence of bridging between filaments, it has yet to be

confirmed whether the behaviour observed here for these two tapes is due to the different filament configuration.

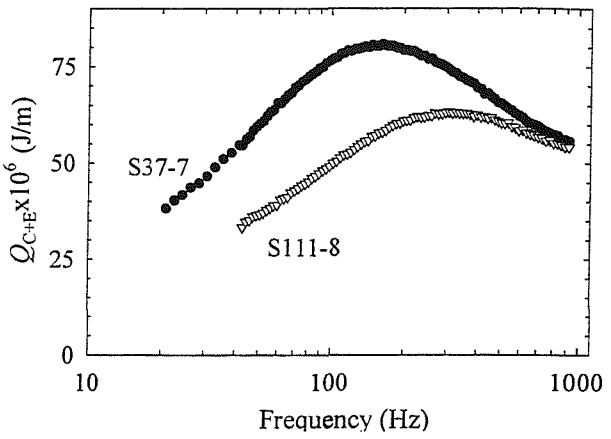

Fig. 64: $Q_C(f) + Q_E(f)$ measured in the S37-7 (•) and S111-8 (▽) tapes at 4 mT.

6.4 Conclusions.

The AC loss of the superconducting multifilament twisted tapes under perpendicular AC fields have been analysed for samples with different number of filaments ($n_f = 37$ and 111), it has been shown that loss reduction has been found as the result of filament uncoupling by twisting. The different loss contributions in this regime, superconducting and current coupling losses have been obtained experimentally with the result of a decrease of the current coupling losses by a factor of two. The contribution of the coupling and eddy current losses have been measured in a wide range of frequencies and compared with the theoretical predictions. The coupling current losses reduction is due to the decrease of the peak value at different frecuencies and the increase of the value τ^{-1}. Both parameters are related respectively to the decrease of the shape factor and the increase of the number of filaments and the alleged transversal resistivity. A discrepancy between the experiments and the theory has been observed at $f < \tau^{-1}$.

6.5 Other configurations.

In order to achieve AC losses reduction, another interesting configurations are braided wires and several experiments have been done in such shape with three and four wires. It has been seen that mechanically, the four wires configuration is more stable and easy to handle during drawing and rolling than the three wires one. This is because the four braided wire has a more homogeneous material distribution during conformation for axial and planar deformation, which will improve filament section homogeneity for each particular wire (See Fig. 65). The AC losses reduction could be also improved if each wire is twisted itself.

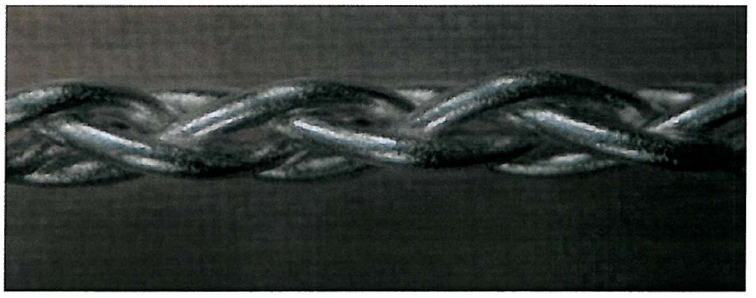

Fig. 65: Four wires braided at an initial pitch of ≈ 11 mm. Each wire is a 37-multifilamentary Ag sheathed wire (Ø= 0.8 mm.).

Four 37 multifilamentary PbBi2223 Ag sheathed wires has been drawn down to 0.8 mm of diameter. The wires has been braided at a certain angle between 15° and 30° with a small tension which did not harm the wire composite in their external face of the wires being possible the later drawing or rolling. The control of the applied tension and the angle will give us the initial pitch of the braided wire. The braiding pitches used are between 11 and 17 mm. The composite wire was drawn until a diameter of 0.8 mm (See Fig. 66).

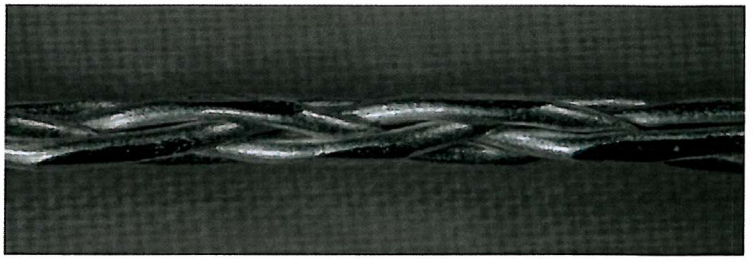

Fig. 66: Braided wire drawn down to 0.8 mm of diameter.

During rolling a special care must be taken in the election of the rolling plane since the shape of the wires along the composite, and therefore, the homogeneity of the filaments are greatly variable depending on such parameter. The wire must be placed parallel to the rolling plane whith the filaments stacked in a square shape when no transposition is done and that means that the change in position of the wires in the rolling plane is only done vertically by two wires each time (See Fig. 67 and Fig. 68).

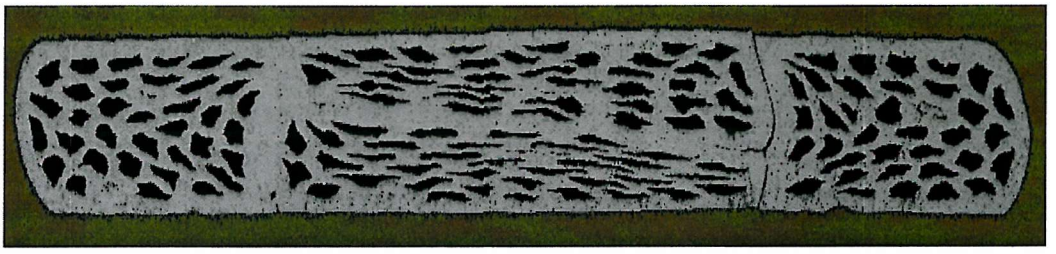

Fig. 67: Braided tape rolled with the transposition made by only a couple of wires. Transposition is made first between the two wires in the middle and later the two couples of the wires on both extreme are transposed at the same time.

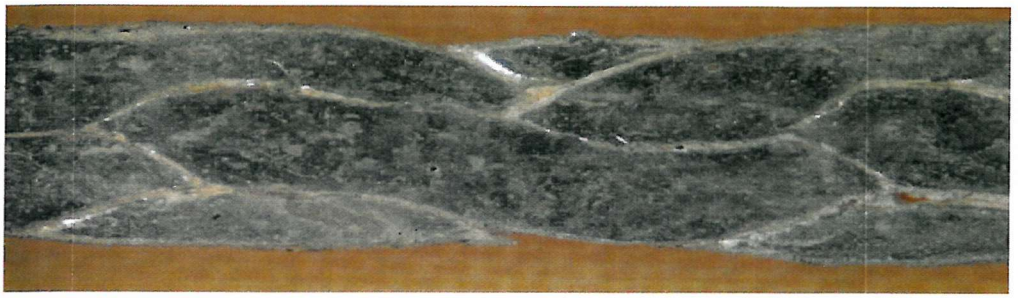

Fig. 68: Braided tape rolled with transposition made vertically.

Otherwise, a 45° turn plane would mean that the change in position is done horizontally by two wires between the other two, a given cross section would see the four wires stacked one on top of the other. As a result, a bulk with very thin filaments sections are followed by four wires spread along the width and therefore the filaments would be much thicker than previous position (See Fig. 69), creating a kind of sausaging that is not desirable for achieving high critical currents.

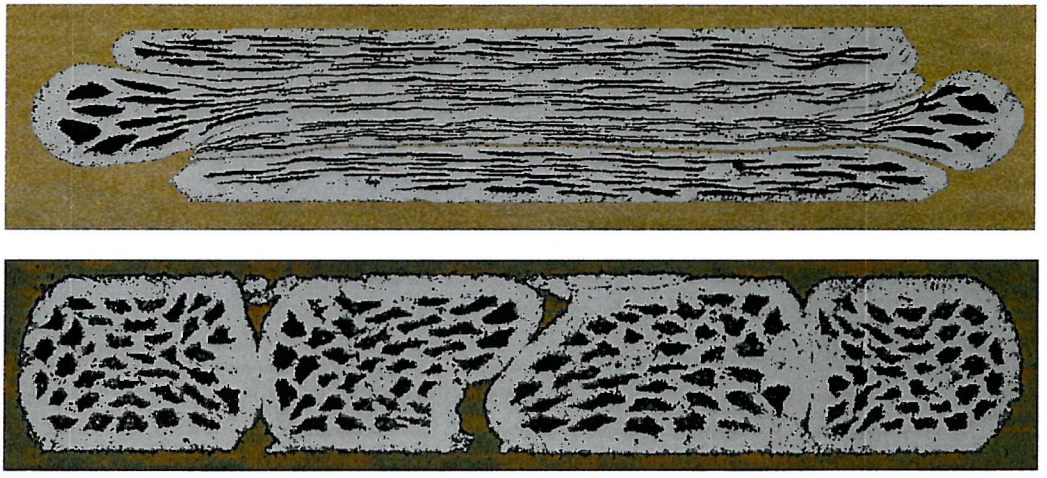

Fig. 69: Cross section of a braided tape rolled by the diagonal angle of the wire at different rolling lengths, the transposition of the wires is produced in between the other wires. As a result filam ents shape is inhomogeneous along the tape and easy to break by shear stress on the edges (see right edge on the top picture).

The transition in the wire between the different position (aligned/stacked wires) is very abrupt. As it is shown in Fig. 70 the shear stress produced in the wire when the rolling plane is turned 45° causes the breaking of the external wires in the transition of aligned-stacked wire position.

Fig. 70: Braided wire broken by the shear stress produced on the transposition of the external wires when the rolling plane is turned 45°.

During conformation of the tape, several annealings must be done at 400°C for 5 minutes in a vacuum atmosphere. The final tape is rolled until a thickness of about 250 μm. Due to the high deformation, the filaments are slightly made out on the surface of the sheath showing the trace of the filaments (see Fig. 71).

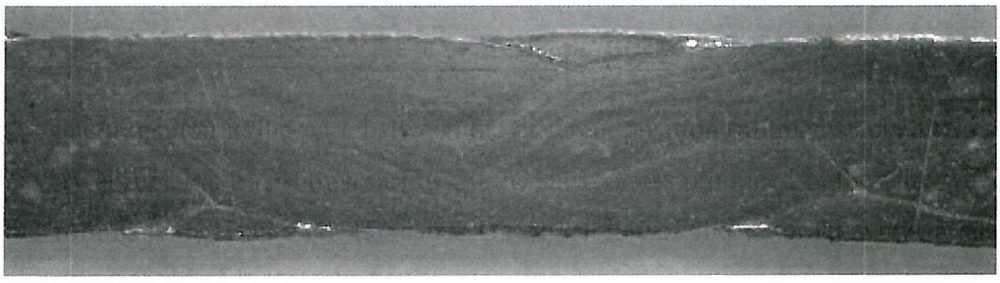

Fig. 71: Braided tape as rolled, it can be seen the filam ents trace on each wire.

The tape was processed thermomechanically with the parameters shown in Table 12. An intermediate rolling reduction of 10% give us a final thickness of the tapes of about 220 μm.

Atmosphere: Ar-8%O_2	Ramp	Anneal/sinter. Temperature	Dwell time(hour)
1st sintering-ramp	200°C/h	600°C	1 h
1st sintering	200 °C/h	826 °C	20 h
1st sintering-cooling	60 °C/h	0 °C	0 h
2nd sintering-ramp	400 °C/h	820 °C	60 h
2nd sintering+annealing	1 °C/h	800 °C	30 h
2nd sintering-cooling	60 °C/h	0 °C	0 h

Table 12: Thermomechanical parameters used for Braided tapes.

The results obtained with braided tapes at different twist pitches and braided pitches are shown in Table 13.

Twist pitch/Braided pitch (cm.)	5/15	3/16	3/18
Ic(1μV/cm,77K)	12,54 A	11,6 A	9,03 A

Table 13: Final critical current results on braided tapes.

By these results, it seems that the braiding pitch is not as influent as the twist pitch for a better critical current but the results are not so homogeneous at different lengths with decrements of 30% in current in some areas. That could mean some filament cracks or bursting that must be solved by a better thermomechanical processing, for this reason and with the lack of a better critical current optimization, the analysis of the AC losses was not possible to be made. Further improvements must be done and hopefully results can be interesting for the understanding of AC losses in BSCCO superconducting tapes.

REFERENCES

[1] H. Kamerlingh Onnes, Leaden Commun., 120b, 122b, 124c (1911).
[2] W. Meissner and R. Oschendfeld, Naturwissenschaften 21, 787 (1933).
[3] J.G. Bednorz and K.A. Müller, Z. Phys. B 64, 189 (1986).
[4] J. Nagamatsu, N. Nakagawa, T. Muranaka, Y. Zenitani, and J.Akimitsu, Nature 410, 63 (2001)
[5] F. London and H. London, Proc. Roy. Soc. (London), A149, 71 (1935); also F. London, Superfluids, Vol. 1, Wiley, New York, 1954.
[6] L. M. Shubnikov et al; 1937 Sov. Phys.-JETP 7 221
[7] V. L. Ginzburg and L. D. Landau, Zh. Eksp. Teor. Fiz. 20, 1064 (1950).
[8] H. Frölich, Phys. Rev. 79, 845 (1950).
[9] C. A. Reynolds, B. Serin, W. H. Wright and L. B. Nesbitt. Phys. Rev. 78, 487 (1950)
[10] J. Bardeen, L. N. Cooper and J. R. Schrieffer, Phys. Rev. 108, 1175 (1957).
[11] A.A. Abrikosov. 1957, Sov. Phys.-JETP 5 1174
[12] Clarke, 1988; Nature 333, 6168, 29-35
[13] F. and H. London, Proc. Roy. Soc. (London) A149, 71 (1935).
[14] M. Tinkham, "Introduction to Superconductivity". Krieger, FL(1985).
[15] A. L. Fetter and J. D. Walecka," Quantum theory of many particle Systems.". Mc Graw-Hill, New York, 1971.
[16] Akimitsu et al, Nature 410, 63 (2001).
[17] R. M, Hazen, "Physical Properties of High Temperature Superconductors II "(ed. D. M. Ginsberg), World Scientific, Singapore, 1990, p. 121.
[18] H. Maeda, Y. Tanaka, M. Fukutomi amd T. Asano, Jpn. J. Appl. Phys. 27 L209 (1988).
[19] P Majewski. J. Mater. Res., (2000)15, 4 854.
[20] H G von schneering et al. Angew. Chem. 1988 27, 574
[21] De Guire et al. Phys. C 1991 179 333
[22] R Flukiger et al. Sup. Sci. Tech. 1997 10 A68
[23] B.W. Statt et al. Physica C 1988 157, 251
[24] S. A. Sunshine et al., Phys. Rev. B 38 1,1988, 893
[25] M. Takano et al., Jap. J. of Appl. Phys. 27, 8 1988, L1041
[26] B. Raveau, C. Michel and M. Hervrieu. J. solid state Chem. 88 140 (1990).
[27] J. B. Goodenough and A. Manthiram. J. Solid state Chem. 88 115.(1990).
[28] K. Kitazawa Am. Ceram. Soc. Bull. 68 880. (1989).
[29] P. H. Kes. Phisica C 153-155 1121 (1988).
[30] P. L. Gammel, L. F. Schneemeyer, J. V. Waszczak and D. J. Bishop. Phys. Rev. lett 61 1666. (1988)
[31] http://www.rtri.or.jp/rd/maglev/html/english/maglev_frame_E.html
[32] Casello et al., Transportation Quarterly, spring 2002, vol 56, 2, 33-49
[33] http://faculty.washington.edu/jbs/itrans/odumag.htm
[34] http://www.maglev2000.com/apps/apps-06.html
[35] http://www.physicscentral.org/action/action-01-3d.html
[36] http://lhc.web.cern.ch/lhc/general/gen_info.htm

[37] http://www.fnal.gov/
[38] Sykulski et al., Proceedings ICEC 17, 1998, Bournemouth, PS19
[39] M Spiller et al. Supercond. Sci. Technol. 14 (2001) no. 3, pp.168-72
[40] Mosawi et al. Physica C 2002 372-6(P3):1539-1542
[41] http://www.abb.com/global/abbzh/abbzh251.nsf!OpenDatabase&db=/global/abbzh/abbzh262.nsf&v=24D86&e=us&m=9F2&c=FB5FDE285E19292CC125688D005940ED
[42] http://www.aclstafford.co.uk/superconductors/index.htm
[43] http://www.igc.com/superpower/products/hts_components/15kV.htm
[44] http://www.nkt.dk/object.php?obj=d000f&base=2e22774
[45] http://www.amsuper.com/html/newsEvents/news/105120628731.html
[46] Heine et al. Appl. Phys. Lett. 1989 55 23 2441
[47] R Navarro. Sup. Sci. Techn. 2000 13 R147
[48] R Flükiger et al. Sup. Sci. Techn. 1992 5 S61
[49] P Haldar et al. Appl. Phys. Lett. 1992 60 4 495
[50] C N R Rao et al. Sup. Sci. Techn. 1993 6 1
[51] S X Dou et al. Sup. Sci. Techn. 1993 6 297
[52] Yamada Y et al., Jpn. J. Appl. Phys. 1988 27 996
[53] Sastry P et al., Solid State Commun. 1989 71 935
[54] D.M. Spiller et al., Physica C 1999 319 50
[55] A. Tampieri et al., Pysica C 1994 227 300
[56] M Yavuz et al., Sup. Sci. Techn. 1996 11 1166
[57] C N R Rao et al., Sup. Sci. Techn. 1993 6 1
[58] B Wolf et al. Sup. Sci. Techn. 1996 9 589
[59] F A A Crane Mechanical working of metals, 1964, Macmillan
[60] M Satou et al. Appl. Phys. Lett. 1994 64 5 640
[61] D A Korzekwa. Appl. Superc. 1994 2 261
[62] H Utsunomiya et al. Physica C 1999 311 23
[63] Wang et al. Sup. Sci. Techn. 1996 9 1066
[64] J Yoo et al. Physica C 1996 269 109-114
[65] D Shi et al. Appl Phys. Lett. 1989 55 7 699
[66] Y Yamada et al. Sup. Sci. Techn 1991 4, 165
[67] U. Endo et al. Jap. J. of Appl. Phys. 27 1988 L1476.
[68] K Sato et al. IEEE Trans. Magn. 1991 Mag 27 1231.
[69] Y Iwai et al. Physica C 1990 170 319
[70] J W Anderson et al IEEE Trans. On Appl. Superc. 1997 7, 2, 1422
[71] S Li et al. Sup. Sci Techn. 1998 11 1011
[72] D M Spiller et al. Cryogenics 1997 37, 623
[73] D M Spiller et al. Physica C 1994 235, 3419
[74] M Penny et al. Cryogenics 1997 37 601
[75] W Zhu et al. J. Mater Res. 1992 7 38
[76] Y B Huang et al. Sup. Sci. Techn. 1994 7 759
[77] T J Rand et al. Appl. Supercond. 1993 2 ed. H. C. Freyhardt 121
[78] W G Wang Physica C 1997 291 1
[79] W G Wang Physica C 1998 297 1

[80] J W Anderson et al, Sup. Sci Techn. 1999 12 617
[81] I Husek et al, Sup. Sci Techn. 1995 8 617
[82] J W Anderson et al. Sup. Sci. Techn. 1999 12 617
[83] M. Penny et al., Cryogenics 37 (1997) 601
[84] R Flukiger et al, Sup. Sci Techn. 1997 10 A68
[85] Endo U et al, 1988 Jap. J. of App. Phys. 27, 8 L1476-9
[86] Y. Yamada et al. Physica C 185-189 1991, 2483.
[87] M Satou et al. Appl. Phys. Lett. 1994 64 5 640
[88] D F Lee et al. Sup. Sci. and Techn. 1997,10 702
[89] R Zeng et al. Sup. Sci. and Techn. 1998, 11 299
[90] H Utsunomiya et al, Phys. C 1999, 311 23
[91] P Kovac et al. Sup. Sci. and Techn. 1997, 10 982
[92] F Marti et al. Sup. Sci. and Techn. 1998, 11 1251
[93] J Muller et al. Sup. Sci. and Techn. 1998, 11 238
[94] U. Endo et al. Jap. J. of Appl. Phys. 1988, vol. 27, 8, L1476
[95] Y Iwai et al. Physica C 1990, 170 319
[96] D M Spiller et al. Cryogenics 1997 37 623
[97] M Lelovic et al Sup. Sci. and Techn. 1996 9 965
[98] Y B Huang et al Sup. Sci. and Techn. 1994 7 759
[99] E. Young, "A Study of the Heat Treatment Time, Temperature and Ramp Rate on the Transport Current Properties and Bi-2223 Grain Growth in (Bi,Pb)2223/Ag Superconducting Tapes", thesis submitted for PhD, 2002, University of Southampton
[100] S. P. Feltham et al. "Correlation of critical current density and phase conversion in Ag-sheathed Pb-Bi 2223 tapes at different final cooling rates". Institute of Cryogenics. University of Southampton. A.S.C. Palms Springs, 13th -18th Sept. In press.
[101] Darren M. Spiller. Thesis of A study of the effects of the processing parameters on the transport Jc of (Pb, Bi)2223 superconducting tapes. University of Southampton 1996.
[102] R Zhao et al. Superc. Sci. and Techn. 11 1998 1068
[103] J W Anderson et al. Superc. Sci. and Techn. 12 1999 617
[104] Y C Guo et al. Physica C 300 1998 38
[105] Endo K et al., 1992, Nature 355, 327.
[106] Y. Hakuraku et al., 1993 J Appl. Phys 73, 309.
[107] R. Navarro, Sup. Sci. and Techn. 2000 13 R147
[108] Anderson J W et al 1997 IEEE T on Appl. Superconduct. 7, 2 1422-25
[109] Husek I et al 1996 Supercond. Sci. and Technol. 9 1066-1070
[110] Zeng R et al 1998a Supercod. Sci. Technol. 11 299-303
[111] Willen D W A et al 1997 IEEE T on Appl. Superconduct. 7, 2 2079-82
[112] Karuna M. et al 1995 IEEE T on Appl. Superconduct. 5, 2 1279-82
[113] Fisher et al 1997 Cryogenics 37, 593-6
[114] W G Wang et al. Sup. Sci. Tecn. 1996 9 875-880
[115] G Grasso et al. Sup. Sci. Tecn. 1995 8 827
[116] Kovac P et al 1997 IEEE T Appl Sup vol 7, 2, 2098-101

[117] Young E et al 1999 EUCAS 1999
[118] C. P. Bean Phys. Rev. Lett. 8 (1962), num. 6, 250-253
[119] Y B Kim et al. Phys. Rev. 129 (1963) 528
[120] W. T. Norris. J. Phys. D 3 (1970) 489
[121] Y. Yang et al. Physica C 256 (1996) 378
[122] Y. Yang et al. Superc. Sci. and Techn. 9 (1996) 801
[123] M N Wilson. Superconducting magnets, Oxford Univ. press, 162
[124] E. H. Brandt Phys. Rev. B 48 (1993) 17, 12893
[125] Y. Yang et al. Cryogenics 37 (1997) 627
[126] C. Bean, Rev. Mod. Phys. 36 (1964) 31
[127] Y. Yang et al. Physica C 310 (1998) 147
[128] E. Martinez et al.. Physica C 331 (2000) 216.
[129] W.J. Carr, AC Loss and Macroscopic Theory of Superconductors Hordon and Breach Science Publisher, 1983.
[130] M.N. Wilson, Superconducting Magnets, Monograph on Cryogenics, Clarendon Press, Oxford, 1983.
[131] A.M. Campbell, "A general treatment of losses in multifilamentary superconductors," in Cryogenics, vol. 22, pp.3-16, 1982.
[132] K. Kwasnitza and St. Clerc, "AC Losses of superconducting high-Tc multifilament Bi-2223/Ag sheathed tapes in perpendicular magnetic fields" in *Physica C* vol. 233, pp.423-435, 1994.
[133] H. Eckelmann, M. Quilitz, M. Oomen, M. Leghissa, W. Goldacker "AC losses in multifilament Bi(2223) tapes with and interfilamentary resistive carbonate barrier" in *Physica C* vol 310 pp 122-126, 1998.
[134] M. Dhallé, A. Polcari, F. Marti, G. Witz, Y.B. Huang, R. Flükiger, St Clerc, K. Kwasnitza, "Reduced filament coupling in Bi(2223)/$BaZrO_3$/Ag composite tapes" in *Physica C* vol 310 pp 127-131, 1998.
[135] E.H. Brandt, M. Indenbom, "Type-II-superconductor strip with current in a perpendicular magnetic field" in *Phys. Rev. B* vol 48 p 12893-12906, 1993.
[136] F. Zeldov, J.R. Clem, M. McElresh and M. Darwin, "Magnetization and transport currents in thin superconducting films" in *Phys. Rev. B* vol 49, pp 9802-9822, 1994.
[137] E. Martínez, Y. Yang, C. Beduz and Y.B. Huang "Experimental study of loss mechanisms of AgAu/PbBi-2223 tapes with twisted filaments under perpendicular AC magnetic fields at power frequencies" in *Physica C* vol. 331, pp.216-226, 2000.